VISCOELASTIC BEHAVIOR OF THE HUMAN INTERVERTEBRAL DISC UNDER CONSIDERATION OF MOISTURE MIGRATION

AIR FORCE OFFICE OF SCIENTIFIC RESEARCH

GRANT NO. 77-3139

(Interim Progress Report)

Prepared by

N. D. Panagiotacopulos

R. Bloch

W. G. Knauss

P. Harvey

M. Patzakis

CALIFORNIA INSTITUTE OF TECHNOLOGY

PASADENA, CALIFORNIA

June 27, 1977

FORWARD

This report summarizes work carried out at the California Institute of Technology on the viscoelastic behavior of the human intervertebral disc. The initial work was performed through sponsorship of the Caltech President's discretionary fund while the follow-up work was supported by the Air Force Office of Scientific Research in cooperation with Dr. Leon Kazarian of the United States Air Force-AMRL and Lt. Col. D. Maio, Biological and Medical Science, Air Force Office of Scientific Research. In order to document our work in a coherent fashion and also incorporate information extracted from the open literature for a somewhat comprehensive view we summarize these developments in a single report. Although the Air Force Office of Scientific Research is kind enough to print this report for wider distribution we wish to acknowledge the support of the Caltech President's Fund which gave us the start in this research.

ABSTRACT

The human intervertebral disc is a highly inhomogeneous fiber composite pressure vessel. If damaged in the post-infant stage, the disc does not repair and may need surgical correction. Diagnosis of whether a disc is damaged is difficult at best and, at this time, involves invasive techniques which are not free of danger (injection of x-ray opaque liquids). Starting from a desire to develop a non-invasive diagnostic technique based on x-ray and computer aided image enhancement, we became interested in the mechanical properties of the disc. These would be important in gaging the x-ray detected deformations of the disc under various loads. During the course of this work we became aware of another need of diagnostics related to estimating the proclivity of an intact disc to sustain damage under unusual loads. It turns out that the water content of the disc material dominates its mechanical behavior. Since modern medical equipment such as the EMI-x-ray body-scanner may record quantitatively the water content of the internal body organs, the possibility exists to gage in-vivo water content measurements with the mechanical performance of discs.

Because the layers of the disc's annulus fibrosus are so thin, we have had difficulty in preparing single-layer specimens. So far, we have worked mainly with three-layer specimens. That test geometry has been sufficient to establish several important aspects of the mechanical properties.

We find that the relaxation behavior is very sensitive to moisture content. Accordingly we have worked with carefully controlled environments including saline solutions claimed to represent body conditions. A major difficulty in obtaining repeatable results is obtaining straight test specimens and holding them in the clamps of the testing apparatus. If moisture and temperature conditioning was repeated without reclamping the specimen, reasonably repeatable results were obtained. No aging was observed after repeated drying and moisturizing cycles.

We also found that water diffuses slowly in the layers. The water apparently acts similar to a solvent in a polymer, effecting a change in the relaxation times. Increasing water content causes shortening of relaxation times, drying having the opposite effect. Upon controlling the water content of the specimen we are thus able to measure the relaxation behavior in various time domains. Data covering a wide spectrum of relaxation times is presented which includes all time scales experienced by the human body. This mechanical characterization gives us an estimate of how discs respond to different rates of deformation and loading conditions.

It is of interest to note that with age (past age 30) the moisture content of the human disc decreases (possible other changes involving increased cross-link density of the mucopolysaccharides as well as an exchange of mucopolysaccharides for collagen). As a result one would expect the human intervertebral disc to react more stiffly with increasing age under nearly constant speeds of motion. Combining this observation with the changes in the vigor of motor/muscle activity as a function of age allows a tentative explanation of the statistic that the largest incidence of disc problems occur around age 40-50.

TABLE OF CONTENTS

TABLE OF CONTENTS

TABLE OF CONTENTS

TABLE OF CONTENTS

ILLUSTRATIONS

TABLE OF CONTENTS

TABLE OF CONTENTS

TABLE OF CONTENTS

TABLE OF CONTENTS

TABLES

I. INTRODUCTION

The human spine consists of a series of vertebrae which are separated from each other by intervertebral discs and surrounded by ligaments and muscles. The main mechanical function of the spine is to support the upper body and transmit the weight/force to the legs. The discs, which contribute approximately one-quarter to one-third of the overall length of the spine, allow deformations of the spine, act as energy absorbers and redistribute the forces, that occur primarily in the vertical axis of the spine, evenly in all directions. The low back region of the spine, known as the lumbar region, is subjected to most of the load which may cause lumbar disc problems. Since a large percentage of the world's population suffers from back disorders, these problems are important in present-day society from both social and medical points of view. It has been reported that in the United States alone, 6.5 million people have back or spine impairments, and about 500,000 workers per year suffer back injuries (Refs. 1 and 2). However, detailed statistical information is not available to us at this time.

A frequent problem is that of the "herniated disc" or "annular rupture," often improperly called "slipped disc," which is defined as the extrusion of the jelly-like material from the center of a disc (nucleus pulposus) through the disc wall (annulus fibrosus). This extrusion occurs most frequently in the posterior portion of the disc. Although it rarely results in death, morbidity is high, inconvenience great, and economic burden significant.

Some of the known causes of disc herniation are:

(1) Improper weight lifting (This is a major source of disability, suffering, and expense to industrial workers.)

(2) Any fall in which the lower extremities slip forward, causing a person to land directly on his buttocks.

(3) Cyclic stress (i.e., "marching stress" in people marching under heavy packs for an extended time period).

(4) Improper posture for an extended time period.

(5) Jet pilot seat ejection.

(6) Paratrooper landing.

(7) Snowmobile and horseback riding injuries which can occur when the buttocks repeatedly impact the seat during a rough ride.

All of these causes may result in lumbar disc herniation problems, such as annular rupture or end-plate rupture known as Schmorl's node, which are discussed in detail in Section III-3. Furthermore, the traumas caused by automobile accidents, certain athletic activities (where improper twisting and bending may occur), some kinds of dancing, and the influence of age are considered as additional significant factors in the occurrence of this problem.

In combatting these lumbar disc problems, reliable diagnostic methods are needed for their identification. Presently, the

techniques in use are exterior or superficial physical examination and conventional radiograms of the lumbosacral spine. Neither of these has proved to be really satisfactory. Let us briefly look at these techniques and their limitations.

The exterior physical examination is based on testing joint motions in the back and the legs. In addition, the neurological activity is checked by testing the muscle and sensory activity. However, although low back pain is a very well-recognized symptom, disc herniation may occur at sites where nerve roots do not exist, so that pain is not always associated with this problem.

On the other hand, conventional diagnostic radiograms, necessary in the clinical evaluation of all patients with such problems, are based on crude qualitative visual measurements of the space between vertebral bodies. Unfortunately, these measurements as well as more accurate ones do not give a satisfactory correlation to clinical studies (Ref. 13). That is, in the majority of patients, the specific cause of low back symptoms is not always clearly demonstrated by these radiograms. In addition, these radiograms can show, very faintly, some features of the intervertebral disc only if properly taken. Presently, the only way to improve the diagnosis of such problems is by the use of contrast-producing materials. More precisely, a better visualization of the spinal canal, and indirectly of the disc, is usually achieved by means of myelographic (Refs. 3 and 4) studies (injection of contrast material in the lumbar subarachnoid, or spinal canal space).

In addition to myelography, discography (injection of contrast material into the nucleus pulposus via a needle) is used when more detailed information regarding the intervertebral disc itself is required (Refs. 3 and 4). Both techniques are "invasive"; that is, they require the penetration of foreign substances into the body and, as such, are potentially dangerous to the individual and may cause significant discomfort during and after the examination. There are many possible side effects associated with these examinations. (See Section III-4 for details.) One alternative to myleography is the use of electromyography which is used to define the specific nerve root or roots involved as manifested by changes of electrical potential of muscles (Refs. 3 and 4). Neither of these methods is foolproof; therefore, there is a great need for the development of noninvasive diagnostic techniques that would be safer and more accurate than the existing ones.

It was recognized that another approach would be to attempt computer enhancement of conventional radiograms by means of digital image processing techniques without the use of contrast materials. These techniques, developed in connection with the space program, have been applied to the analysis of diagnostic radiograms in a number of recent investigations (Refs. 6-9). They help to emphasize selected features, modify the contrast range, remove unwanted data, perform desired measurements, and detect differences between pictures. They are most useful where specific dimensions have clinical significance or where certain abnormalities have a predominant spatial frequency. In situations of more general interest, clinical applications of processed images are restricted

by the degradation of the original image that is introduced by rapid scanning and the subsequent video display. These techniques were utilized for the detection of the human intervertebral disc edges from conventional radiograms of the spine. These radiograms were lateral views of the spine taken by means of optimum exposure (i.e., 80 KVP, 100 MAS).

The diagnostic information recorded in these radiograms regarding the disc is difficult to be extracted with the unaided eye. However, as it is demonstrated by this study, the application of digital image processing techniques can provide an improved visualization of the human disc. We believe that this is important in that it opens a new and safer approach in the detection of disc problems. It is needless to say that this diagnostic information is greatly needed by the neurosurgeon and orthopedist surgeon prior to disc surgery.

At this point, we feel it is worth mentioning that the disc herniation is primarily a mechanical problem of failure and the proclivity to herniation with age depends on the biochemical changes that occur in the material of the disc during its maturation process. However, a careful mechanics-based analysis of failures adequate to the need is not available today. It appeared that the treatment, as well as the possible prevention of the disc herniation problems, would be greatly aided by an improved understanding of the mechanical behavior of the human intervertebral disc under various modes of deformations and motions of the human spine.

A review of the work done in this field (see Section III-6-a) has shown that, so far, experimental work on the human intervertebral

disc has been carried out on autopsy specimens, such as segments of the spine consisting of two vertebral bodies with their intervening disc or small sections of the annulus fibrosus (Ref. 1). These experiments were directed to obtain mechanical properties of the total disc, assuming that the disc material has elastic behavior. However, to the best of our knowledge, only three experiments (Refs. 10-12), not including our experiments, recognize the viscoelastic behavior of the disc. To date, no use has been made of this observation in treating the limited analysis of the disc's mechanical behavior.

In studying the viscoelastic properties of the disc, we observed that the water content of the disc material is important in that it controls the relaxation behavior of the material. This was done by subjecting small sections of the disc's lamellae (layers from which the annulus fibrosus consists of) to simple tension tests under closed system conditions (i.e., permitting no mass flow in or out of the disc specimen). Based on this observation, on data obtained from literature review, and on the fact that the water content of the disc decreases with age (Refs. 23-27), a qualitative hydrorheological model for the behavior of the disc's material is proposed. This model, although qualitative, provides the basis for discussion regarding the maturation of the disc. It is our purpose to quantify and check the validity of this model in a future study. We expect that the long term medical significance of this work will be in the fields of preventive and diagnostic medicine.

II. OBJECTIVE

The overall objective of this research is to advance the present knowledge of the physiology of the human intervertebral disc and subsequently of the spine. However, its immediate purpose was to determine, in-vitro, the viscoelastic material properties of sections from the annulus fibrosus of human lumbar intervertebral discs. In addition, an attempt was made to visualize the human intervertebral disc from conventional radiographic data without injection of contrast material.

III. BACKGROUND

1. Anatomical Review

a. The Human Spine

The human vertebral column is formed by a series of 33 vertebrae:

(1) 7 cervical (neck region)

(2) 12 thoracic (chest region)

(3) 5 lumbar (low back region)

(4) 5 sacral

(5) 4 coccygal.

The cervical, thoracic, and lumbar vertebrae remain distinct and separate from each other throughout life. They are considered as movable vertabrae and are separated from each other by intervertebral discs. In contrast, adult sacral and coccygeal vertebrae are fused (united) with each other to form two bones, the sacrum and the coccyx. Figure 3.1 shows a lateral view of the vertebral column in the erect position together with the names and locations of its basic constituents.

b. The Intervertebral Disc

The intervertebral discs contribute between a quarter to one-third of the overall length of the vertebral column.

It is customary to distinguish three domains of the disc, though the demarkation of these domains is not sharp:

(1) The annulus fibrosus

(2) The nucleus pulposus

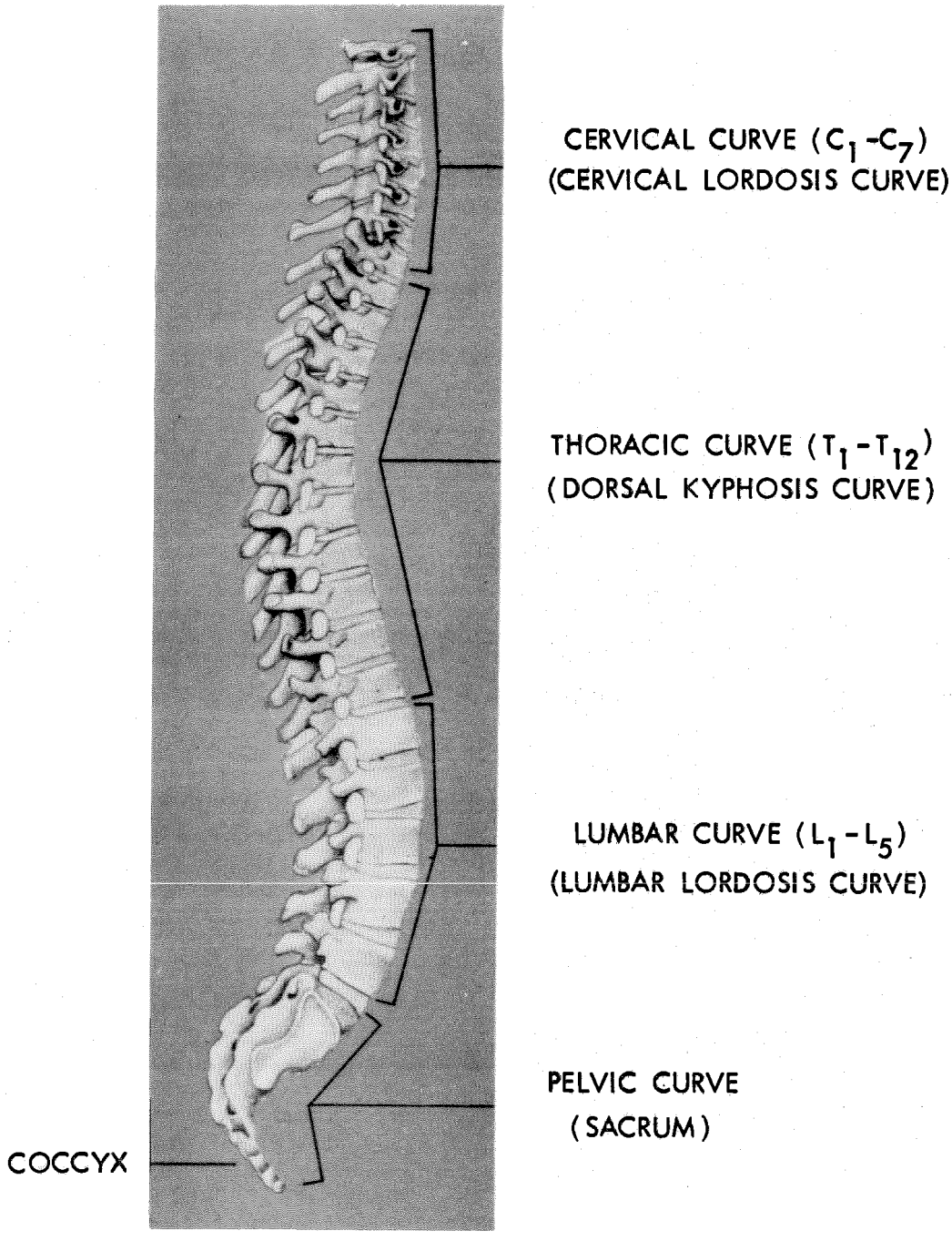

Figure 3.1. Lateral View of the Vertebral Column

(3) The cartilaginous end plates.

Each disc is named by the two surrounding vertebrae; for example, the disc L4-L5 is surrounded by vertebrae L4 and L5.

1) The Annulus Fibrosus

The annulus fibrosus is the outer fibrous part of the intervertebral disc (Figures 3.2(b) and 3.2(c)). It is formed by a series of 12-14 (or more) concentrically encircling lamellae (Refs. 3 and 4). A lamella is defined as a layer from the disc's annulus fibrosus in which collageneous fibers embedded in a mucopolysaccharide matrix run in a single direction.

In order to give an approximate representation of the lamellae structure as far as the direction of the fibers is concerned, let us consider two adjoining lamellae. In both lamellae the fibers run approximately a uniform course. In the first one the fibers form an angle (Refs. 14 and 15) approximately $+50^{\circ}$ to $+60^{\circ}$ with respect to the disc axis; in the next one the fibers form an angle -50° to -60°. Figure 3.2(b) gives a simplified schematic representation of the layered structure of the inhomogeneous disc. The two macroscopic pictures presented in Figures 3.3(a) and 3.3(b) show the direction of the fibers for the cases of a single lamella and two adjacent lamellae correspondingly.

In the lumbar region (Ref. 10) the lamellae vary in thickness from tenths to several millimeters. It is thicker anteriorly (front of the disc) where the lamellae are more numerous than posteriorly (rear of the disc). It is worthwhile mentioning

that some interweaving is present between adjoining posterior lamellae (Ref. 16). The outermost lamellae attach themselves to the bony edge of the vertebral body (bony epiphyseal ring) while those remaining continue into the cartilaginous plates. In the front, intimate connections exist with the anterior longitudinal ligament, while the posterior longitudinal ligament is less firmly attached to the annulus (Ref. 3).

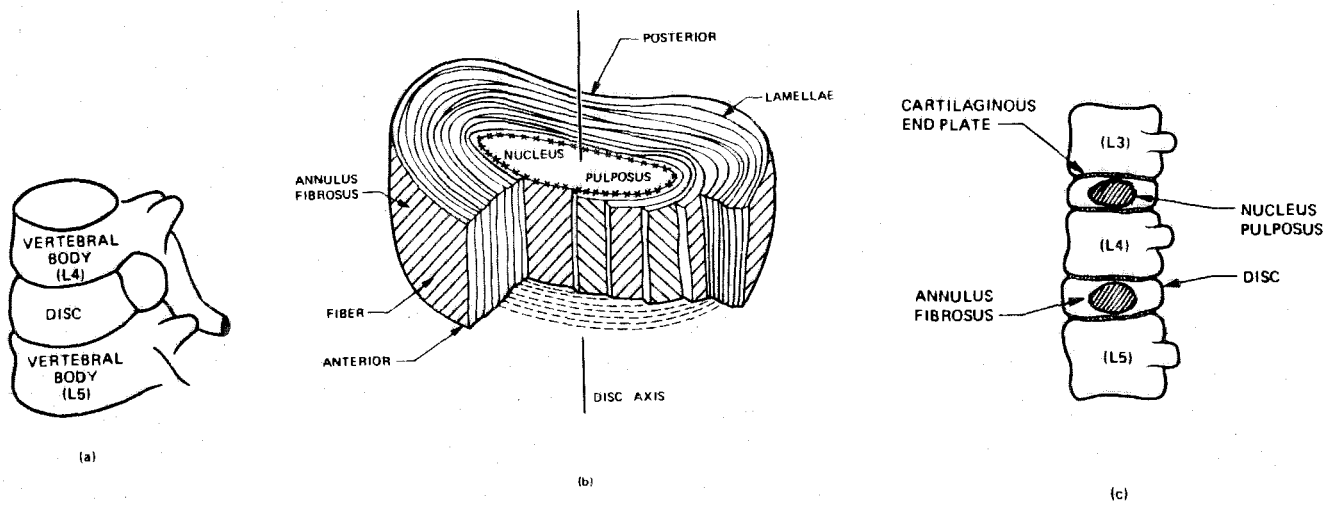

Figure 3.2 A Schematic Representation of the Human Intervertebral Disc and Vertebral Bodies

2) The Nucleus Pulposus

The nucleus pulposus is centrally situated (Figures 3.2(b) and 3.2(c)) it consists of a three dimensional network of non-oriented collagen fibrils enmeshed in a mucoprotein gel and occupies about 25-50% of the disc volume (Refs. 3 and 4).

(a) Single Lamella

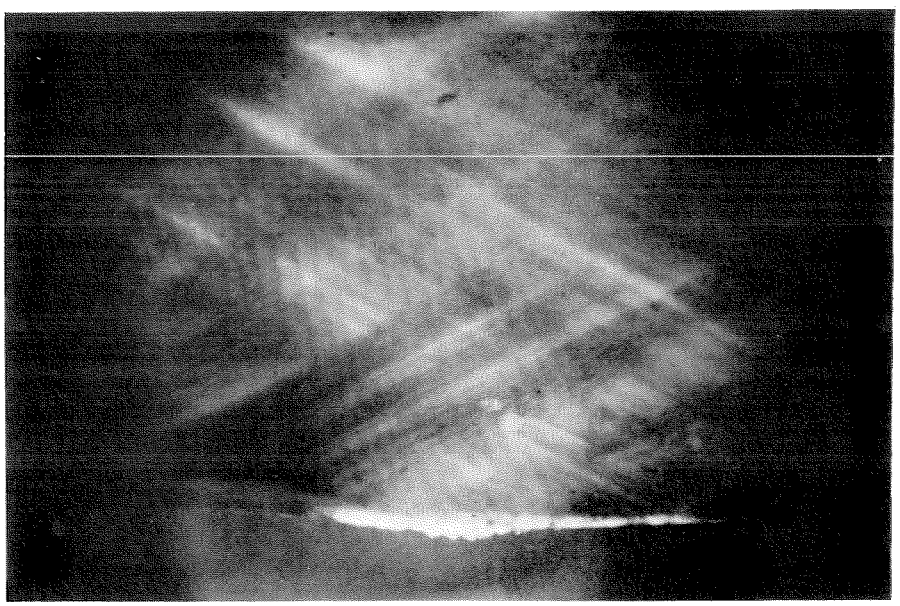

(b) Multiple Lamellae

Figure 3.3. Direction of the Fibers Via Microscopic Pictures

3) The Cartilaginous End-Plates

The cartilaginous end-plates (Fig. 3.2(c)) connect the disc with the vertebral bodies above and below. Peripherally they are attached to the bony epiphyseal ring (Refs. 3 and 17). We are of the opinion that these thin plates are firmly attached to the vertebral bodies.

4) The Disc Shape and Dimensions

The disc is somewhat kidney-shaped. However, it appears that the pattern of the disc shape varies considerably from individual to individual or even in the same individual. The following parameters shown in Figure 3.4 are normally used to characterize the disc's geometry. They are its major diameters (B, b), its minor diameters (D, d) and its height(h). In Table 1. some measurements for these parameters taken from radiographs of lumbar intervertebral discs are presented.

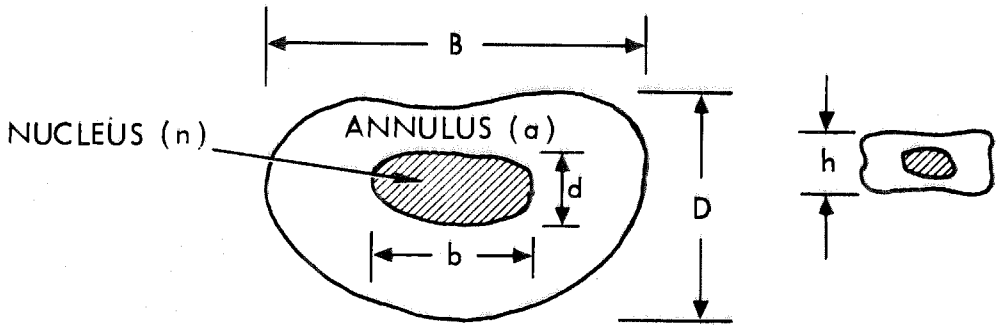

Figure 3.4 Parameters Characterizing the Disc's Geometry

Table 1. Typical Lumbar Intervertebral Disc Dimensions

Disc Level	Major Diameter (cm)		Minor Diameter (3m)		Vertical Disc Height (cm)
	Disc	Nucleus	Disc	Nucleus	
L1-L2	5.26	2.83	3.81	1.78	.69
L2-L3	5.46	2.67	3.81	1.55	.87
L3-L4	2.57	2.64	3.58	1.71	.82
L4-L5	5.59	2.54	3.86	1.49	.96

c. The Vertebral Bodies and the Ligaments

1) The Vertebral Bodies

The somewhat kindey-shaped vertebral body (Figure 3.5) consists of an outer shell of dense bone about 0.5 mm thick. The inner portion of the body is composed of trabecular or spongy bone. Its upper and lower flattened, slightly concave surfaces are covered by the vertebral end plates which are approximately 1 mm thick (Refs. 3 and 17).

2) The Ligaments

The vertebral bodies and the intervertebral discs are surrounded by fibrous bands in tension called ligaments. The names and locations of these ligaments are shown in Figure 3.6.

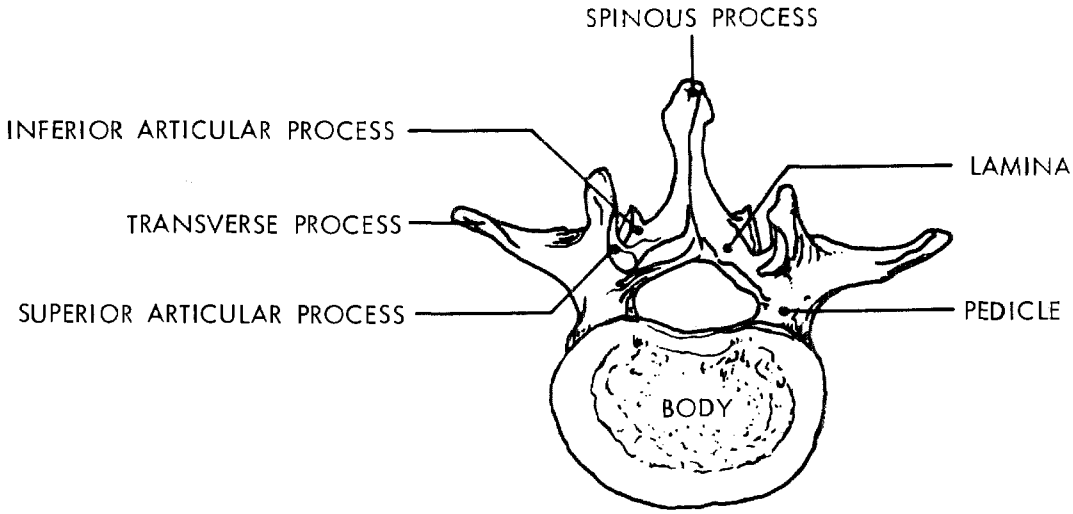

(a) Top View

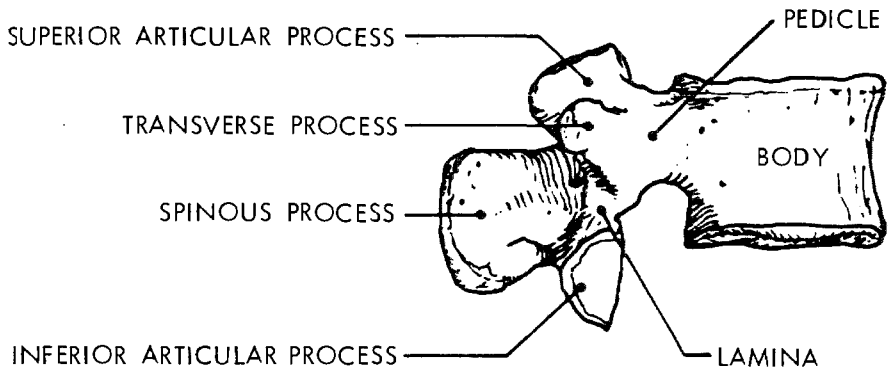

(b) Side View

Figure 3.5. A Typical Lumbar Vertebra

(1) The Anterior Longitudinal Ligament. The anterior longitudinal ligament (Figure 3.6) is a broad strong band of fibers extending along the anterior surfaces of the vertebral bodies. Essentially, it consists of 3 layers of dense fibers, all of which run in a longitudinal direction. The innermost layer extends from one vertebrae to the next, adhering intimately to the intervertebral discs and the epiphyseal ring. It blends with the outer fibers of the annulus and cannot be separated from it easily. The middle layer extends between 2 or 3 vertebrae, and the outermost is the longest and extends over 4 or 5 vertebrae (Refs. 3 and 17).

(2) The Posterior Longitudinal Ligament. The posterior longitudinal ligament (Figure 3.6) lies within the vertebral canal, extending along the posterior surfaces of the vertebral bodies. It consists of 2 layers; the outermost layer extends over 3 or 4 vertebrae, and the inner layer extends between adjacent vertebrae. It is considered to be a much more delicate (thinner) structure as compared to the anterior one (Refs. 4 and 17).

(3) The Lateral Vertebral Ligament. The lateral vertebral ligaments (Figure 3.6) are situated between the anterior and posterior longitudinal ligaments. They consist of short fibers firmly adherent to the intervertebral discs

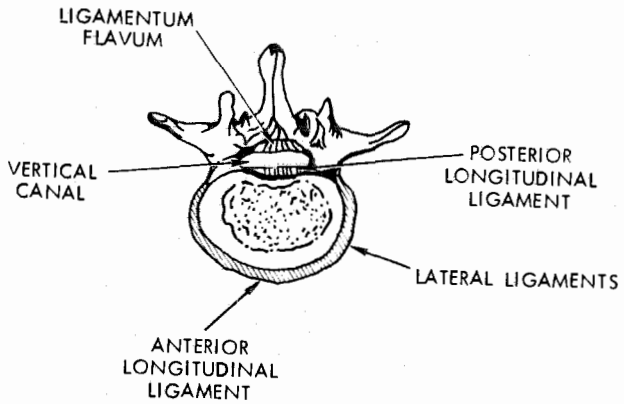

(a) Top View

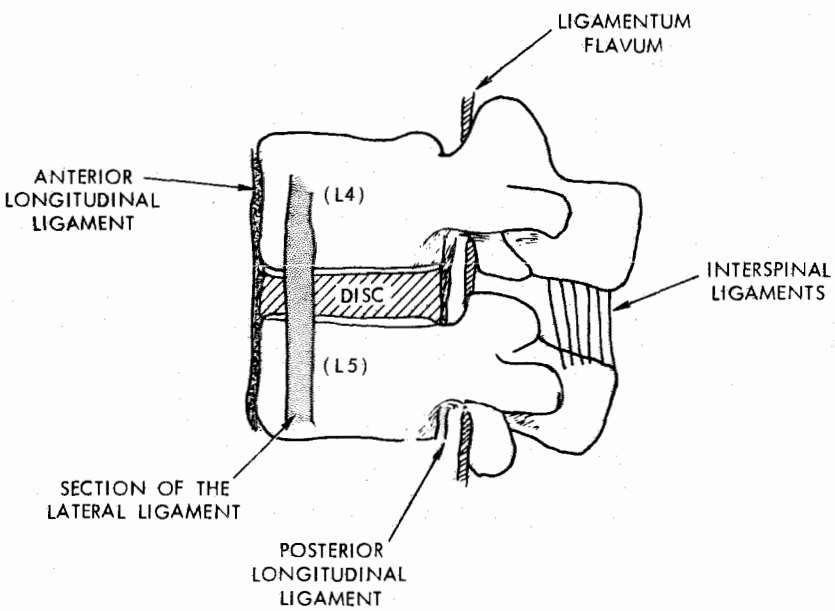

(b) Side View

Figure 3.6. The Ligaments

and passing over the vertebral body to the adjacent intervertebral disc.

(4) The Ligamentum Flavum. This is a structure composed of thick (3 mm), strong fibers. It bridges the gap between the edges of two adjacent laminae as it is shown in Figure 3.6 (Refs. 3 and 17).

(5) The Interspinal Ligaments. These ligaments are fibers which connect the root of one spinous process to the tip of the next. Although they are thin and membranous in the cervical and thoracic area of the spine, they are thick and well developed in the lumbar region (Ref. 3).

d. The Muscles

1) General

The muscles involved in the vertebral column are numerous, and their arrangement is complicated (Refs. 3 and 18). There are three main groups:

(1) Flexors (allow flexion or forward bending).
(2) Extensors (allow extension or backward bending).
(3) Abductors (allow side movements and rotations).

Some of these muscles are shown in a tomographic EMI picture taken from the lumbar area of the spine (Figure 3.7).

In the following paragraph we will describe briefly only the

most important from the group of flexors, namely the erector spinae or sacrospinal muscles.

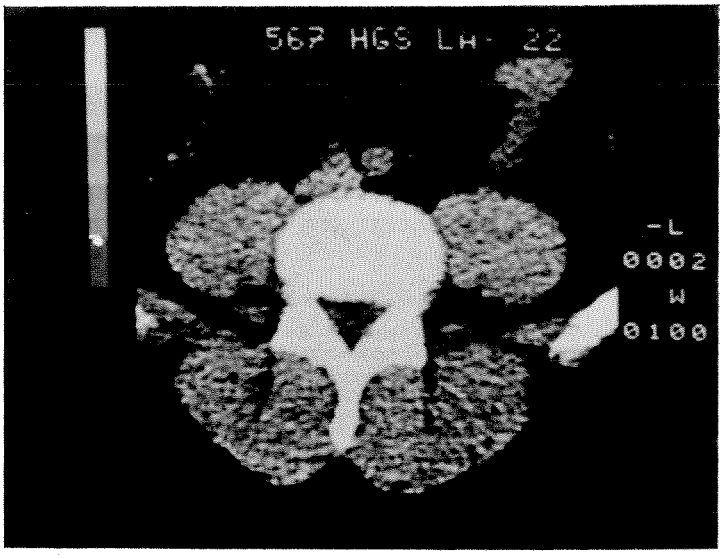

Figure 3.7 The Muscles Surrounding the Spine (Sectional View)

2) The Erector Spinae or Sacrospinal Muscles

These muscles exist between the ilium and the sacrum (Figure 3.8) with their upper parts attached to the spinous processes of all the lumbar and four thoracic vertebrae (Ref. 3). They serve as a powerful extensor of the spine.

e. Blood Supply of the Intevertebral Disk

It has been reported (Refs. 3 and 17) that in children and young adults one can find small blood vessels within the periphery of the cartilaginous end-plates. These vessels gradually disappear so that by the second decade the intervertebral disc is found to be completely evascular. There are only a few small vessels in the outermost layers of the ligaments, but these vessels

never penetrate into the annulus.

The disc's limited nutritional demands are probably fulfilled by the diffusion of lymph from the marrow cavity to the cartilaginous end-plates, which permits some lymph supply to diffuse through the disc.

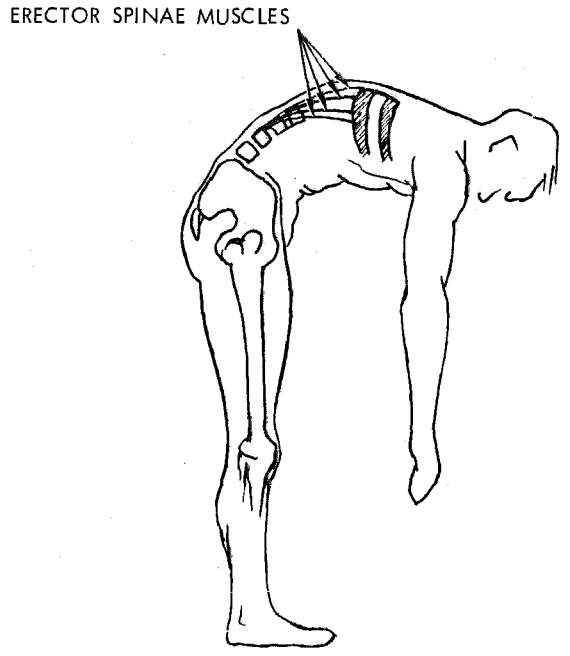

Figure 3.8. The Erector Spinae Muscles

2. Biochemical Review

As it was described earlier, the structure of the disc lamella is made of collageneous fibers embedded in a mucopolysaccharide matrix. Next we document some general information regarding the disc's biochemical constituents.

a. General Information

1) Collagen

The collagen fibers appear as bundles of individual non-branching fibrils (Refs. 19 and 20). The structure of the fibrils consists of a core and an annulus as is shown in Figure 3.9.

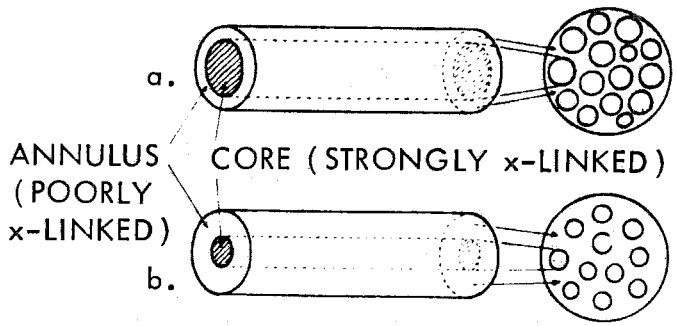

(a) Old Fibril
(b) Young Fibril

Figure 3.9. Structure of a Fibril

Electron microscope studies have shown that in a given fiber the diameter of the fibril's core increases with age at the expense of the fibril's annulus, as shown in Figure 3.9.

The fibrils are made of tropocollagen molecules. Each tropocollagen molecule is composed of three strands forming a triple helix (Ref. 19). Each strand is made of amino acids with glycine, proline and hydroxyroline being the primary ones. The amino acid composition of the tropocollagen molecules appears to be almost constant with age. Fibril growth and development

occurs by accumulating newly formed tropocollagen molecules on its surfaces. Furthermore, it is accepted that the tropocollagen molecules are strongly bonded between themselves (highly cross-linked) in the core area and poorly cross-linked in the fibril's annulus. Since the annular collagen is easily extractable by various solutions (i.e., acetic acid, NaOH, etc.), the strength and number of the cross-links will be weaker than that of a young fibril. Correspondingly, the annulus will be narrower in older fibrils than in younger ones. As growth continues, the fibril will move toward complete three-dimensional cross-linking and the annulus will decrease until the whole fibril is uniformly cross-linked.

The maturation of collagen involves the intra-and inter-molecular cross-linking of the tropocollagen. This cross-linking process leads to the relative insolubility of collagen and it may be related to the aging process.

2) The Mucopolysaccharides

According to References 10 and 21, mucopolysaccharides are composed of: Hyaloronic Acid, chondroitin sulfate (A, B, C), heparitin sulfate, keratosulfate, and heparin. The majority of these mucopolysaccharides appear to be nonbranched amorphous polymers. They are covalently bound to proteins resulting in a compound called protein-polysaccharides or mucoprotein. To the best of our knowledge, the variation of these compounds with age is not known for the human intervertebral disc material. However, for the case of the skin where similar components are present,

it is known that the percentage of hyaloronic acid decreases and the percentage of chondroitin sulfates increases with age.

Some of the functions of the mucoproteins are (Ref. 22):

(1) To Stabilize Mechanically the Collagen Fibrils. The mucoproteins act as the bonding agent between the collagen fibrils as shown in Figure 3.10.

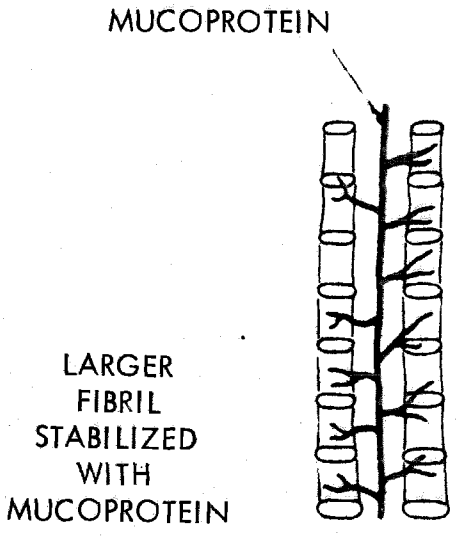

Figure 3.10. Stabilization of Collagen Fibrils

(2) To Bind Water. These high molecular weight polymers trap large amounts of water within their domain, an important factor in determining their physical and mechanical properties.

(3) To Control the Synthesis of Collagen

(4) To Regulate the Growth and Differentiation of Cells. This is important in wound healing.

b. The Chemical Constituents of the Human Intervertebral Disc

Dickson, Naylor et al reported the percentage of hydroxyproline, and thus the collagen content, as a function of age (3-89 years) for dry nucleus pulposus and annulus fibrosus (Ref. 23). They found that in nucleus pulposus, the hydroxyproline content remains fairly constant after the age of 10 until the age of 65 and then decreases slightly. In the annulus fibrosus they reported that the percentage of hydroxyproline decreases until the age of 62 and then remains constant. The mucopolysaccharides are present in larger amounts in the nucleus and their highest level is reached in the 30-40 age group, declining to its lowest level in later years. Moreover, they found that for a protruded disc in a younger man, the hydroxyproline content (or collagen) of both nucleus and annulus was increased and their mucopolysaccharide content was reduced (Ref. 24). This is consistent with what is found in nonprotruded discs from older individuals. Lyons et al felt that disc degeneration represents a premature aging process (Ref. 25). Also there is little doubt that severe damage in the disc material is a manifestation of excessive production and aberrant arrangement of collagen in the affected disc material. Many of the chemical details of the various processes related to the synthesis and deterioration of these constituents are not yet known.

Besides these relatively solid components, the disc contains a large amount of water (trapped by the mucoprotein macromolecules as it was discussed earlier) which influences strongly its mechanical

response characteristics. The following table gives the approximate water variations in the disc as a function of age (Ref. 10).

Püschel indicated that with advancing age, the water content of the disc is progressively decreased (Ref. 26). Later DePukey reported that the average person is one percent shorter at the end of the day when compared to body length in the morning on first rising (Ref. 27). It was observed that the average daily oscillation in body length is two percent in the first decade and only 0.5 percent in the eighth decade. This difference was attributed to decreasing water content of the disc.

Table 2. Approximate Water Variations in the Human Intervertebral Disc

Age	At birth	30 yrs.	77 yrs.
Nucleus Pulposus	88%	gradually decreases to 65%	constant
Annulus Fibrosus	78%	gradually decreases to 70%	constant

3. Some Lumbar Intervertebral Disc Problems

Its unique construction and composition enable the disc to withstand stresses varying in duration and magnitude. Both the annulus and the nucleus act to absorb forces that occur primarily in the vertical axis of the spine and redistribute them evenly in all directions. We may think of the annulus as a flexible pressure vessel with the less structured nucleus as the pressure medium. Its

nearly incompressible behavior converts the spine-axial load into (tangential) tension stresses in the annulus. The disc's reaction to pressure is nicely demonstrated in Figure 3.11.

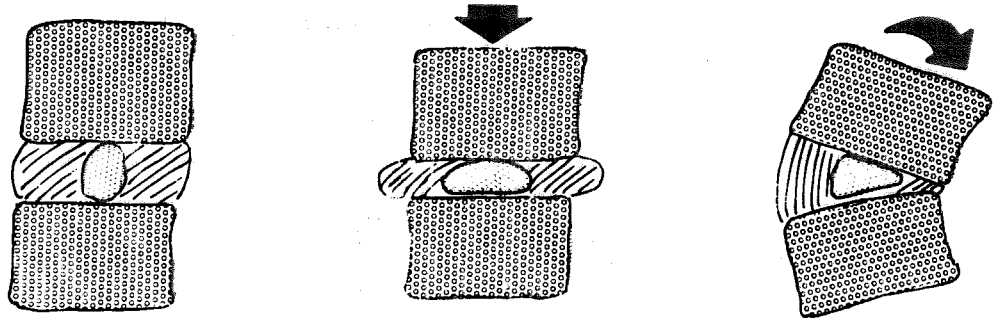

(a) (b) (c)

Figure 3.11. The Reaction of the Disc to Pressure (After Cailliet)

As one can see, the normal disc has a rounded well-hydrated intact nucleus (Figure 3.11(a)) and under normal pressure maintains normal vertebral separation. Compression deforms the nucleus and "bulges" the annulus physiologically (Figure 3.11(b)). Flexion or extension deforms the disc nucleus and permits the motion (Figure 3.11(c)). Upon release of compression or bending forces, the disc resumes its normal position as a result of the intrinsic intervertebral disc pressure.

Somehow, in a still unknown way, the above mentioned physiological behavior is perturbed, subsequently allowing the spinal axial load to cause ruptures. Furthermore, biochemical changes due to aging or early maturation of the disc may be the cause of another problem known as disc degeneration.

a. Ruptures

1) Annular Rupture

The annular rupture (frequently referred to as disc herniation) of the disc is shown in Figure 3.12(a). It is the extrusion of material from the nucleus pulposus through the posterior part of the disc

(Refs. 3 and 4). This extrusion can cause pain by pressing on nerve endings in the ligamentous layers surrounding the vertebrae, or on the spinal nerve.

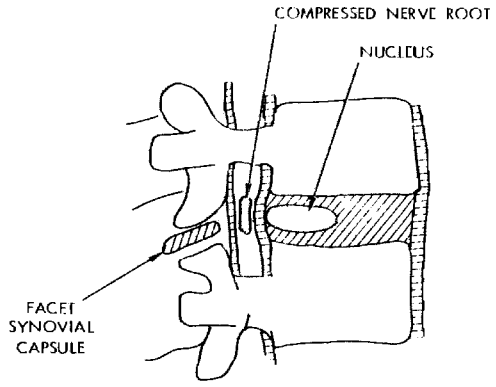

Figure 3.12(a). Annular Disc Rupture (Herniated Disc)

2) End Plate Rupture (Schmorl's Node)

This pathological occurrence is defined as the penetration of nuclear material through the cartilaginous end plates into the spongy bone of the vertebral body (Figure 3.12(b)).

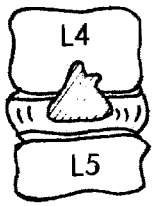

Figure 3.12(b). Schematic Representation of Schmorl's Node

b. Disc Degeneration

Degeneration of the disc implies dehydration and fragmentation of the lamellae with some radial tearing. The nucleus material escapes into the adjacent annulus and loses its intradiscal pressure thus allowing the narrowing of the intervertebral space (Figure 3.13). This narrowing can cause the posterior facets

of the vertebrae to press against one another producing a crushing of their synovial capsule and consequently pain. This may occur as a result of aging or repeated injuries associated with overloading.

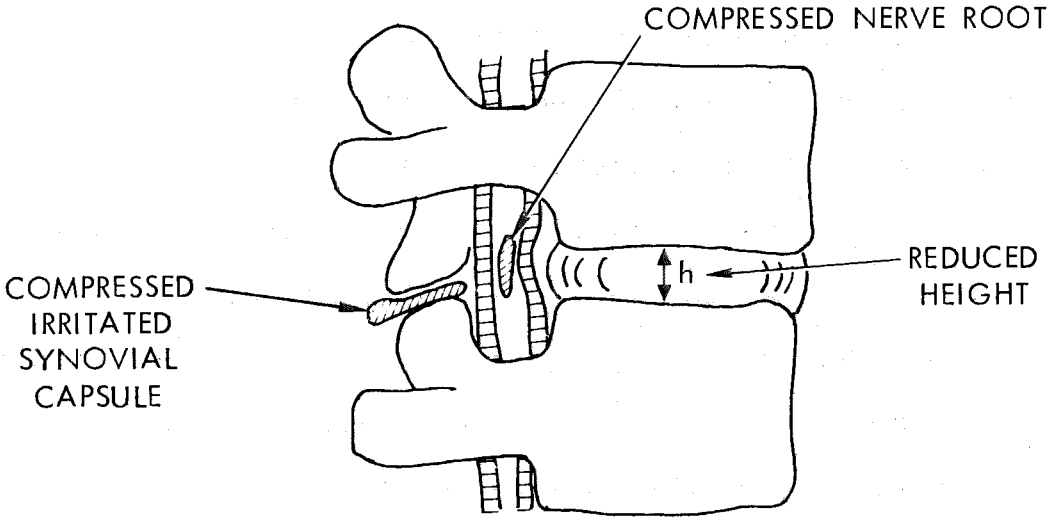

Figure 3.13. Degenerated Disc

4. Diagnostic Techniques Presently in Use

In combating the spine problems discussed earlier, reliable diagnostic methods are needed for their identification. Presently, the techniques in use are: exterior or superficial physical examination, and conventional radiograms of the spine. Neither of these has proved to be really satisfactory.

Let us briefly now look at these techniques and the problems associated with them:

The exterior physical examination is based in testing joint motions in the back and the legs. In addition, the neurological activity is checked by testing the muscle and sensory response.

Although low back pain is a very well-recognized symptom, disc herniation is not always a cause of this pain. On the other hand, disc herniation may occur at sites where nerve roots do not exist, so that pain is not always associated with this problem.

Conventional diagnostic radiograms, necessary in the clinical evaluation of all patients with such problems, are based on measurements of the space between vertebral bodies. Unfortunately, these measurements do not give a satisfactory correlation to clinical studies (Ref. 13). That is, in the majority of patients, the specific cause of low back symptoms is not always clearly demonstrated by these radiograms. In addition, these radiograms can show, very faintly, some features of the intervertebral disc only if properly taken. Presently, the only way to improve the diagnosis of such problems is by the use of contrast producing materials. More precisely, a better visualization of the spinal canal, and indirectly of the disc, is usually achieved by means of myelographic studies (Refs. 3 and 4). When myelography is performed, a radiopaque substance, heavier than the spinal fluid, is introduced via a needle into the subarachnoid or spinal canal space. By tilting the patient up and down under fluoroscopic guidance, one can follow the column of dye along the length of the spine, thus providing some diagnostic information for the presence of disc herniation (Figure 3.14). Myelography is used on a routine basis prior to lumbar disc surgery, even though it is not an accurate detection method (it is claimed that the method is 80-85% accurate). For instance, in some cases the myelogram was interpreted as nonrevealing, although surgery revealed a disc protrusion.

Furthermore, faulty lumbar puncture techniques used in performing the myelogram may deposit radiopaque substance outside the subaracnoid space making removal much more difficult and at times impossible. Several reports of more severe and even fatal reactions attributed to a unique hypersensitivity to the radiopaque substance have appeared in the literature. As a result of the increased sensitivity to this radiopaque material, a widespread aseptic leptomeningitis may occur, involving not only the spine but extending into the brain, with some cases terminating in death.

The low frequency of occurrence of these tragedies makes it impossible to establish reasonable criteria to prevent similar future complications. Intradermal radiopaque skin tests have been used, but have proven to be unreliable (Ref. 3). Until satisfactory

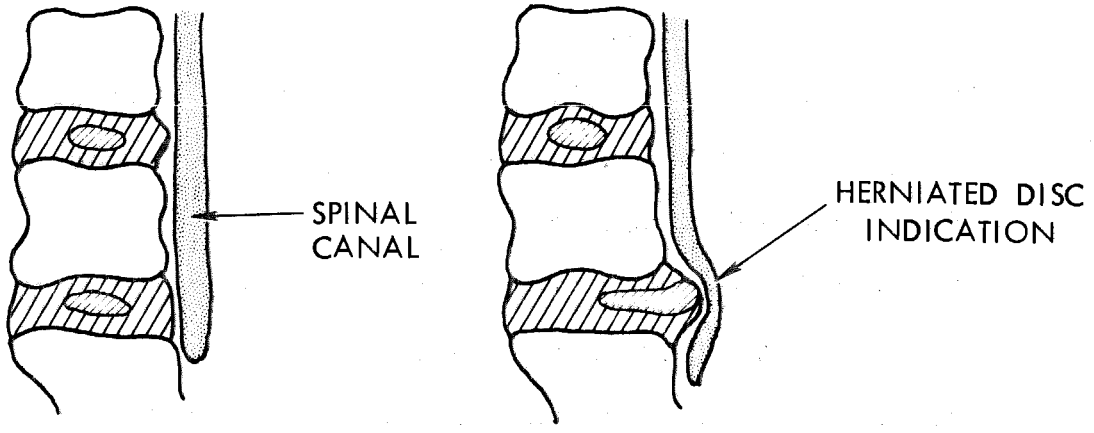

Figure 3.14. Schematic Representation of (a) Normal, and (b) Herniated Disc Myelograms

guidelines can be developed, patients with a severe allergic background, including a specific allergy to iodine, should probably

not have radiopaque myelography. However, to date there is research going on on the development of safer contrast materials which, hopefully, will reduce these dangers.

In addition to myelography, discography, injection of contrast material into the nucleus pulposus via a needle, is used when more detailed information regarding the intervertebral disc itself is required (Refs. 3 and 4). Both techniques are "invasive"; i.e., they require the penetration of foreign substances into the body and, as such, are potentially dangerous to the individual and may cause significant discomfort during and after the examination. There are many possible side effects associated with these examinations.

The side effects associated with myelography are:

(1) Pain during the performance of the myelogram.

(2) Postmyelogram radiculitis resulting from nerve root trauma.

(3) Postspinal headache.

(4) Meningeal irritation, in reaction to introduction of a foreign material into the subarachnoid space.

(5) Bacterial menengitis.

(6) The irritative effects of the radiopaque substance may produce adhesive arachnoiditis.

(7) Dye retained in the subarachnoid space may flow into the basilar cisterns and cerebral ventricles and produce a basilar adhesive arachnoiditis, which may lead to obstructive hydrocephalus.

(8) The incidence of a ten percent error inability to visualize laterally placed discs may cause the surgeon to withhold indicated surgery.

(9) Radiopaque substance sensitivity. (Spinal fluid examination one or two days following radiopaque myelography will usually show from two to twenty white blood cells per cubic centimeter associated with a moderate increase in the spinal fluid protein, resulting in nuchal rigidity, headache, low grade temperature elevation and malaise.)

In the case of discography, the possible side effects are:

(1) Pain during the performance of the discogram.

(2) Nerve root trauma.

(3) Long-term effects of injecting a needle into a normal disc may accelerate the normal degenerative changes of age and stress.

(4) Infection following injection into an interspace.

Reviewing this large list of side effects, one should rightly pause before considering the use of these tests.

One alternative to myelography is the use of electromyography (Refs. 3 and 4). This technique is used to define the specific nerve root or roots involved as manifested by changes of electrical potential of muscles. Neither of these methods is foolproof.

The last alternative to the diagnostic techniques discussed earlier is exploratory surgery of the spine which seems to be even more undesirable. Therefore, there is a great need for the development of noninvasive diagnostic techniques that would be safer and more accurate than the existing ones.

5. Engineering Fundamentals

a. Viscoelasticity

1) Definition

Viscoelasticity is a material property possessed by solids and liquids which, when deformed, exhibit both viscous and elastic behavior through simultaneous dissipation and storage of mechanical energy (Ref. 28). The material constants connecting stress and strain in the linearized theory of elasticity become time dependent material functions in the constitutive equations of viscoelastic theory.

Example: A viscoelastic material when subjected to a constant deformation, the forces required to maintain that deformation decrease with time.

2) Boltzmann's Superposition Principle (Linear Theory)

At sufficiently small strains, the behavior of anisotropic linear viscoelastic materials is well described by the following constitutive equation:

$$\sigma_i(t) = \int_{-\infty}^{t} C_{ij}(t-u)\,d\varepsilon_j(u) \quad (i,j = 1, 2, \ldots, 6) \tag{1}$$

where:

t = time

$\sigma_i(t)$ = the six components of the symmetric stress tensor

$\varepsilon_j(t)$ = the corresponding strains

$C_{ij}(t)$ = the time dependent stiffness matrix (it characterizes the memory of the material).

Equation (1) states that the stress at time t under an arbitrary strain history is a linear superposition of all strain increments applied at previous times u and the relaxation time corresponding to the time interval t-u which has elapsed since imposition of the

respective strains.

By taking the Carson transform (a special case of Laplace transform) of Equation (1), we obtain the following equation:

$$\sigma_i(s) = C_{ij}(s) \quad \varepsilon_j(s) \tag{2}$$

where: $\sigma_i(s)$, $C_{ij}(s)$ and $\varepsilon_j(s)$ are the Carson (Laplace) transforms of $\sigma_i(t)$, $C_{ij}(t)$ and $\varepsilon_j(t)$ respectively.

Equation (2) is the associated Hooke's law of linear elasticity (see the correspondence principle (Ref. 31) of the theory of viscoelasticity). Therefore, the expressions for the components of the $C_{ij}(s)$ matrix from the linear theory of elasticity can be applied in the Laplace s-plane for viscoelastic materials.

(1) Expressions for the $C_{ij}(s)$ Matrix for Various Types of Materials. Next, we present the form of the stiffness matrix $C_{ij}(s)$ for anisotropic, orthotropic, transversely isotropic and isotropic materials (Refs. 29 and 30).

(a) For Anisotropic* Materials

$$C_{ij}(s) = \begin{bmatrix} C_{11}(s) & C_{12}(s) & C_{13}(s) & C_{14}(s) & C_{15}(s) & C_{16}(s) \\ 0 & C_{22}(s) & C_{23}(s) & C_{24}(s) & C_{25}(s) & C_{26}(s) \\ 0 & 0 & C_{33}(s) & C_{34}(s) & C_{35}(s) & C_{36}(s) \\ 0 & 0 & 0 & C_{44}(s) & C_{45}(s) & C_{46}(s) \\ 0 & 0 & 0 & 0 & C_{55}(s) & C_{56}(s) \\ 0 & 0 & 0 & 0 & 0 & C_{66}(s) \end{bmatrix} \tag{3}$$

where $C_{11}(s), \ldots, C_{66}(s)$ are 21 distinct material properties.

* A material for which its mechanical properties are different in all directions at a point in a body (no plane of material symmetry) is called anisotropic.

(b) Orthotropic* Materials. (When the planes of material symmetry coincide with the stress-strain coordinate system.) In this case, the $C_{ij}(s)$ matrix has the form

$$C_{ij}(s) = \begin{bmatrix} C_{11}(s) & C_{12}(s) & C_{13}(s) & 0 & 0 & 0 \\ C_{12}(s) & C_{22}(s) & C_{23}(s) & 0 & 0 & 0 \\ C_{13}(s) & C_{23}(s) & C_{33}(s) & 0 & 0 & 0 \\ 0 & 0 & 0 & C_{44}(s) & 0 & 0 \\ 0 & 0 & 0 & 0 & C_{55}(s) & 0 \\ 0 & 0 & 0 & 0 & 0 & C_{66}(s) \end{bmatrix} \tag{4}$$

where the functions $C_{11}(s)$, $C_{12}(s)$, $C_{13}(s)$, $C_{22}(s)$, $C_{23}(s)$, $C_{33}(s)$, $C_{44}(s)$, $C_{55}(s)$ and $C_{66}(s)$ are functions of the Young's moduli, Poisson's ratios, and shear moduli via the relations:

$$C_{11}(s) = \frac{E_1(s)\left[1 - \nu_{32}(s)\ \nu_{23}(s)\right]}{\Delta(s)}$$

$$C_{12}(s) = \frac{E_1(s)\left[\nu_{12}(s) + \nu_{32}(s)\ \nu_{13}(s)\right]}{\Delta(s)} \tag{5}$$

$$C_{13}(s) = \frac{E_1(s)\left[\nu_{13}(s) + \nu_{12}(s)\ \nu_{23}(s)\right]}{\Delta(s)}$$

$$C_{22}(s) = \frac{E_2(s)\left[1 - \nu_{13}(s)\ \nu_{31}(s)\right]}{\Delta(s)}$$

* A material for which its mechanical properties are different in three mutually perpendicular directions at a point in the body is called orthotropic.

$$C_{23}(s) = \frac{E_2(s)\left[\nu_{23}(s) + \nu_{13}(s)\,\nu_{21}(s)\right]}{\Delta(s)}$$

$$C_{33}(s) = \frac{E_3(s)\left[1 - \nu_{12}(s)\,\nu_{21}(s)\right]}{\Delta(s)} \qquad (5)$$

$$C_{44}(s) = G_{23}(s)$$

$$C_{55}(s) = G_{13}(s)$$

$$C_{66}(s) = G_{12}(s)$$

where:

$$\Delta(s) = 1 - 2\nu_{12}(s)\nu_{23}(s)\nu_{31}(s) - \nu_{13}(s)\nu_{31}(s) - \nu_{12}(s)\nu_{21}(s) - \nu_{23}(s)\nu_{32}(s)$$

(c) Transversely* Isotropic Materials (Orthotropic sheets).

In this case, the matrix (4) reduces to

$$C_{ij}(s) = \begin{bmatrix} C_{11}(s) & C_{12}(s) & C_{13}(s) & 0 & 0 & 0 \\ C_{12}(s) & C_{11}(s) & C_{13}(s) & 0 & 0 & 0 \\ C_{13}(s) & C_{13}(s) & C_{33}(s) & 0 & 0 & 0 \\ 0 & 0 & 0 & C_{44}(s) & 0 & 0 \\ 0 & 0 & 0 & 0 & C_{44}(s) & 0 \\ 0 & 0 & 0 & 0 & 0 & \frac{C_{11}(s)-C_{12}(s)}{2} \end{bmatrix} \qquad (6)$$

where the five unknowns $C_{11}(s)$, $C_{12}(s)$, $C_{13}(s)$, $C_{33}(s)$ and $C_{44}(s)$ are functions of the Young's moduli $E_1(s)$, $E_3(s)$, the Poisson's ratios $\nu_{12}(s)$, $\nu_{13}(s)$, and the shear modulus $G_{13}(s)$ via the relations:

---

* A material for which at every point there is one plane in which the mechanical properties are the same is called transversely isotropic (i.e., Properties are the same in 1 and 2 directions).

$$C_{11}(s) = \frac{1 - \nu_{13}(s)\nu_{31}(s)}{E_3(s)A(s)}$$

$$C_{12}(s) = \frac{\nu_{12}(s) + \nu_{13}(s)\,\nu_{31}(s)}{E_3(s)A(s)}$$

$$C_{13}(s) = \frac{\nu_{13}(s) + \nu_{12}(s)\,\nu_{13}(s)}{E_3(s)A(s)} \qquad (7)$$

$$C_{33}(s) = \frac{1 - \nu_{12}^2(s)}{E_3(s)A(s)}$$

$$C_{44}(s) = G_{13}(s)$$

where:

$$A(s) = \frac{1 - \nu_{12}^2(s) - 2\left[\nu_{13}(s)\nu_{31}(s) + \nu_{12}(s)\nu_{13}(s)\nu_{31}(s)\right]}{E_1(s)E_3(s)}$$

(d) Isotropic Materials*. For this case, the $C_{ij}(s)$ matrix reduces to:

$$C_{ij}(s) = \begin{bmatrix} C_{11}(s) & C_{12}(s) & C_{12}(s) & 0 & 0 & 0 \\ C_{12}(s) & C_{11}(s) & C_{12}(s) & 0 & 0 & 0 \\ C_{12}(s) & C_{12}(s) & C_{11}(s) & 0 & 0 & 0 \\ 0 & 0 & 0 & \frac{C_{11}(s)-C_{12}(s)}{2} & 0 & 0 \\ 0 & 0 & 0 & 0 & \frac{C_{11}(s)-C_{12}(s)}{2} & 0 \\ 0 & 0 & 0 & 0 & 0 & \frac{C_{11}(s)-C_{12}(s)}{2} \end{bmatrix} \qquad (8)$$

* A material for which its mechanical properties are the same in every direction at a point in a body is isotropic.

In this case, there are only two unknowns: $C_{11}(s)$ and $C_{12}(s)$ which depend only on $E(s)$ and $\nu(s)$ via the relations:

$$C_{11}(s) = \frac{E(s)}{1 - \nu^2(s)}$$

$$C_{12}(s) = \frac{E(s)\nu(s)}{1 - \nu^2(s)} \qquad (9)$$

The Young's moduli, the Poisson's ratios and the shear moduli must be determined experimentally. However, since such tasks involve considerable technical difficulties, only experiments associated with the determination of Young's moduli have been performed, and some ideas for the determination of the Poisson's ratios and the shear moduli are discussed in Appendix A and will be the subject of future research.

3) Material Properties

We think that the following effects are operative in affecting the mechanical properties of the disc material:

(1) The Relaxation of the Macromolecules (Ref. 32). In a polymer, each molecule occupies an average volume considerably larger than atomic dimensions. It changes shape continuously because of the possiblities of motions (due to thermal energy) around its atomic bonds. To characterize its various configurations it is necessary to consider: Global (long-range) contour relationships, somewhat more local (shorter range) relationships, and so one, eventually including the orientation of bonds, in the polymeric chain, with respect to each other on an atomic scale. Rearrangements on the atomic scale are relatively rapid. On the

other hand, rearrangements can be very slow on the long-range scale.

Under stress, new configurations of the polymer molecules are obtained. The response of the polymer to such excitation is very fast on the local scale. This response is characterized or represented) by the "short time" or glassy behavior. On a larger-range scale the response is slower and is represented by the transition region. For the very long-range scale this response is very slow, and it is represented by the rubbery plateau.

The curve in Figure 3.15 is known as relaxation curve and it shows the mechanical behavior for an amorphous (single phase) rubber-like material.

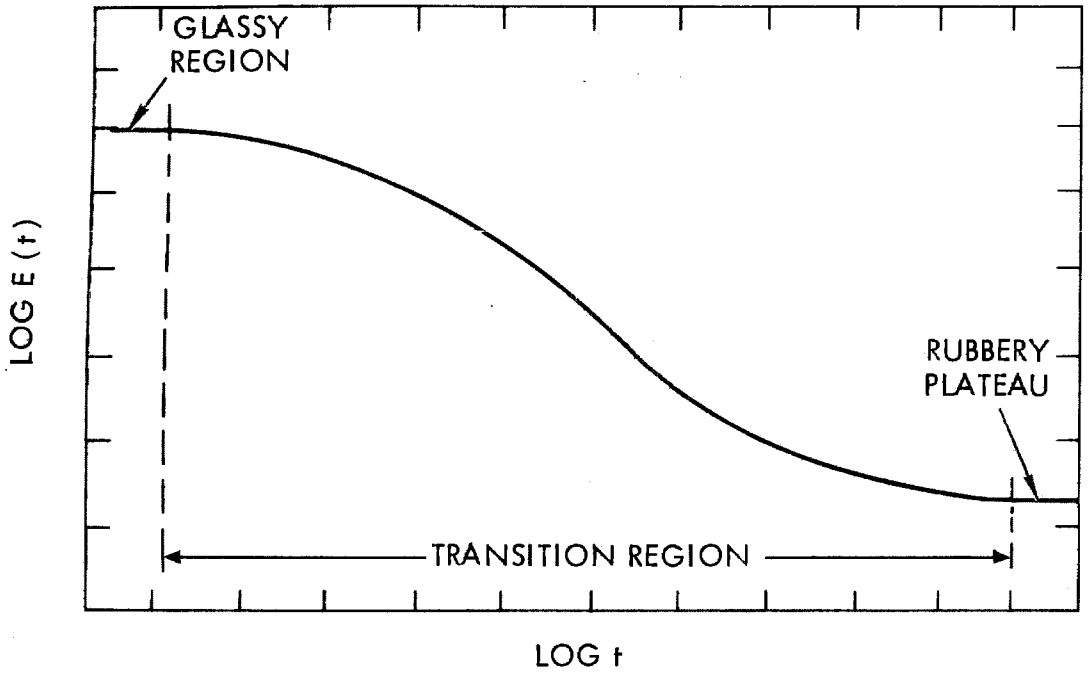

Figure 3.15. Single Phase System Relaxation Curve

However, the disc lamellae can be considered as a two phase material. The first phase is associated with the mucopolysaccharides and the second one with the collagen. For such a material the relaxation

modulus curve may have two (or more) transition regions. The presence of more than two transition regions, if they exist, is probably due to entanglements, change of crystaline structure, etc. A two phase relaxation curve may look like the one given in Figure 3.16

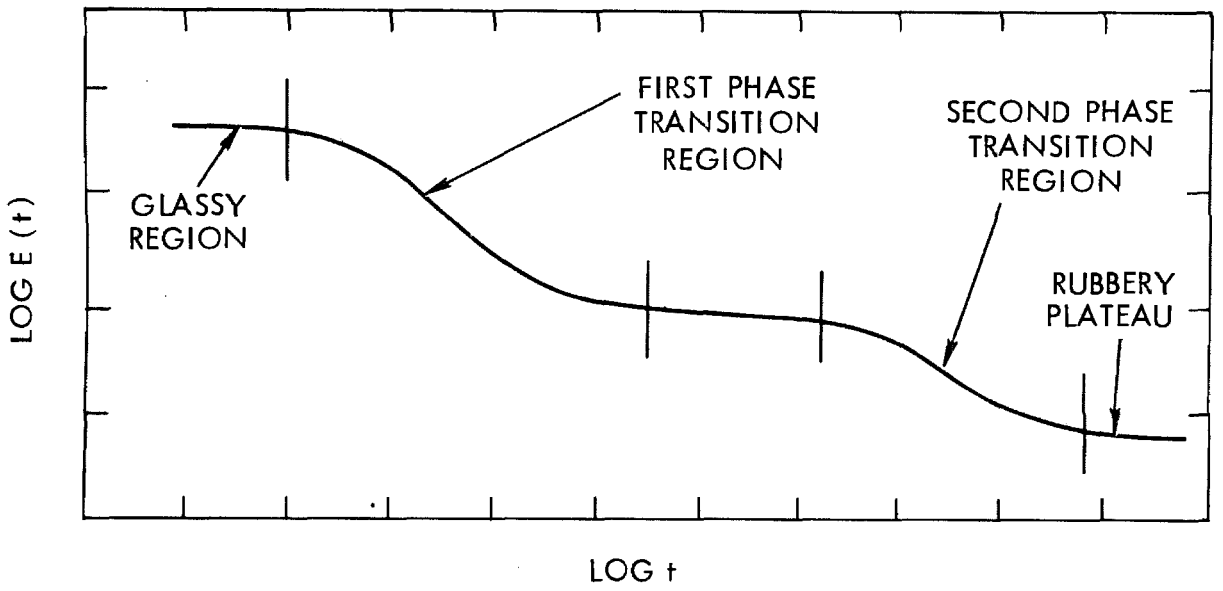

Figure 3.16 Two Phase System Relaxation Curve

(2) Relaxation of Swollen Polymers. For the present purpose let us consider only closed* swollen systems. Ferry explains such molecular behavior as follows (Ref. 32):

"When a polymer is diluted with a solvent of low molecular weight with which it forms a true solution in the sense that the solvent is molecularly dispersed, the local friction coefficient is sharply reduced. Each polymeric chain unit has in its vicinity diluent molecules as well as other polymeric segments, and the former can be displaced in translatory motion much more easily,

---

*A system is considered to be closed if there is no net flow of its constituent phases across the system boundary.

thus lowering the effective local viscosity. The resulting reduction in all relaxation times is the most striking effect on viscoelastic properties."

This effect is visible as a horizontal shift in the (log) time axis of the relaxation modulus, and it is shown in Figure 3.17 for an amorphous rubberlike material. In other words, if the water concentration increases, the relaxation process speeds up, the speed-up being given by the factor a_c that multiplies the time.

From experiments performed in the same time range window but varying the solvent composition one obtains a family of curves as shown in Figure 3.17.

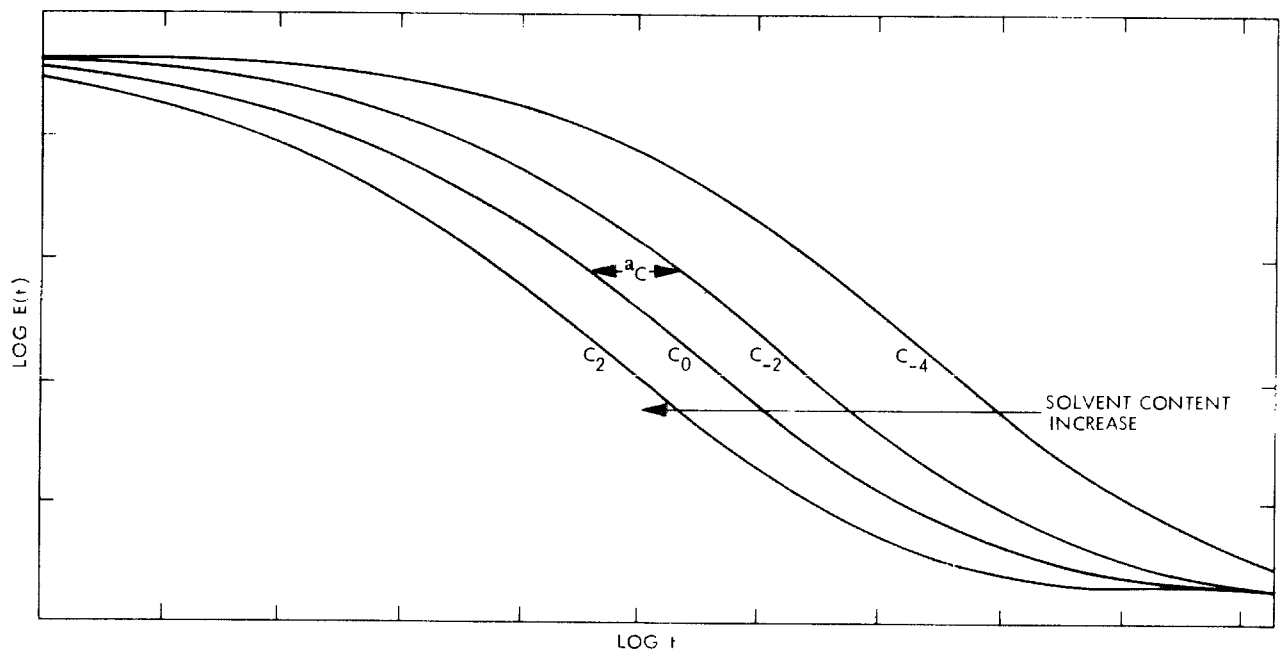

Figure 3.17. Effect of Solvent in the Relaxation Modulus (Schematic Representation)

By shifting* horizontally and vertically one obtains the curve shown in Figure 3.18, known as the master relaxation curve (Refs. 28 and 31).

* Similarly as obtained through the use of time-temperature shifts.

where:

t = the time,

E(t) = the relaxation modulus,

C = the concentration, (C_0,C_2,C_{-2}, C_i represent concentrations of solvent, constant during any test)

a_c = the horizontal shift factor (shift along the time axis)

There is also a vertical shift factor (along the modulus axis) which is due to the volumetric changes in the specimen.

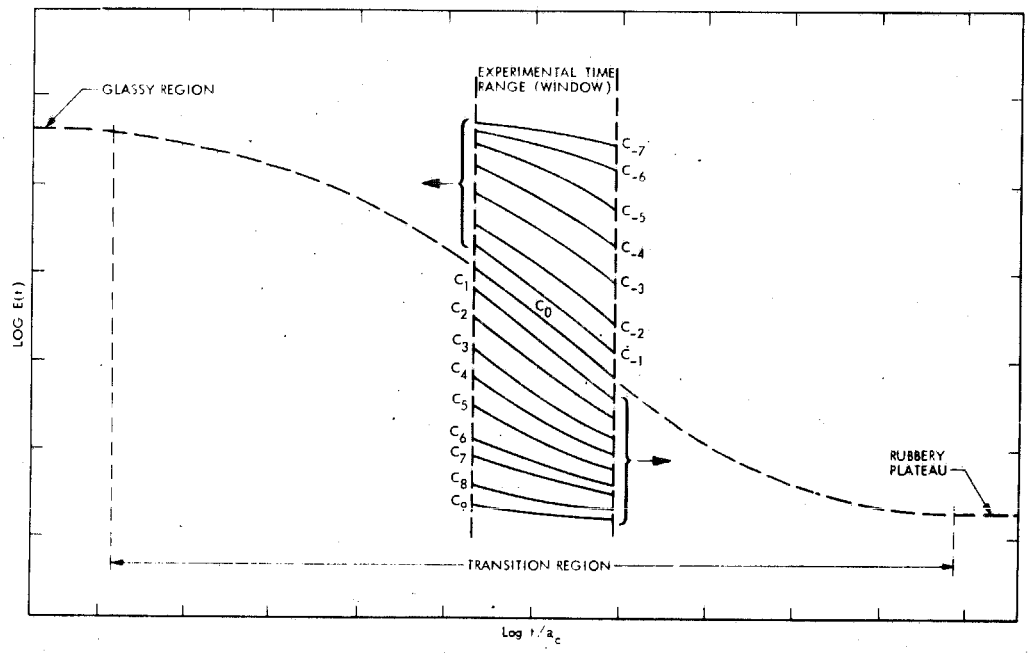

Figure 3.18. Master Relaxation Curve at C_o Concentration

For the case of a two phase system the relaxation behavior is altered by the presence of a swelling agent as follows:

(a) Non-uniform shifting. The transition region portions of the relaxation curve (Figure 3.16) for both phases are shifted to shorter times when the material is swollen by a solvent compatible with the two phases. However, if this shifting is not uniform, the shape of the relaxation curve will depend

on the concentration of the swelling agent. In this case the procedure for the construction of the master relaxation curve for an amorphous rubber-like material will not be applicable. Therefore, a different procedure should be utilized. Such a procedure is in general a combination of short, intermediate, and long-term experiments.

For example: A wave propagation experiment will correspond to short time ($\sim 10^{-8}$ min to $\sim 10^{-5}$ min), a dynamic testing (forced-sinusoidal excitation) will cover the intermediate region ($\sim 10^{-6}$ min to $\sim 10^{-1}$ min) and a relaxation will cover the long time ($\sim 10^{-2}$ min to $\sim 10^{3}$ min).

(b) Uniform shifting. In this case we consider two types of behavior. The first one corresponds to a true uniform shifting (the shape of the relaxation modulus curve does not depend on the concentration of the swelling agent although its horizontal and vertical shifting does). The second type corresponds to a special non-uniform shifting with the two transition regions widely separated. If this is the type of behavior, in practice, only one transition region is important within the time domain we are interested in. In this case the effect of the other transition is negligible. This implies that the shifting can be

considered as uniform. For these two cases the procedure already discussed for amorphous rubberlike material is applicable. We think that uniform shifting is possible for the disc specimens as it is shown earlier. Furthermore, in a two-phase system we must consider volumetric effects such as the changes in volume due to the swelling of the collagen fibers and the muco-polysaccharides matrix. These changes, which in the case of amorphous rubberlike material produce only a vertical shift (shift along the modulus axis) in the relaxation curve, may also introduce non-linear effects in the material behavior. These effects are due to the presence of stresses in the fibers-matrix interface. However, if the difference in swelling between the two phases is not large enough we may expect that the two phase system will behave like the one phase system.

(3) Transients Caused by the Diffusion of the Solvent.

Let us now consider the example of the swelling of a polymer in a solvent. It is assumed that the polymer is a cross-linked material which does not dissolve in the solvent due to the existence of intermolecular bonds, but it can absorb some of the solvent (swelling). Considering such a polymer-solvent interaction the solvent will diffuse into the polymer and equilibrium will be reached after some time. The diffusion process involves the penetration of the small molecules into the solid (which may obey Fick's law of diffusion), and the changes of the material properties induced by the presence of the solvent as was discussed previously.

For the study of the interaction between the mechanical behavior of the disc material and the diffusion of water, three cases will be discussed. For these cases the disc specimen will be considered as:

Case 1: A closed system for all time (i.e., the specimen is properly coated with silicon grease or other inert materials).

Case 2: An open system (i.e., the specimen without coating) in water or saline solution environment which permits swelling.

Case 3: An open system in an environment at low humidity (room environment) which dries the specimen.

Figure 3.19 represents the expected responses for cases 1, 2 and 3, due to a step of strain excitation for the same specimen.

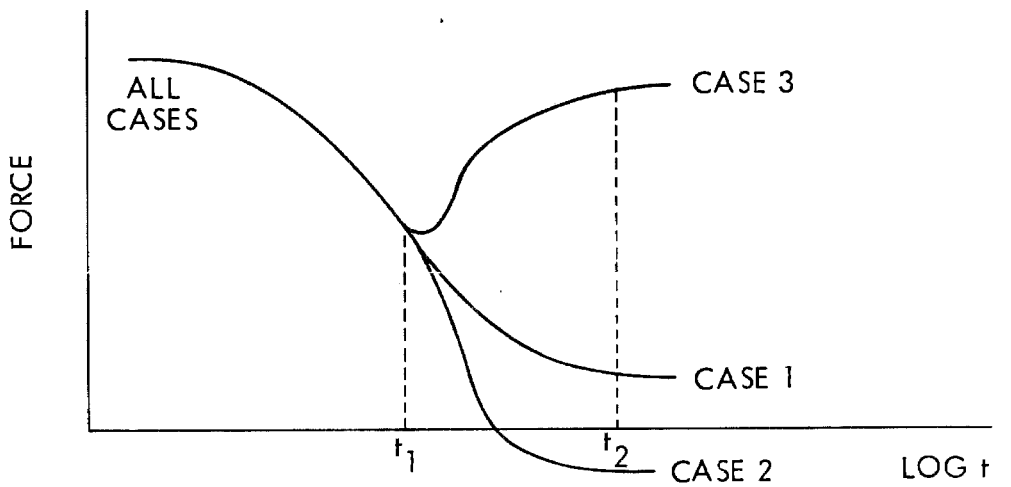

Figure 3.19 Times for Equilibrium Diffusion and Diffusion-Relaxation Interaction to a Step of Strain Excitation

We define t_1 as the time for which we begin to detect deviation from case 1, caused by diffusion, in the relaxation behavior of the specimen, and t_2 as the time for which no further changes with respect to the time are detectable in the relaxation behavior of cases 2 and 3.

The system will be considered closed in all cases for $t < t_1$. For times $t > t_2$ the system is considered to be in equilibrium with its environment and the stresses have been completely relaxed. It must be mentioned here that for a given specimen the determination of the exact values of the times t_1 and t_2 is limited by the sensitivity of the experiment (measurement of forces, elongations, concentrations, temperature, etc.). These times are not material parameters, because they depend on the geometry of the specimen. They depend on: type of materials (lamellae, nucleus), concentration of water in the specimen, concentration of water in the environment, geometric shape, area of the specimen exposed to the environment, cross-sectional area, stresses, strains and temperature. We think that t_1 is related to an interaction of diffusion and relaxation processes.

b. Equilibrium Properties of Polymers Embedded in Solvent

The state of equilibrium is defined as the state in which there will be no change of the mechanical properties with respect to time and no net flow of solvent. Let us now consider the application of a strain (stress) to the swollen polymer. This is equivalent to the introduction of mechanical energy which by the application of thermodynamical principles implies that a new equilibrium state will be reached after some time.

This effect has been reviewed by Treloar for amorphous rubberlike materials (Ref. 33). He found that the equilibrium states are related to the following properties:

(1) The molecular volume (V_1) of the solvent (cc per mol).

(2) The molecular weight (M_c) between crosslinking points for the polymer.

(3) A parameter (μ) which characterizes the interaction between the polymer and the solvent.

(4) The composition of the swollen polymer, volume fraction (U_2).

(5) The applied strain ($\varepsilon = \lambda - 1$, where λ is the stretch* ratio).

(6) The density (ρ).

These parameters are related by the Flory-Huggins equation (Ref. 33):

$$\sigma_\alpha = \frac{RT}{V_1}\left\{\ell n(1 - U_2) + U_2 + \mu U_2^2 + \frac{\rho V_1}{M_c} U_2 \lambda_\alpha^2\right\} \quad (10)$$

where:

R = the universal gas constant

t = the temperature

α = 1, 2, 3 (Principal directions)

This equation represents a particular constitutive equation for polymeric isotropic materials with zero sol-fraction in the presence of solvents. The sol-fraction is the part of the material which is uncrosslinked in the crosslinked material or gel. The sol-fraction will flow out of the gel when the material is placed in solvent (water).

For the case of simple tension we have:

$$\sigma_1 = \sigma, \quad \sigma_2 = \sigma_3 = 0$$

$$\lambda_1 = \lambda, \quad \lambda\lambda_2^2 = \frac{1}{U_2}, \quad \lambda_2 = \lambda_3 \quad (11)$$

and Equation (10) reduces to a set of two equations.

---

* Stretch ratio (λ) is defined to be the ratio of the deformed over the undeformed dimensions.

c. Non-Linear Viscoelastic Behavior

1) Isotropic Nearly Incompressible Polymers

The nucleus pulposus is considered to be an isotropic almost incompressible soft polymer. Therefore, we think the recently developed theory of the "n" (Refs. 34-37) measure of strain can be applied to account for the stress-strain non-linearity. For discussion purposes we will only consider the equilibrium (elastic) simple tension case of this theory. This theory yields for moderately large deformations (up to 100% or more for some materials) in simple tension to the equation

$$\bar{\sigma} = \frac{2G}{n} \left\{ \lambda^n - \lambda^{-\frac{n}{2}} \right\} \qquad (12)$$

where: G is the shear modulus

$\bar{\sigma}$ is the true stress (force over deformed area).

This theory has been extended to account for the viscoelastic behavior for materials for which it is possible to separate time effects from strain non-linear effects. For these materials when they are excited by a particular strain function (that is the step of strain) their response can be factorized into a strain dependent function (strain effect) and a time dependent one (time effect) as it can be seen in Section V-6-b.

2) Anisotropic Polymers

In naturally occurring polymers isotropy is a rarely encountered phenomenon. A large class of them can be characterized as transversely isotropic (material with a principal axis such that at any plane perpendicular to this axis the elastic properties are

identical in all directions). Examples of such materials are human intervertebral disc lamellae, skin, tendons, ligaments, etc., all of which are of a "fibrous" nature. Green and Adkins (Ref. 38) have documented that for the special case of transversely isotropic materials under large deformations the constitutive relations can be expressed in terms of five invariant functions of the deformation gradient (they remain invariant for the special transformation pertinent to the summetry of the material) which are in turn related to the principal stretch ratios λ_1, λ_2, and λ_3. To the best of our knowledge, only two attempts have been made to develop such elastic constitutive equations for such materials (Refs. 39 and 40). The extension of these elastic theories to viscoelastic materials has not been explored sufficiently. However, we know that for some materials the simplistic approach (separation of strain and time effects) that was valid for isotropic materials do not hold for anisotropic behavior. An example of such non-linear viscoelastic constitutive equation is given by Cheung and Hsiao (Ref. 40) for blood vessels.

d. Irreversible Effects

In testing for material behavior it is always probable that the specimen may be permanently damaged either because of strain (stress) induced damage (Refs. 41-45) or bio-chemical changes (oxidation, crosslinking or decomposition of the polymer during the experiments).

Neither effect was studied in the course of this work.

e. Digital Image Processing Techniques

Images, in the form in which they usually occur, are not directly amenable to computer analysis. Since computers work with numerical data, an image must be converted to numerical form before processing. This conversion process is called "digitization," and is done using film digitizers (i.e., DICOMED 57 scanner). The image is divided into small rectangular regions called "pixels." (Figure 3.20). For each pixel an integer number (grey level*) is generated, associated with the degree of brightness of the image at that point. Then the image is represented by a rectangular array of integers (digitized image) with some noise introduced by the film digitizer. Perception of low-contrast features in an image depends upon existing visual characteristics (i.e., sharp edges). When these characteristics do not exist and noise is added to the image, the detection of these low-contrast features becomes impossible. Since film readers can detect film density changes of less than 1%, it is possible to enhance desirable features of the picture.

This enhancement can be done by means of digital image processing (Ref. 5). Actually, linear contrast stretching and filtering techniques are applied for the change of the point by point intensity of the initial digital image and for the removal of noise. Digital image processing starts with an image and produces a modified version of that image. After processing, the final image may be displayed by reversing the process of digitization.

* The grey level of each pixel is used to determine the brightness or darkness of the corresponding point on a display screen.

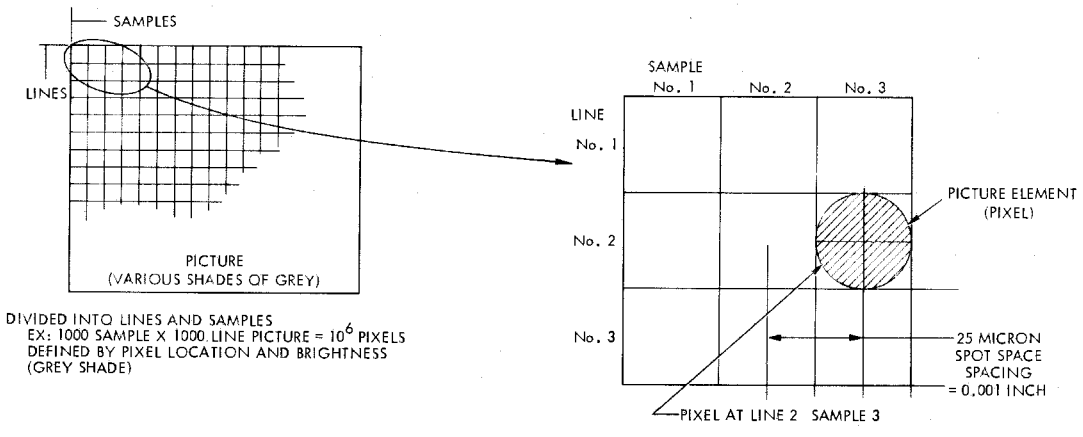

Figure 3.20. Array of Pixels

'Digital image analysis' is taken to mean a process which takes a digital image into something other than a digital image, such as a set of measurement data. For example, if a digital image contains a number of objects, a program might analyze the image and extract measurements of the objects. This would take the original digital image into a set of object measurements and would be an application of digital image analysis. The term digital image processing, however, is loosely used to cover both processing and analysis.

6. Biomechanical Review

a. On Material Properties.

First, we present a review of the literature on the experimental work done for the determination of the mechanical properties of the human intervertebral disc material. Compression experiments have been carried out by Virgin (Ref. 11) using as a specimen the entire disc with thin slices of bone at each of its ends. The specimen was kept in Ringer's solution* before and during testing and at room temperature.

The main finding of Virgin's work was that the disc possesses a nonlinear viscoelastic behavior with significant energy dissipation depending on the age of the subject (Figure 3.21).

Brown, Hansen and Yorra applied axial compression to the entire disc with large portions of the vertebral bodies at both ends (Ref. 46). They also perform tensile tests using discs which were cut into block samples as shown in Figure 3.22, excluding samples corresponding to the nucleus pulposus. Their experiments were performed under uncontrolled humidity and temperature (room conditions).

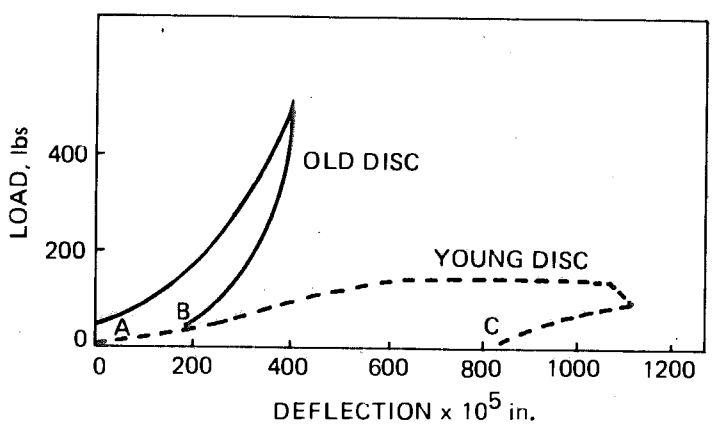

Figure 3.21 Effect of Loading to 500 lb and Unloading. (After Virgin)

* 0.9 gr of NaCl, 0.04 KCL, 0.025 gr $CaCl_2$, 0.02 gr $NaHCO_3$, in 100 ml solution

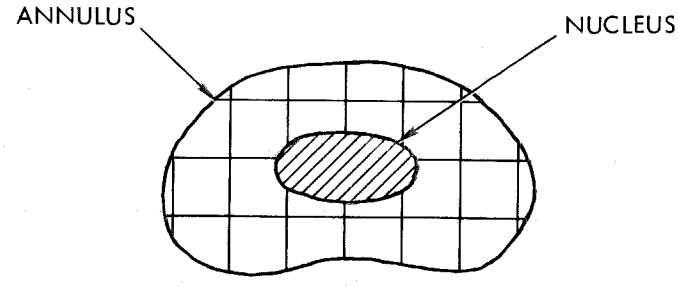

Figure 3.22. Sampled Intervertebral Disc.

They demonstrated a strong nonlinear stress-strain behavior of the disc material in both tension and compression. Similar results were reported by Yamada (Ref. 47) and are shown in Figures 3.23 and 3.24.

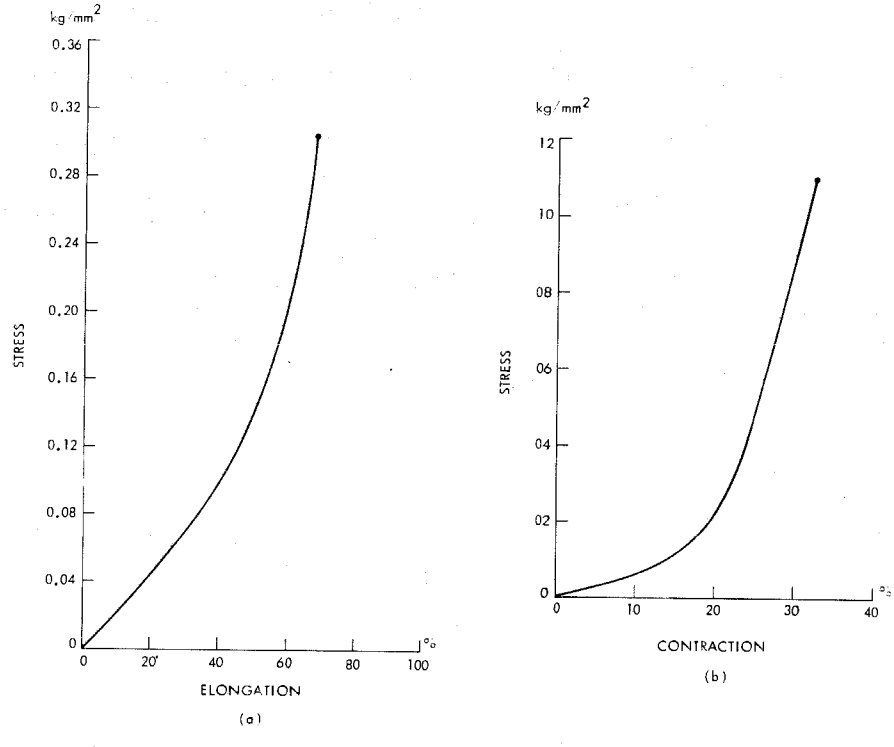

Figure 3.23 Stress-Strain Curves of Fresh Human Intervertebral Disc (a) In Tension, (b) In Compression (After Yamada)

Similar but more refined measurements were performed by Galante (Ref. 10) who measured the tensile properties of thick sections of the annulus fibrosus. His main assumption was that the water loss from the specimen influences the mechanical response of the material.

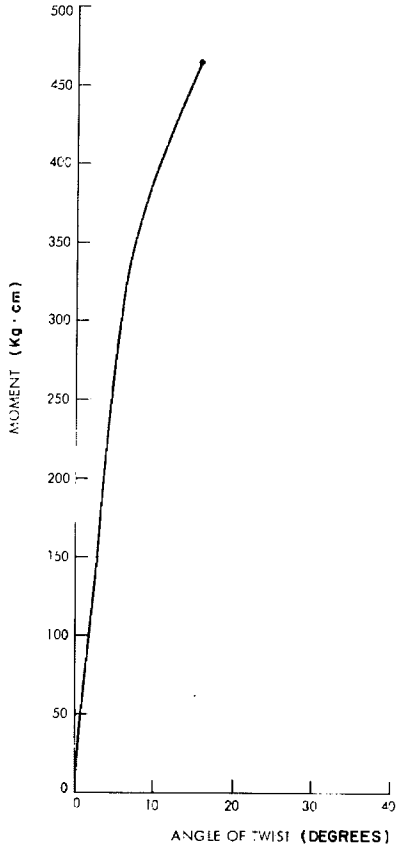

Figure 3.24. Moment-Angle of Twist Curves of Wet Human Intervertebral Disc (After Yamada)

In his effort to minimize the water loss to the environment during the experiment, he immersed small samples from the annulus into various solutions (distilled water, 0.9% sodium chloride, human plasma, and 10% dextran) until equilibrium was reached. He found that these solutions produced significant swelling, therefore altering the tensile properties of the disc specimen. Furthermore, he exposed the specimen to air at different relative humidities and temperatures (maximum 90% relative humidity at 25°C temperature and 80% at 37°C temperature). He found that water loss occurred in every humidity and temperature condition that he employed. However, the diffusion process was rather slow so that short time duration

(one minute) mechanical experiments could be performed by considering the water content of the specimen almost constant for this time interval. He also concluded that at a 100% relative humidity the rate of water loss was very small. Therefore, longer duration relaxation experiments could be performed.

Galante's measurements show that the mechanical properties (stiffness and energy dissipation) depend on the direction and position of the specimen in the annulus. He also confirmed the nonlinear viscoelastic behavior of the annulus fibrosus.

Kazarian (Ref. 12) studied the creep behavior of whole discs including the end plates and showed that the viscoelastic response depends not only on the position of the disc (lumbar, thoracic) but also on its degree of degeneration.

Wu and Yao (Ref. 48) have performed short duration (10 min) tensile experiments using an INSTRON tester at room environmental conditions (65% relative humidity and 24°C temperature). Their specimens were dog-bone shaped of 2 mm thickness (several lamellae thick).

The analysis was based on Spencer's (Ref. 49) composite theory for incompressible materials that contain identical fibers running in alternate angles. This theory yields a constitutive equation which seems to fit the nonlinear stress-strain data over the range of $1 \leq \lambda_1 \leq 1.35$, ($\lambda_1$ = uniaxial stretch ratio). Wu and Yao (Ref. 48) recognize the problem associated with the definition of a reference state (state at which the specimen begins to transmit load) and explain it in terms of a gradual transition

from the stage of pure fiber straightening motion to the stage of fiber elongation, as the specimen deforms. The same problem was already recognized by Fung (Ref. 50) for other biological tissues. Kulak et al (Ref. 51) also proposed an elastic constitutive equation and fit it successfully to Galante's (Ref. 10) nonlinear stress-strain data.

In conclusion, this review reveals that the disc material is:

(1) Nonlinearly viscoelastic (at sufficiently large strains)
(2) Sensitive to its environment (properties depend on water content)
(3) Anisotropic and inhomogeneous

However, the linear viscoelastic properties of the disc's material are known only for a narrow experimental time window. This is mainly due to limitations imposed by the influence of the environment. In the present work we overcome this limitation and therefore obtain the viscoelastic properties in a large experimental time window which will cover times from 10 min to 10 min.* This covers the study of time ranges** important for short duration effects (shocks, accidents) as well as for long-time ones such as sitting, slipping, etc.

---

* Short duration effects, such as shocks, occur in the time intervals of 1 m sec (10^{-5} min). In order to predict viscoelastic responses at such times, properties corresponding to shorter times are involved as required by the Boltzmann superposition principle.

** This range is probably a bit wider than needed for actual human body response. However, in this initial study it was easy to extend the time range. We should continue to work in this range until we are certain of the actual time range at which the human body operates.

For the case of larger deformations (nonlinear viscoelastic behavior) the existing experimental data do not separate time and strain (stress) effects. Therefore, the equilibrium constitutive equations developed have not been adequately tested.

b. On the Modeling of the Disc.

Analytical, experimental and numerical treatments of the human intervertebral disc have been carried out by various investigators. As a consequence, a number of disc models have been developed. They start with the simplest barrel-type model of the disc and end up with the more sophisticated ones based on finite element methods (Refs. 3 and 52-56). All of them are based on in-vitro studies and can give some idea of the stress distribution in the disc as the disc is subjected to various modes of deformation. In the structural analyses performed to date, via finite element methods, the material behavior has always been assumed to be elastic, implying that the stress relaxation of the material can be neglected. In these analyses, the nucleus pulposus is considered to be imcompressible and in a hydrostatic state of stress. However, the material of the nucleus is not a fluid but a solid of low modulus and its contribution to the stress bearing capability is appreciable in viscoelastic studies. In addition, Nachemson has provided an in-vivo estimate of the pressure in the nucleus pulposus of the disc as a function of the human body position.

IV. NON-INVASIVE DIAGNOSTIC TECHNIQUES

1. Introduction

The intervertebral disc and the disc herniation problem have been discussed in Section III. Coming out of the back side of each disc level are the nerves which carry pain and regulate muscles. As it was pointed out, a lumbar disc problem often causes nerve root pressure which may result in pain and muscle spasms. A schematic representation of this problem is shown in Figure 4.1 by the shaded portion. In cases of severe pain, the part of the shaded portion of the disc that may cause this pressure must be removed surgically.

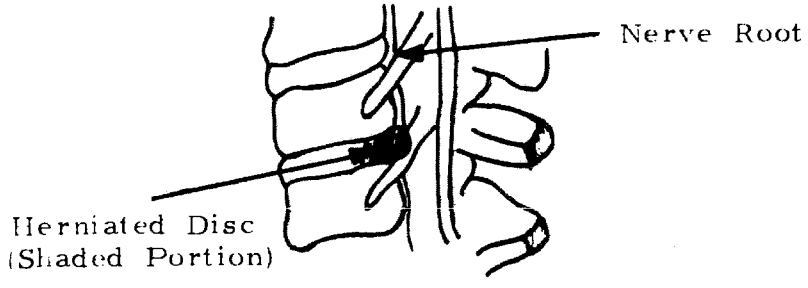

Figure 4.1. Herniated Disc

Obviously, the determination of the exact shape of the disc and more specifically of its posterior edge (shaded portion) is very important for diagnostic purposes prior to surgery. Since the only effective diagnostic techniques used today are invasive, (Section III-4), a new non-invasive approach based on computer image processing of conventional spine radiograms is investigated. We report here the results obtained from the application of this technique.

2. Problem Statement

The problem was given a radiographic film (lateral view) of the lumbosacral spine taken without injection of contrast material to determine the edges of the anterior and posterior portion of the intervertebral disc using computer image processing techniques.

3. Approach

In this study selected radiograms of the lumbosacral spine (lateral views), taken without injection of contrast materials, were used. These radiograms are available in a form which is not directly suitable for computer processing. Since computers work with numerical data, the radiogram must be converted into numerical form before processing. The conversion process, known as "digitization," was done using JPL's DICOMED D57 film digitizer. Presently, the digitizer can handle only an image area of 50 x 50 mm . Since the disc, including small portions of the vertebral bodies, is larger than this area, only the anterior (A) and posterior (P) portions have been digitized (Figure 4.4). This process actually takes the initial radiogram into a digitized image with some noise introduced by the film digitizer. Perception of low-contrast features in an image depends upon existing visual characteristics (i.e., sharp edges). When these characteristics do not exist and noise is added to the image, the detection of these low-contrast features becomes very difficult. Since film readers can detect film density changes of less than 1%, it is possible to enhance features by rescaling the digital form of the picture. Figure 4.2

is an example of the gray level distribution (histogram*) of the anterior and posterior portions of a disc image, respectively.

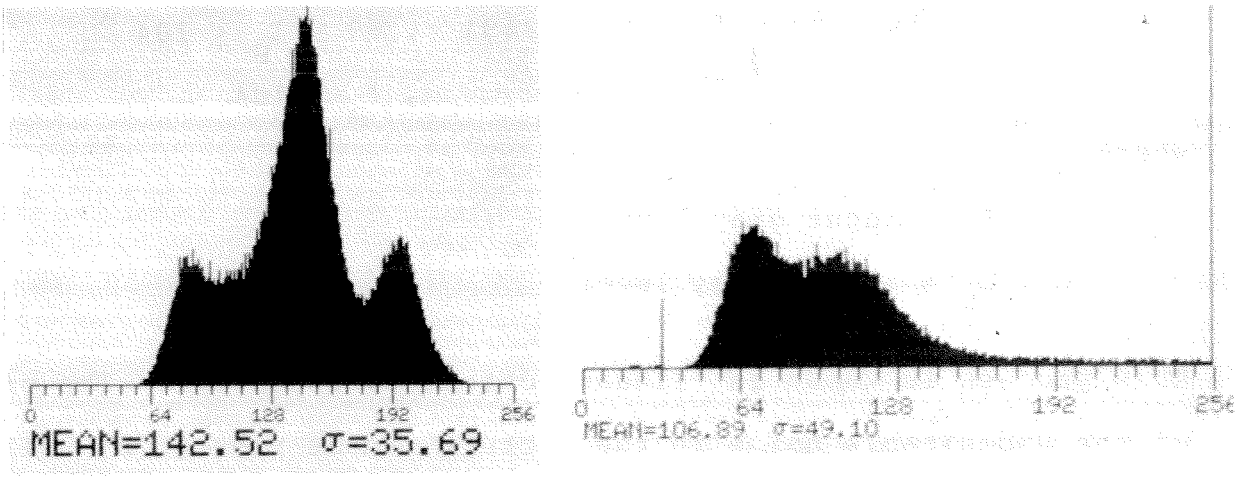

(a) (b)

Figure 4.2. Histograms of (a) Anterior and (b) Posterior Portions of the Disc

From these histograms, one can see that the information associated with the anterior portion (A) of the disc is between gray levels 72 and 176 and for the posterior portion (P) between gray levels 69 and 104. Changing the point by point intensity of the digitized radiograms we achieve an improved version of the initial picture. This was done by generating the following linear transfer functions (Ref. 5).

For anterior (subscript 'A' denotes anterior)

$$O_A = \begin{cases} 0 & , \quad I_A < 72 \\ 2.55\,(I_A - 72) & , \quad 72 \leq I_A \leq 176 \\ 255 & , \quad I_A > 176 \end{cases} \qquad (1)$$

* "Histogram" is the summary of the gray level distribution of an image.

For posterior (subscript 'p' denotes posterior)

$$O_p = \begin{cases} 0 & , I_p < 69 \\ 2.55\ (I_p - 69) & , 69 \leq I_p \leq 104 \\ 255 & , I_p > 104 \end{cases} \qquad (2)$$

where:

I_A, I_p = input gray level

O_A, O_p = output gray level

This process is known as "linear contrast stretching." The effect of the undesirable noise in the picture can be reduced by "filtering" processes. VICAR's program FILTER (Ref. 5) performs two-dimensional convolution filtering. It convolves the given digital image with a properly chosen digital function known as the "matrix of weights" (Refs. 6 and 57):

$$O(i,j) = \sum_m \sum_n I(m,n) W(i-m,j-n) \qquad (3)$$

where:

$I(m,n)$ = digitized input image point

$O(i,j)$ = digitized output image point

$W(i-m,j-n)$ = matrix of weights

The size of the matrix of weights must be chosen large enough to remove the noise but not so large as to remove the image of the disc.

In this application, due to the existence of noise which makes low contrast features difficult to see, N x N equal weight

low-pass and Gaussian* filters were used. Furthermore, for edge enhancement, convolution with a positive peak and negative side lobes function was used.

The determination of the edge points was done using the maximum slope of the density curve approach discussed in Reference 58. In the plot for the smoothed density profile along a single line across the image (Figure 4.3) there exists a point such that the slope of the desnity curve becomes a maximum. This point is defined as the "edge point" for this line. This process was repeated for all the lines in the image. The set of the edge points so determined constitute the edge of the disc.

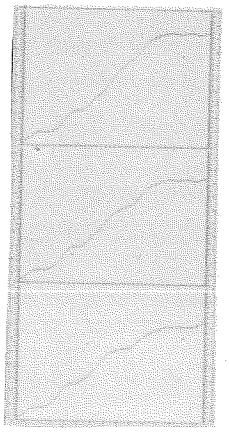

Figure 4.3. Smoothed Density Profiles for Various Lines Across the Filtered Disc Image

---

* A filter that follows Gaussian (or normal) distribution.

4. Examples of Digital Image Processing Techniques to Conventional Radiographic Data

- Example 1

Let us consider the radiogram shown in Figure 4.4. Our objective is to enhance the posterior (P) and anterior (A) sections of the disc.

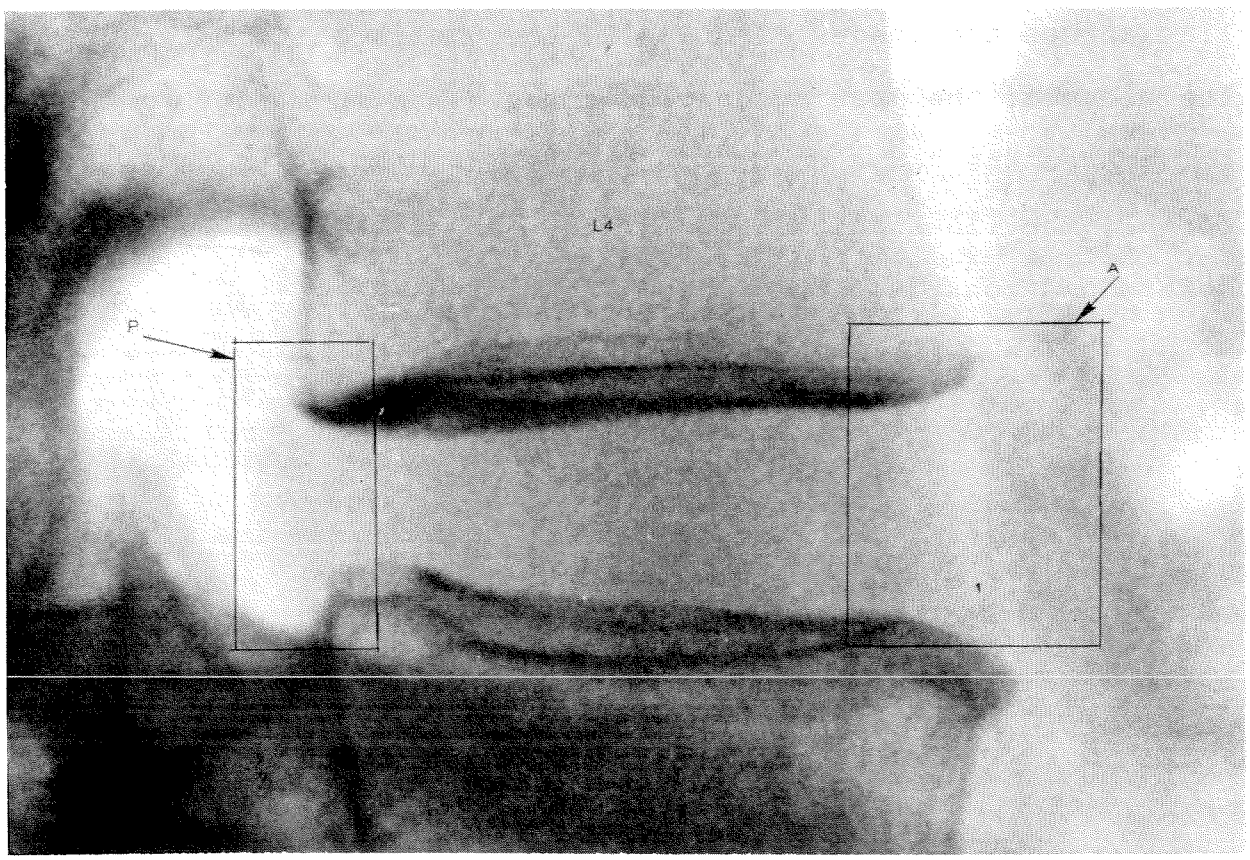

Figure 4.4. Selected Unprocessed Radiogram of the L4-L5 Disc

The photometric information recorded on the radiographic film transparency was converted to digital form suitable for computer processing.

Only the anterior (A) and posterior (P) portions shown in Figure 4.4 have been digitized in this application.

Figures 4.5(a) and 4.5(b) show the digitized pictures of the anterior and posterior portions of the intervertebral disc.

In these pictures one cam see that in the digital version of the initial radiogram there is a substantial amount of X-ray absorption present at the site of the disc with some noise present.

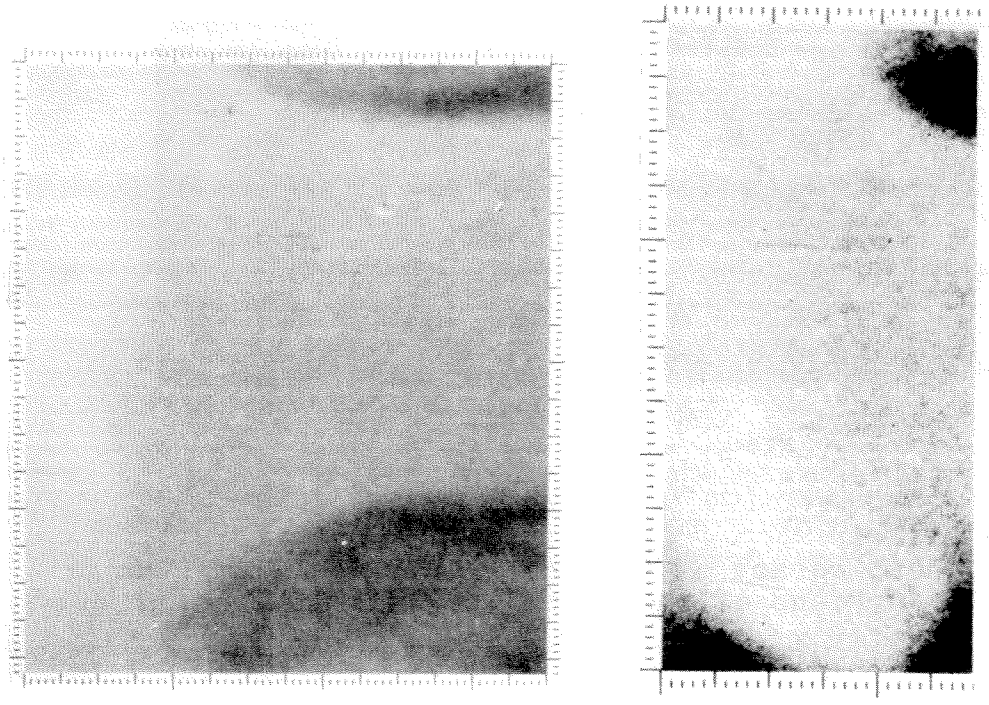

(a) (b)

Figure 4.5. Unprocessed Radiograms of (a) Anterior, and (b) Posterior Portions of the Disc

a. Image Contrast Stretching.

Contrast stretching of the digitized pictures provides an interesting improvement in picture usefulness. The results are shown in Figures 4.6(a) and 4.6(b).

These pictures clearly show the existence of the anterior and posterior edges of the disc.

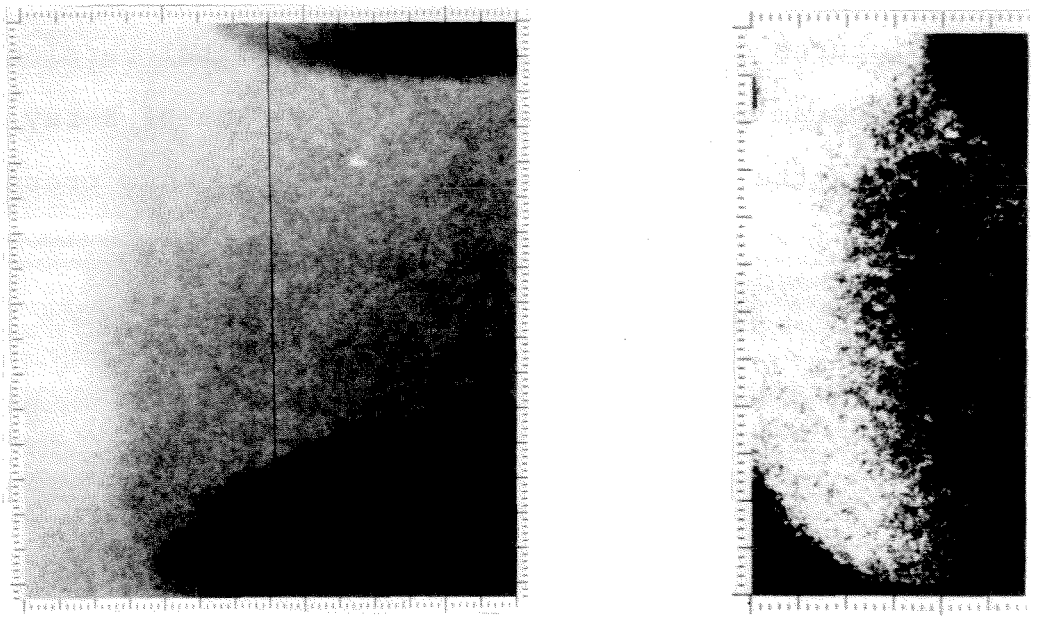

(a) (b)

Figure 4.6. Radiograms of (a) Anterior, and (b) Posterior Portions of the Disc After Linear Stretching

b. Image Filtering.

For the filtering of the anterior portion of the disc (Figure 4.6(a), the matrix of weights selected was a 15 x 15 array of equal weights. The size was chosen large enough to remove the noise but not so large as to remove the image of the disc. The resulting filtered picture* is shown in Figure 4.7.

For the filtering of the posterior portion of the disc, the image on Figure 4.6(b) was convolved with an 11 x 11 matrix of equal weights resulting in Figure 4.8.

* Only the portion between the vertical lines in Figure 4.6(a) was filtered (left side).

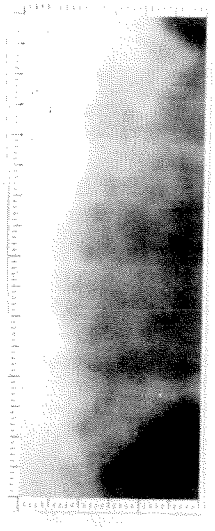

Figure 4.7. Anterior Portion of the Disc After 15 x 15 Equal Weight Low-Pass Filter

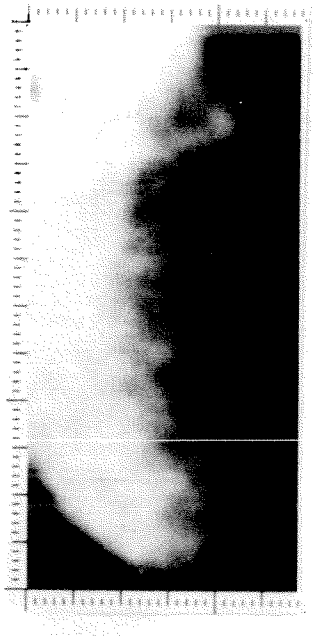

Figure 4.8. Posterior Portion of the Disc After 11 x 11 Equal Weight Low-Pass Filter

The edge of the anterior portion of the disc is shown in Figure 4.9. Observe that in the top left portion of the image, the detected edge is the edge of the thickening portion of the anterior longitudinal ligament.

Figure 4.10 shows the edge of the posterior portion of the disc.

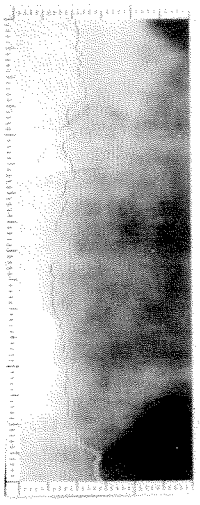

Figure 4.9. Anterior Edge of the Disc

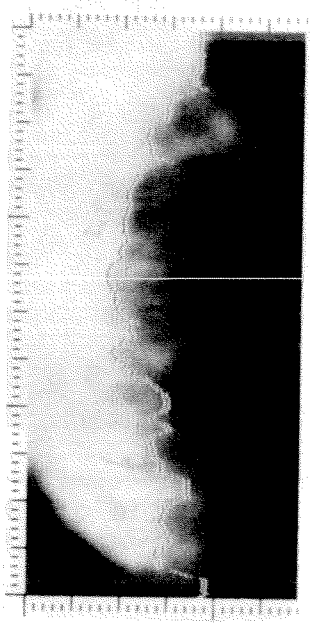

Figure 4.10. Posterior Edge of the Disc

c. Gaussian and Special Feature.

Figure 4.11 shows the results of the application of a Gaussian filter.

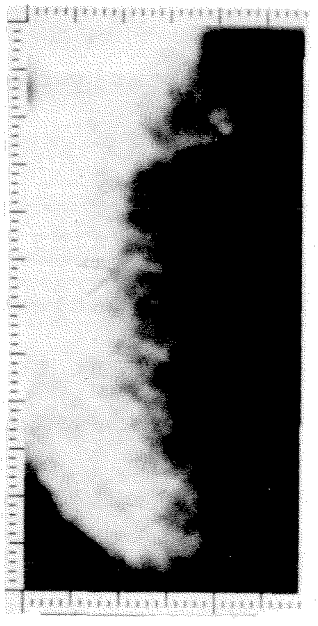

Figure 4.11. Posterior Portion of the Disc After Application of 11 x 11 Gaussian Filter

Figure 4.12 shows the effect of reducing the size of the picture by one-half and subsequently applying a special feature (edge enhancement) filter.

Figure 4.12. The Poster Edge After Application of Special Feature Filter

The effect of computer image processing is clearly demonstrated by comparing the enhanced pictures (Figures 4.9, 4.10, 4.11 and 4.12) with the unenhanced original radiogram (Figure 4.4).

In a second example, the potential of utilizing digital image processing techniques to improve the diagnostic quality of raw radiographic data is even more clearly demonstrated.

- Example 2

In this case, due to difficulties encountered in obtaining radiographic data from cadavers or patients, it was decided to use a phantom disc which is equivalent to a human intervertebral disc as far as absorption features are concerned. The phantom disc was constructed based on the estimated absorption characteristics of real L4-L5 discs obtained from conventional radiograms via densitometric studies. Figure 4.13 shows the original radiogram of this phantom and Figure 4.14 shows the processed one. The result was encouraging since the disc material, which was almost invisible in the original data, is now clearly shown after the enhancement took place.

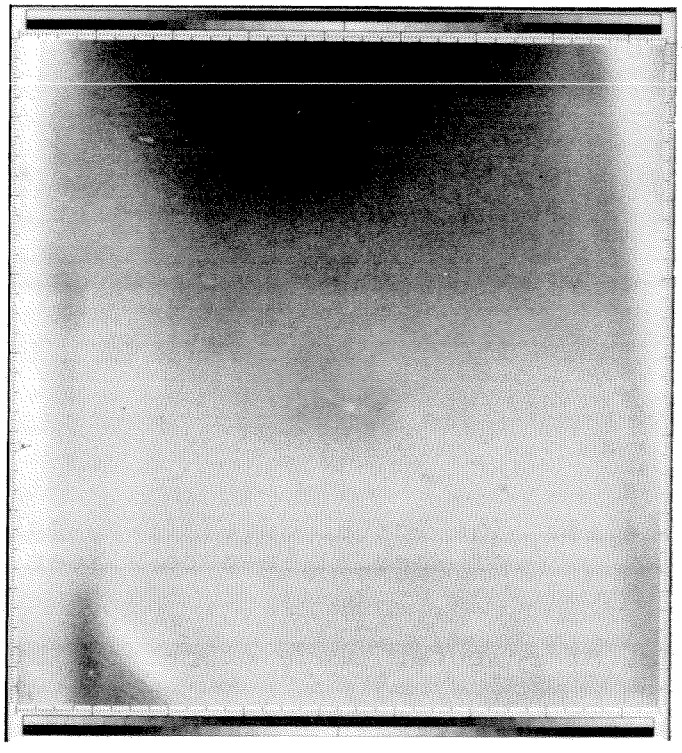

Figure 4.13. The Original Radiogram of the Phantom Disc

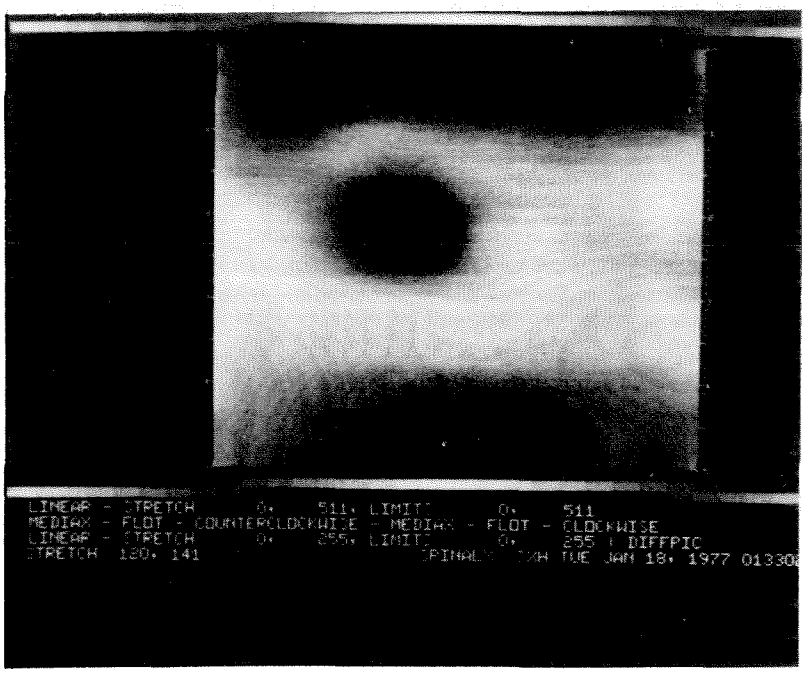

Figure 4.14. The Enhanced Version of the Original Radiogram

5. Conclusions and Discussion

This study shows that the diagnostic quality of the unprocessed radiogram of the spine can be improved significantly by using digital image processing techniques. This is clearly demonstrated here by the visualization of the disc and the detection of its anterior and posterior edges in two cases. However, while the results of this study have been interesting and encouraging, there is no question that much work needs to be done until such methods will be clinically available.

At this point, it may be of interest to enumerate the problems associated with digital image processing of X-ray films.

(1) Obtain spine radiograms by means of optimum exposure.

(2) Minimize image losses from film scanning by using better scanners.

(3) Decrease processing time (time required to take an X-ray film, scan it, process it in the computer and reconstruct the computer output into a photograph) by having a computer tied directly to the scanner and having instant display of the pictures stored in memory.

We think that these problems are not difficult to overcome and that the clinical application of image processing techniques may be the hope for a non-invasive solution to the diagnosis of low back problems.

V. WATER EFFECTS ON THE VISCOELASTIC PROPERTIES OF THE HUMAN INTERVERTEBRAL DISC

1. Introduction

From the simple observation that a dry disc is similar to a hard piece of plastic or leather, and that a wet one is soft as a rubber, we had initially suspected that the water content in the disc affects its mechanical properties. Based on this observation we studied the viscoelastic material properties of disc specimens as a function of their water content, as well as their diffusion and equilibrium swelling characteristics by immersing them into saline solutions of various concentrations. These properties, together with realistic environmental and loading conditions, are necessary for the disc's structural analysis. Although the disc's geometry is complicated, existing finite element methods give us a tool to work on this problem, provided that a suitable geometric breakdown of the disc can be established.

It is conceivable that a refined geometric representation of the disc, which accounts for the fibers (number, geometry and direction) embedded in a continuous isotropic matrix, is the most realistic solution. However, at this time we think that such a detailed representation is cumbersome and prohibitively expensive. We, therefore, believe that a more averaged discretization is appropriate. To this end we would consider each lamella to be represented by an orthotropic material layer connected to adjacent lamellae-layers such that their interface experiences common deformations. However, another less detailed geometric approximation of the disc may be necessary, especially for the areas of the disc's

annulus in which lamella separation is difficult or impossible (i.e., posterior section of the disc). That is, for these areas we may consider the annulus to consist of large pieces of orthotropic material. Furthermore, we consider that the nucleus is made of an isotropic, nearly incompressible substance.

We feel that an alternate, less refined geometric breakdown of the disc, such as the annulus (considered as an orthotropic continuum) and the nucleus (considered as an isotropic medium) is unsuitable for our intended work. Nor would we wish to be concerned in the physical modeling of the disc as a single (average) continuum except where it was necessary to refer to test data of other investigators.

If the intervertebral disc was made of a dry crosslinked polymeric material, the only material properties needed for its structural analysis would be its viscoelastic mechanical properties; i.e., $E_{ij}(x,y,z,t)$ and $\nu_{ij}(x,y,z,t)$.

However, due to the fact that the disc material contains water which migrates in and out of the disc, its response to loads and/or deformations may be affected by its water content. Therefore, for a realistic structural analysis, information of how the water flows and interacts with the disc material is needed besides the classical viscoelastic properties; these properties depend also on the water concentration (C) in the disc i.e., $E_{ij}(x,y,z,c,t)$ and $\nu_{ij}(x,y,z,c,t)$.

To the best of our knowledge there is no generalized theory that explains how these interactions can be quantified. However,

there exist some theories which are valuable only for special cases. They are:

1) The Free Volume Theory. This theory has been developed only for a few simple cases such as the case of the effect:

(1) of temperature on the viscoelastic mechanical properties (Ref. 32).

(2) of concentration on the viscoelastic mechanical properties* (Ref. 33).

(3) of concentration on the diffusion properties ignoring mechanical interactions (Ref. 59).

2) The Thermodynamical Theory of Swelling: i.e., Flory-Huggins* Theory (Ref. 33). This theory explains how the stresses and strains, the environment, and the equilibrium concentration of water in an isotropic polymer are related.

Although not directly applicable to the problem at hand, both theories can still provide some valuable physical insight. We feel that the following material properties need to be determined.

(1) The viscoelastic (linear and nonlinear) mechanical properties for disc specimens obtained under closed system conditions as a function of water concentration in the specimens. (Free volume theory)

(2) The diffusion coefficients for water into the disc's specimens without the influence of any external load. (Free volume theory)

(3) The properties needed for the characterization of the equilibrium swelling (thermodynamical theory of swelling).

* This case has been extensively discussed in Section III of this report.

In the following section we discuss in detail our work on the viscoelastic mechanical properties. For the cases of diffusion and equilibrium swelling we present only preliminary studies that are useful for a qualitative view of the physical problem and at the same time serve as the basis for future quantitative work.

We discuss how measurements of the viscoelastic mechanical properties were made. In order to obtain these properties, specimens of well defined geometry are needed. Details for the preparation of such specimens are discussed in Section V-3-a. Furthermore, since we want to obtain data under closed system conditions, special environments were chosen under which these experiments were performed. A description of these environments with some discussion of diffusion and swelling effects is presented in Sections V-3-b and V-4.

For the determination of these viscoelastic properties a particular strain history is required. We have chosen relaxation experiments which together with an error analysis discussion are presented in Section V-5 and V-6.

To date, we have obtained sections of master relaxation curves for:

(a) a non-uniform fresh wet specimen from the annulus fibrosus referred to an unknown percent of water.

(b) a single lamella specimen referred to a dry state of about 40% water;

(c) a triple lamella specimen referred to a dry state of about 46% water;

(d) a triple lamella specimen referred to a wet state of about 82.8% water.

These master relaxation curves cover a wide time range. However, before they are applied to human body conditions they should be referred to states of about 70% water. We also determined how the water affects this relaxation spectrum and found that this effect is dominant. Furthermore, we observed that this relaxation spectrum does not depend on the applied strain on the specimen.

In addition, from equilibrium swelling experiments performed by immersing the previously mentioned specimen in saline solutions of various concentrations, we observed that its dimension did not change in the length direction of the specimen (i.e., circumferential with respect to the disc).

2. Experimental Setup

a. INSTRON Tensile Tester

The testing apparatus used for our experiment was a floor model INSTRON tensile machine (Figure 5.1). This machine allows tests to be performed under very limited and special time histories of tensile deformation.

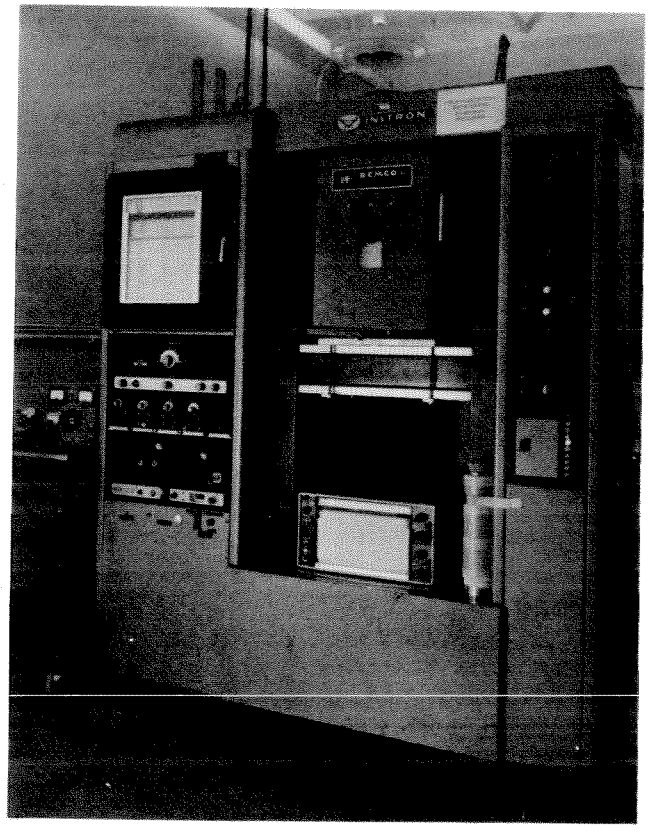

Figure 5.1. The INSTRON Tester and the BEMCO Environmental Chamber

b. Environmental Chambers

A large size TENNEY environmental chamber was used to produce and control temperature and humidity conditions (Figure 5.2). Furthermore, a smaller size BEMCO environmental chamber (Figure 5.1) attached to the INSTRON cross-head and to the TENNEY environmental chamber was used to maintain the specimen at the desired temperature and humidity conditions during the time of the experiment.

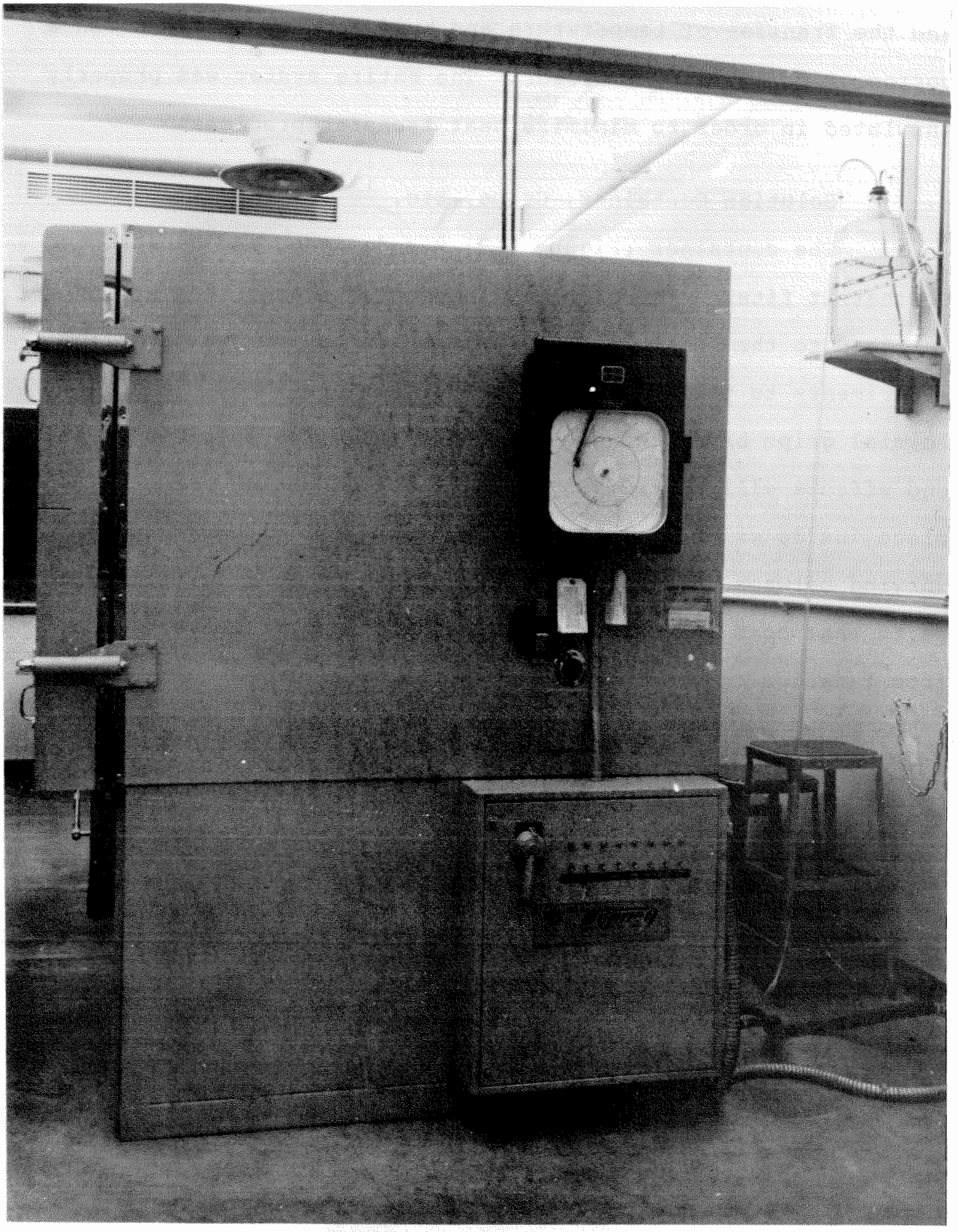

Figure 5.2. The TENNEY Environmental Chamber

The connection between the two chambers was done via plastic hoses and the transfer of temperature and humidity was achieved via a corrosion resistant PAR blower. The entire system was properly insulated in order to minimize heat transfer problems.

c. Solution Container, Grips, Etc.

The container (Figure 5.3) was designed and constructed so that it fits in the small environmental chamber and it can be attached to the INSTRON's crosshead. Its purpose was to allow experiments to take place inside special solutions. In addition, special grips have been constructed to hold the specimen so that end effects will be reduced. Since some of our experiments took place inside saline solution environments, with temperatures varying between $36^{o}C$-$49^{o}C$ and were of rather long duration, the parts that come in contact with the saline solution were made from titanium in order to avoid corrosion.

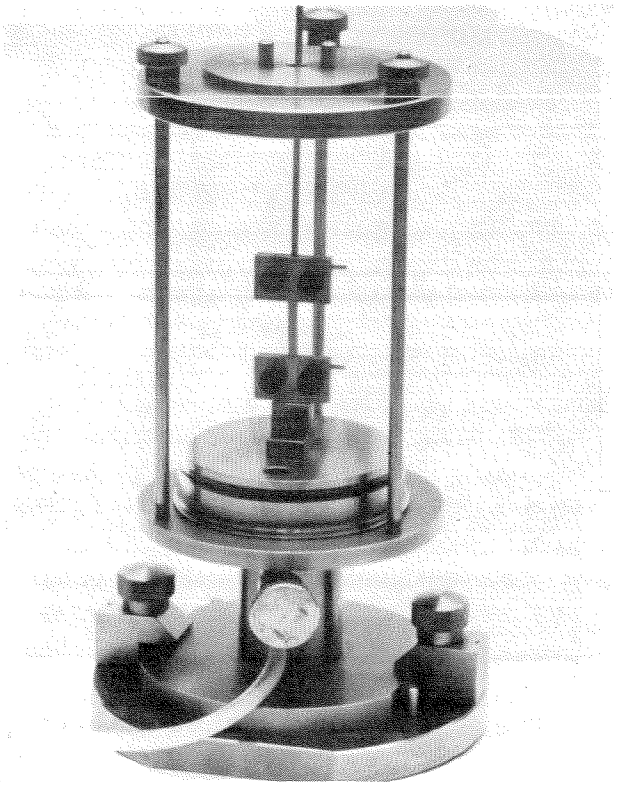

Figure 5.3. The Container

For the proper specimen preparation, a special cutter with sharp razor blades separated by adjustable spacers was made. Also, a microscope, a micrometer, and a precision mechanical balance were used (Figure 5.4).

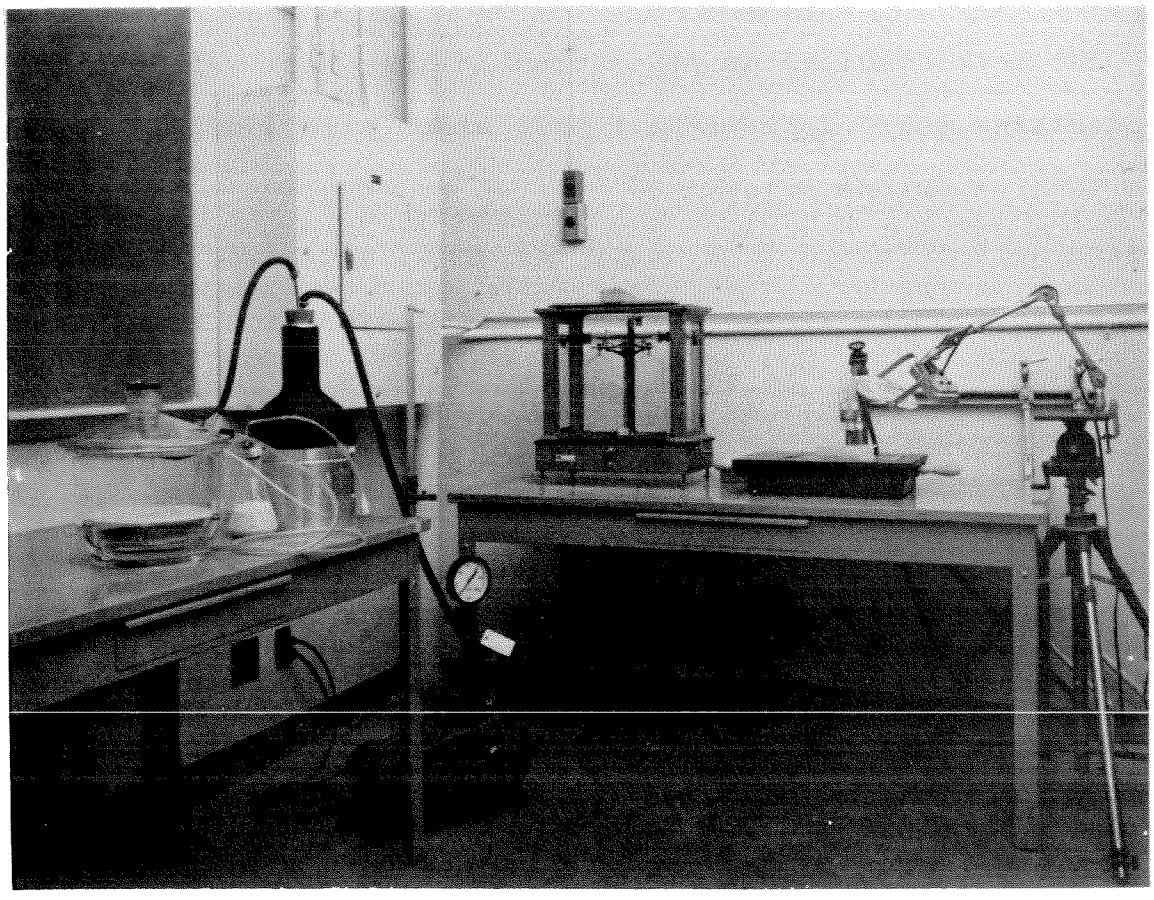

Figure 5.4. The Balance, the Vacuum Device, and the Micrometer

3. Experimental Procedures

In this section the experimental procedures followed in the course of this work are presented. We will describe first the preparation of the specimen, and then discuss measurements of its mechanical properties.

a. Specimen Preparation

The term specimen as it is used in this work will mean small sections taken from human lumbar discs (i.e., single or triple lamella prisms or cylinders* from the nucleus pulposus). The discs were obtained from newly deceased, unclaimed bodies or donors approximately 24 to 48 hours after death which have been refrigerated and were not embalmed. The supply of these discs, actually sections from the lumbar region of the spine consisting of two vertebrae bodies with their intervening disc, was provided by the Pathology Department of the University of Southern California Medical Center. From the time of the disc removal until the time of specimen cutting, the disc was kept in sealed plastic containers and in temperatures below $0^{o}C$. This was necessary for the minimization of moisture exchange between the disc and the environment and for keeping deterioration of the disc material to a minimum.

It is known that the disc's material properties depend on the age of the subject. Furthermore, material properties, within the composite disc, are functions of its age, as well as its physical condition (i.e., herniation, degeneration, etc.). Information about the location and the degree of herniation was employed as a guide for the acceptability of the specimen for mechanical testing. In

* Nucleus Specimens of Cylindrical shape have not been used in this work.

order to ascertain the physical condition of the disc (fractures or other damage), prior to the cutting of the specimen, the disc was subjected to an X-ray examination, by means of conventional radiographic (X-rays) and computerized axial tomographic techniques (EMI - Body Scanner). An example of a ruptured annulus fibrosus is demonstrated in Figures 5.5 and 5.6.

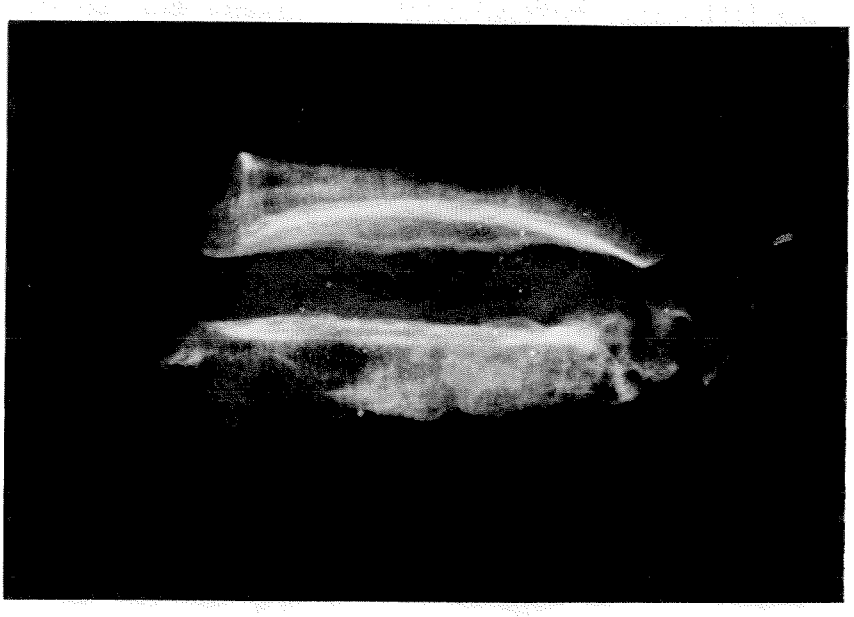

Figure 5.5. Conventional Radiogram (AP-view) of a Damaged Human Intervertebral Disc

We observe that the visibility of the rupture is increased since the disc is expanded when removed from the body. This expansion allows the penetration of air into the rupture, thus enhancing the visibility of the rupture.

At this point, it should be mentioned that cross sectional views of the healthy and damaged discs can be obtained photographically after sectioning the discs with a knife-edge saw. Then, these sectional views may be compared with the corresponding EMI-tomograms for classification purposes.

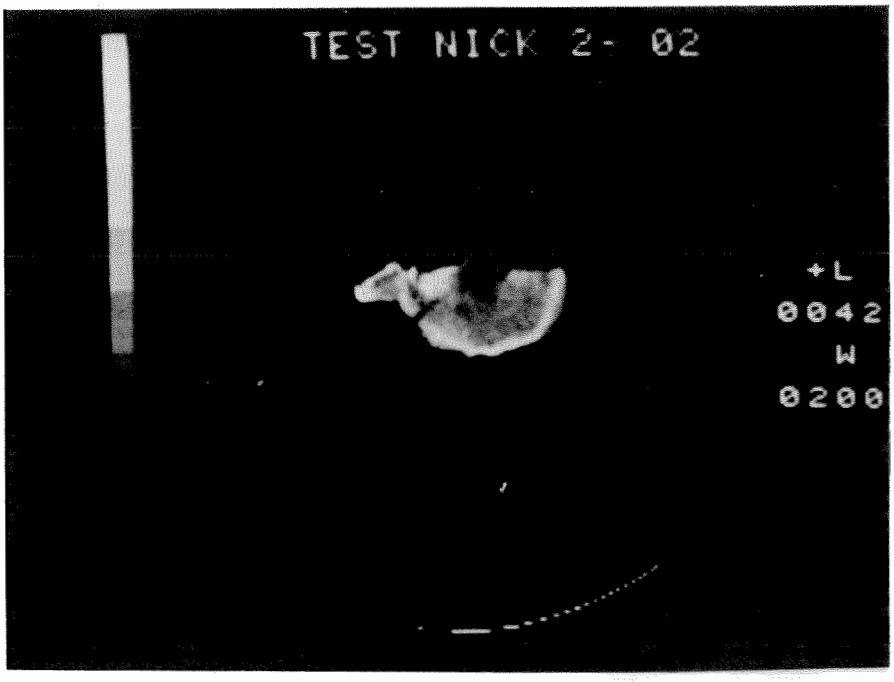

a. The Vertebral Body

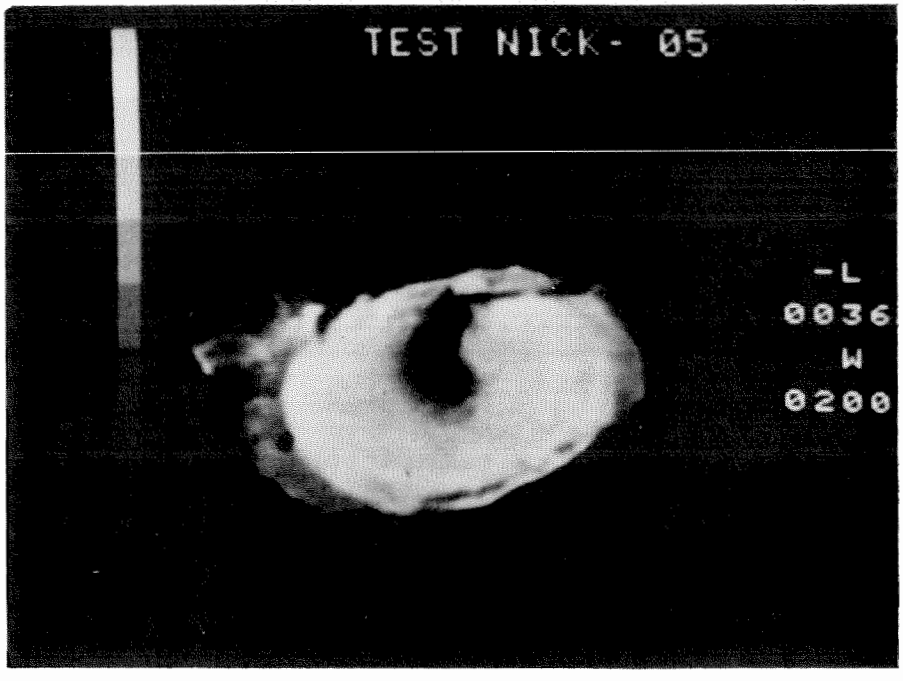

b. The Disc

Figure 5.6. EMI-Tomogram of the Vertebral Body and the Disc

The approximate location of the EMI tomograms presented in Figure 5.6 are shown schematically in Figure 5.7 below.

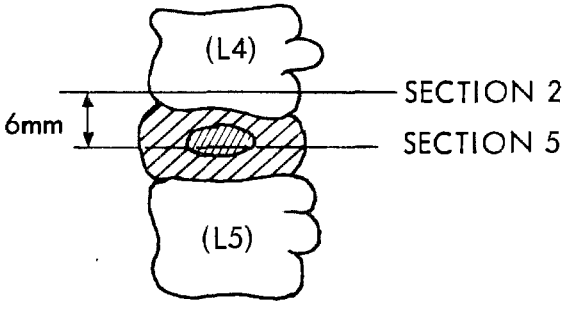

Figure 5.7. Location of the EMI-tomograms.

For our experiments two types of specimens were used. The first one was obtained from the nucleus pulposus and the second from the annulus fibrosus. More precisely, these specimens were prepared as follows:

1) The Specimen From the Nucleus Pulposus. Since the nucleus is a rather soft material it was kept frozen during cutting in order to increase its strength. The freezing was done by using dry ice. The specimens were cut approximately along the major diameter of the nucleus. They were cylinders* with a diameter of about 5mm; their length was a function of the location and the age of the disc and was approximately 2.5 cm. In order to ascertain the exact location of the disc with respect to the adjacent vertebrae, and therefore to facilitate the cutting of the specimen(s), the lateral ligaments were removed first.

The cutting of the cylindrical specimens was done using a hollow drill operated at high speed. In order to minimize thawing of the specimen during cutting, which could cause its rupture, pre-cooling of the drill by means of dry ice was necessary.

---

*Cylindrical type of nucleus specimens were not used in this work (See Section V-6-e)

Furthermore, the specimens' surface areas were checked for smoothness using a low power microscope (X10).

2) The Specimen From the Annulus Fibrosus. The procedure for the separation of a single lamella from the annulus (microsurgery*) is described next. For our present work specimens from the anterior circumferential lamella were obtained as it is shown schematically in Figure 5.8 below.

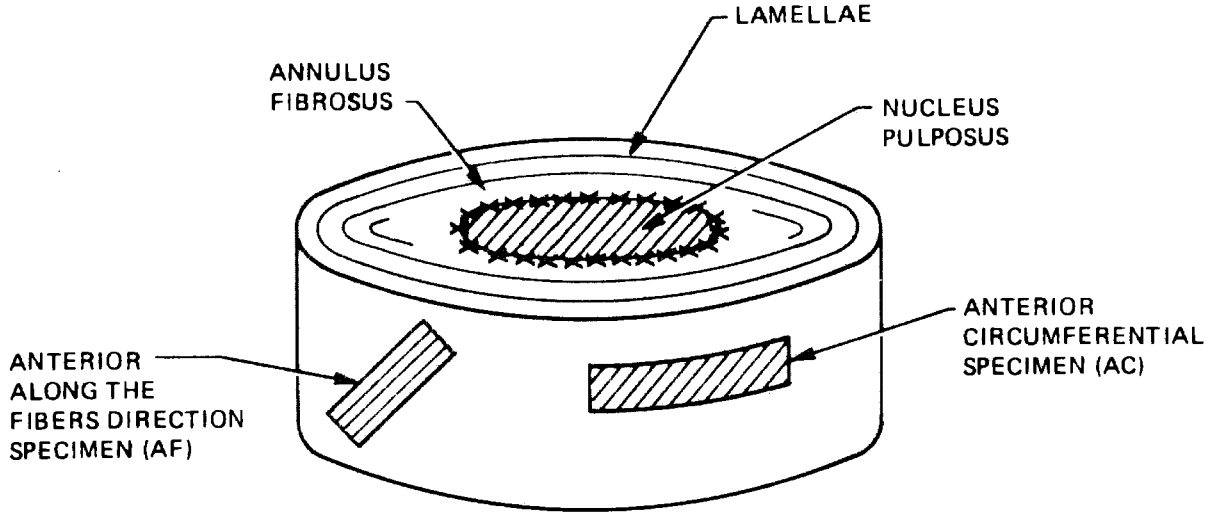

Figure 5.8. A Simplified Schematic Representation of a Disc and the Specimens

A section from the lumbar region of the spine consisting of two vertebral bodies with their intervening disc was utilized. This section was thawed at room temperature (23°C) for about two hours and then the vertebral bodies were gripped, and subsequently stretched, by means of two clamps (Figure 5.9). This step is done to ease both the removal of the ligaments and the separation of the lamellae. The specimen preparation was done manually under room environmental

---

*The microsurgery performed on the annulus fibrosus was done skillfully by Dr. A. Ketenjian, of the Huntington Applied Medical Research Institute, Pasadena, California, assisted by the author.

conditions and under microscopic observation (25X) using a scalpel, forceps, and scissors.

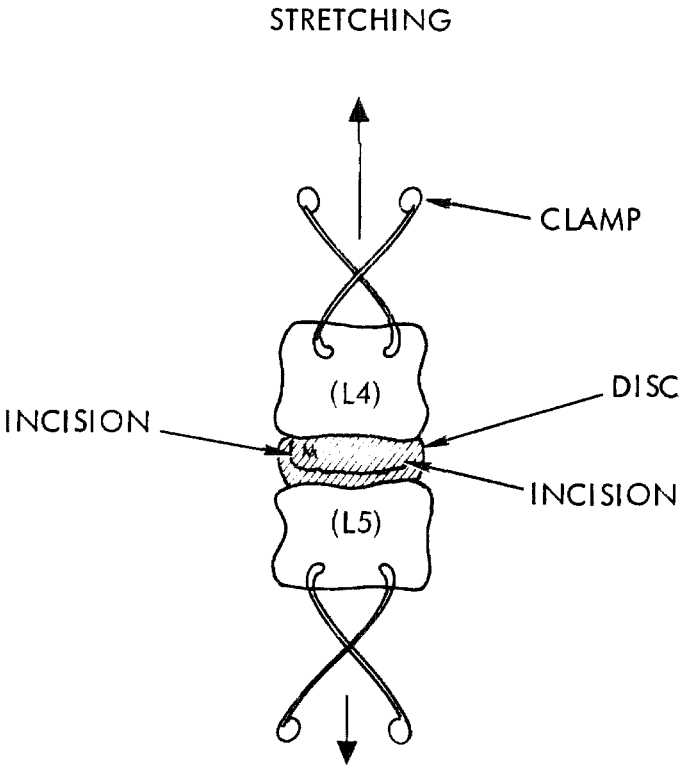

Figure 5.9. Gripping and Stretching of L4-L5 Spine Section

First, the anterior longitudinal ligament was removed using a scalpel and forceps. Next the exterior lamella attached to the ligament was freed from the small remains of the ligament. The first step for the separation of the lamellae was to perform two incisions of 1mm depth each via the scalpel (Figure 5.9). Then the lamella was lifted at the point M with the aid of the forceps and separated from the adjacent lamella (in the neighborhood of the point M) using a scalpel as shown schematically in Figure 5.10.

The peeling was done by holding the lamella at the point M with forceps using minimum force and by pushing the ligament, in the neighborhood of point N, using only the opening motion of the scissors' blunt edges. It was found by trial and error that this

produced the most satisfactory results. Finally, the other ends of the peeled lamella were cut. The lamella specimen was then placed in a sealed plastic container and maintained at dry ice temperature.

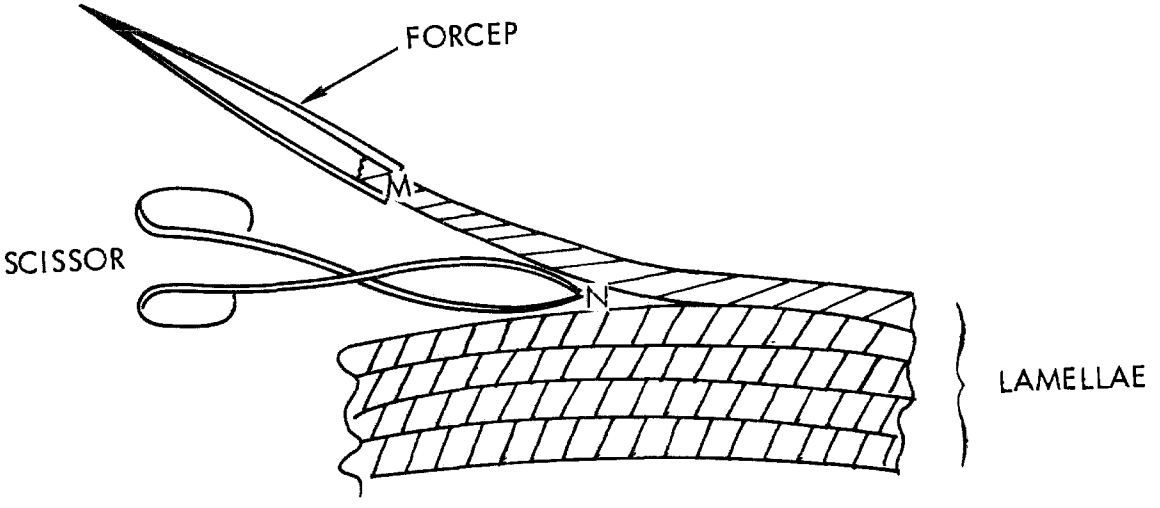

Figure 5.10. Peeling of the Lamella

After the first lamella was removed, the next one was freed from any remainders of the first lamella. The same procedure was then applied for the separation of more lamellae from the anterior portion of the annulus fibrosus.

In order to keep the specimen wet, saline solution (50 gr NaCl/1000 cc solution) was applied via gauze to the surface of the lamella to be cut next. Before the desired specimen is prepared for mechanical testing, the quality of the separated lamella was checked. First, by eye inspection, those specimens containing some cuts (ruptures) were eliminated. These ruptures occurred generally along the direction of the fibers. When these imperfections were removed, the size of the useful lamella was reduced

and in the case that the ruptures were extensive, the lamella was discarded. As an example, Figure 3.3(a) presents a microscopic view of a small section of a lamella. This picture was obtained using a transmission microscope (75X) with green filter and phase contrast. The examination of the entire surface of this lamella showed that with the exception of a few strands, the fibers ran along the same direction. This implies that a single lamella was obtained. Since the drying of the specimen was severe during the microscopic examination, in future work the specimen will be kept in sealed plastic small containers.

The specimens for mechanical testing were then cut at specified directions; i.e., along, perpendicular and at an angle of about 30^{o}. The procedure for cutting these specimens is discussed next.

In order to keep the specimen straight, the lamella was placed between two properly aligned grips, as shown in Figure 5.11 and a slight tension was applied to the grips.

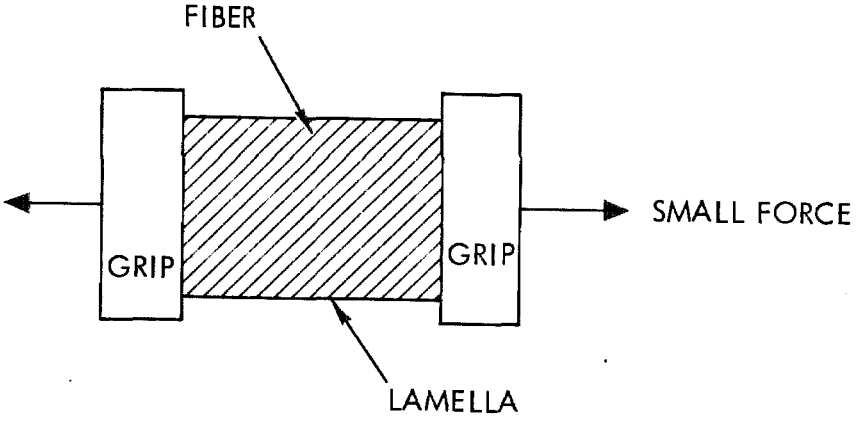

Figure 5.11. Gripping of the Lamella

At this point and under microscopic observation (5X to 10X) specimens of prespecified geometry were cut by using a cutter

made with sharp razor blades separated by adjustable spacers. After the specimens were cut, their dimensions and their weights were measured. Some typical dimensions of such specimens are shown in Figure 5.12.

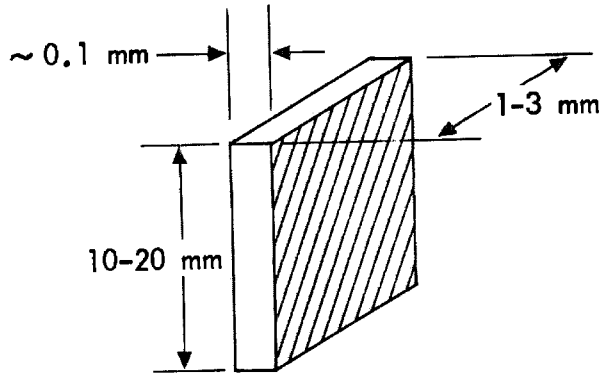

Figure 5.12. Typical Lamella Specimen used in this Research

3) Other Methods of Specimen Excision. We have obtained specimens from the annulus fibrosus by cutting them with a dermatome. Using this cutting technique we can obtain quickly sections of adjustable dimensions from the annulus but with little control as far as the number of lamellae is concerned. A transmission microscopic picture of a dermatome prepared specimen is presented in Figure 3-3.

An examination of the fiber direction at the surface indicates that our specimen has 3 or more lamellae (Figure 3.(b)). Again, as soon as the specimens were prepared they were placed and kept in sealed plastic containers at temperatures below 0 C until the time of mechanical testing.

b. Laboratory Environmental Conditions Necessary for the Mechanical Testing of Specimens Cut From a Disc.

Our experimental procedure used for the determination of

the master relaxation curve, at nearly human body conditions, requires mechanical testing of the disc specimen(s) at various water concentrations (above and below body conditions) under closed system conditions. A system (the specimen) is considered to be closed if there is not net flow of its constituent phases across the system boundary.

In practice an absolutely closed system cannot be achieved. It can be obtained only approximately. However, the following two approaches can lead to a closed (or almost closed) system. They are the controlled environment approach and the uncontrolled environment approach.

1) The Controlled Environment Approach. In this case the specimen is initially in equilibrium (or near equilibrium) with the environment in which it is going to be tested. Therefore, there is no (or only small) net flow of material across the specimen interface. This implies that the specimen can be considered as a closed system. Since we desire to study the material properties at various water concentrations, we must search for environments at which equilibrium exists at various water contents. We can achieve this by changing the osmotic pressure of the water in the environment. For example, one way is by changing the partial pressure (humidity) of water in the air. Another way is by introducing solutes in a liquid environment which effectively drop the osmotic pressure of the water (water with salt or water with chondroitin sulfate). However, there is a limitation of this method when mechanical testing is performed and is due to the mechanical energy introduced to the material. This energy shifts the equilibrium concentration, therefore the system is no longer in equilibrium

and a flow across the interface occurs. However, if this shift is small or the diffusion is slow (see next paragraph), we can still consider the specimen as a closed system for a sufficiently large time interval (i.e., two hours).

Based on this general discussion, the following procedures were applied.

(1) Moist Air Environment. The following experiments were performed for the determination of the time required for the water content of disc specimens to reach equilibrium with its moist air environment as well as for the estimation of the percentage of water content in it. The specimens used were obtained from the anterior circumferential section (AC) of the disc's annulus fibrosus via dermatome (Figure 5.8) and consisted of one and three or more lamellae (See Section V-3-a).

The specimens were first dried in a desiccator over silica gel environment and then their dimensions and weights were measured. In our experiment the drying time* was aribtrary but always longer than 24 hours. Subsequently, the specimens were placed over a wire mesh inside the BEMCO environmental chamber with circulating air at fixed but controllable temperature and humidity conditions. The determination of the time required for equilibrium was done by removing the specimen periodically from the chamber and recording its weight until its weight did not change with time. We tried to minimize the time required to take the specimen out of the chamber, weigh it and then place it back in again. More precisely, as soon as the specimen was taken out of the environmental chamber, it was

*We plan to obtain the time required for a specimen to dry more accurately at a future date.

placed in a small plastic box tightly closed and weighted* with the box. Then the specimen was removed from the box and placed in the environmental chamber again. This operation took less than two minutes. The percentage of water content in the specimen was estimated from the ratio:

$$\frac{\text{wet weight - dry weight}}{\text{wet weight}} \times 100$$

Although this method involves many potential problems (i.e., the evaporation of water during weight measurement, the condensation of drops on the specimen after placing it cool in the moist-warm chamber, etc.) we can obtain approximate values for both the equilibrium time and the percentage of water content in the specimen as a function of time.

Table 5.1 summarizes our experimental findings for the cases of single lamella and triple lamella specimens. In both cases the percentage of water content in the specimen was very low compared to the 70% expected for specimens from discs of advanced age, which was the case for our specimens (see Section III-2).

---

*The weights were obtained with a precision mechanical balance.

Table 5.1 Time for Equilibrium and Percentage of Water for Single and Triple Lamella Specimens

Specimen Description	Time for Equilibrium (minutes)	Percentage of Water Content (%)	Comments
Single lamella	~240	~40	Two experiments were performed in this case
Triple lamella	~40	~14	The equilibrium measurements of weight were obtained from the average of six measurements taken between 40-1500 min.
Environmental Conditions:	Dry bulb temperature $\cong 38^{\circ}C$ Wet bulb temperature $\cong 36^{\circ}C$ via tables and charts Temperature of the environment $38^{\circ}C$ Relative Humidity $\cong$ 90% or Absolute Humidity $\cong$ 0.0305 gr of Water per gr of dry air		

In order to increase the water content of the specimen, the dry bulb temperature must be raised, while maintaining a high relative humidity. That is, the partial pressure of the water vapor in the air will control the water in the specimen and at higher temperatures we can obtain higher partial pressures.

The highest temperature achievable in our experimental

setup was about 50°C because the plastic hoses and the blower used for the connection of the two experimental chambers could not be subjected to higher temperatures (Section V-3-b). Our measurements were based on the three lamellae specimen described earlier. It was shown that, for a dry bulb temperature of 48.1°C and a wet bulb temperature of 47.5°C (which corresponds to an absolute humidity of 0.0755 gr of water per gr of dry air in the environment), the weight of the specimen was 36.8 mgr or that its water content was 46%.

However, the use of high temperatures seems to introduce the following complications:

(1) Oxidation of the specimen

(2) Shifting in the relaxation spectrum due to temperature in addition to the concentration shift being studied.

We investigated the relative importance of both factors and our preliminary results indicated that their contribution to the mechanical behavior was rather small (see next section). Further work is necessary to quantify those effects. We point out here that a change in color of the specimen occurred (the specimen became browner) and we assumed that this was evidence of oxidation.

The results obtained by the use of this environment are summarized below:

(1) Both the triple lamella and single lamella specimens were drier than body conditions at all environments achievable in our experimental setup (14% - 40% H_2O vs. 70% at body). Although we do not have sufficient

data (the only data available are given in Table 5.1), we speculate that in the case of the single lamella it is possible to reach larger percentage of water in the specimen compared to the water content for triple lamella by using higher temperatures in the environment.

(2) There were significant differences between the water content of the single lamella specimens as compared to the triple lamella ones. Namely, the specimens consisting of one lamella contained more water than the multiple lamellae ones (40% vs. 14%).

(3) The time required to achieve equilibrium, for single and triple lamella specimens, was of the order of a few hours, since the water diffuses in or out of the specimen relatively slowly.

(4) The problems with the control of humidity warrant a modification of the control mechanism (i.e., the controller in the TENNEY environmental chamber) for any future work.

The problems associated with the control of humidity are:

(1) Oscillations of $\pm$ 0.5°C in the wet bulb temperature, (See Figures 5-18 and 5-19).

(2) Formation of drops which deposit on the specimen at high relative humidities. (See paragraph 5 of this Section.)

In conclusion, the previously discussed environmental conditions can be used to obtain a large portion of the mechanical data. However, sufficiently large amounts of water in the specimen cannot be achieved and other environments are needed for this purpose. In this type of experiment the percentage of water in the specimen was controlled by the adjustable relative humidity of the air (15% - 95%) via the TENNEY environmental chamber. The upper limit was set by the appearance of mist in the air (that is, trapped drops of water in the circulating air).

(2) Saline Solution Environment. In this case we studied the effects of the environment established through various concentrations of saline solutions on a disc specimen. In doing so, we could control the percentage of water contained in the specimen which was in equilibrium with its environment. The maximum percentage of water was obtained using deionized water and the minimum with saturated NaCl solution. Saturation of NaCl solution occurs at 350 gr. NaCl per 1000 cc solution. However, since such a solution was difficult to prepare, we used 300 gr. of NaCl per 1000 cc solution as the upper limit of NaCl prepared at room temperature (~20°C).

As in the case of moist air, we determined the time required for the specimen to reach equilibrium in this environment (Fig. 5.13), as well as the percentage of its water content at equilibrium. In these experiments one single lamella and two triple-lamella specimens were used. The two triple lamellae specimens were taken from the same disc section as the one used in the case of the moist air. All specimens were first dried in air over silica gel and then their

dimensions and weights were measured. Subsequently they were immersed in saline solutions of various concentrations (60, 180, and 300 gr. NaCl/1000 cc solution) maintained at room temperature (~20°C).

The weight and dimensions of the specimen were monitored during the swelling process in the various solutions. The dimensions were measured inside the solution so any error due to possible drying of the specimen during measurements was eliminated. The weights were obtained with a precision mechanical balance after removing the specimen from the solution. The weighing process took less than one minute so that any evaporation of water from the specimen in this step was minimal. However, large errors in the weight measurements were involved. This was due to the fact that drops of solution tend to adhere to the surface. We reduced that problem by removing the drops, that is, shaking the drops off. Our data, in spite of the large errors involved in these measurements, enable us to obtain an estimate for the time to reach equilibrium and the percentage of water content in the specimen at equilibrium. For all experiments the swelling process reached equilibrium in a few hours* (1 to 2 hrs) as it is shown in Figure 5.13.

---

*In some instances the time to reach equilibrium was not measurable because the change dimensions and weight were small compared to the errors involved in the measurement.

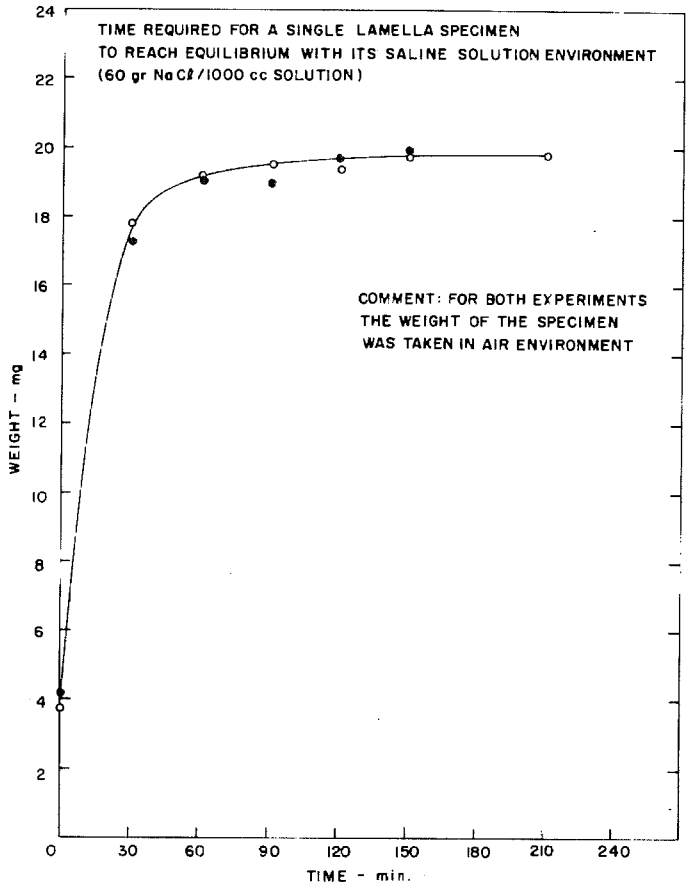

Figure 5.13. Equilibrium Time for a Single Lamella Specimen with its Saline Solution Environment

The dimensions and the weight at equilibrium were the average of several measurements obtained over a certain time interval.

Table 5.2 summarizes our measurements. From these measurements one can observe that the dimensions of the specimens do not vary much as we change solutions. However, by taking the ratios of swollen over dry measurements (Table 5.3), subsequently referred to as "swelling ratios," we observe that the swelling was not identical in all directions (swelling anisotropy). The swelling anisotropy will be discussed further in V-4.

Table 5.2. Equilibrium Swelling Data

Specimen No.	Specimen Description	Dimensions [cm]			Weight [mgr]	Comments
		Length	Width	Thickness		
1	Single-Lamella	1.56	0.107	0.0184	3.8	Dry
		1.63	0.2032	0.0519	19.8	o At 60 gr NaCl/1000cc solution at T≅21°C Density of the specimen: P_{dry} = 1.2329 gr/cc, P_{wet} = 1.148 gr/cc
2	Triple-Lamella	2.23	.096	.0416	7.4±1	Dry
	"	2.19	.23	.17	43.45	o At 60gr NaCl/1000cc solution and T ≅ 21°C o Measurement obtained from the averaging of 16 data points over 70-2830 minutes. o Time for equilibrium swelling ≃ 1 hr.
	"	2.16	.23	.14	44±4	o At 180 gr NaCl/1000cc solution and T ≅ 21°C o Measurement obtained from the averaging of 10 data points over 125-2870 minutes o Time for equilibrium not measurable since dimensions and weight do not change much. Believed to be few hours.
3	Triple-Lamella	2.37	.178	.035±.01	11.5	Dry
	"	2.48	.23	.16	54	o At 300gr NaCl/1000cc solution and T ≅ 21°C o Measurements obtained from the averaging of 10 data points over 40-2820 minutes o Time for equilibrium swelling is about 2 hrs.
	"	2.5	.28±.02	.13±.03	57.5±2.1	o At 180gr NaCl/1000cc solution and T ≅ 21°C o Measurements obtained from the averaging of 16 data points over 140-2890 minutes o Time for equilibrium not measurable since dimensions @ weight do not change much. Believed to be few hrs.

Table 5.3. Equilibrium Swelling Ratios of Water in Swollen Specimen

Specimen No.	Specimen Description	Swelling Ratios			Weight	% of Water in Swollen Specimen	Comments
		Length	Width	Thickness			
1	**Single-Lamella**	1.0448	1.899	2.82	5.21	80.8	**60 gr NaCl/1000cc solution**
2	Triple-Lamella	.982±.02	2.39 ±.2	4.08	5.87	82.9	60 gr NaCl/1000cc solution
		.969	2.39	3.36	5.9	83.1	180 gr NaCl/1000cc solution
3	"	1.046	1.29	4.57	4.69	78.7	300 gr NaCl/1000cc solution
		1.054	1.61	3.71	5.0	80.0	180 gr NaCl/1000cc solution

Table 5.4 gives an average estimate of the water in the triple-lamella specimen at the state of equilibrium with its various saline solution environments.

Table 5.4. Water Content in a Specimen at Various NaCl Solutions

Specimen Description	Solution (gr/100 cc Solution)	% of Water in Swollen State	Comments
Single Lamella	60	80.8	Specimen from Cadaver A
Triple Lamella	60	82.9	Specimen from Cadaver B
	180	81.5	
	300	78.7	

Therefore, the various saline solution concentrations offer a rather narrow range of water content in a triple lamella specimen. This is quite different from the results obtained from a circumferential specimen (AC) consisting of one lamella, taken from the same disc. As before, the specimen was first dried and then placed

consecutively in various saline solutions of decreasing NaCl content and finally in pure deionized water. The results are shown in Fig. 5.14.

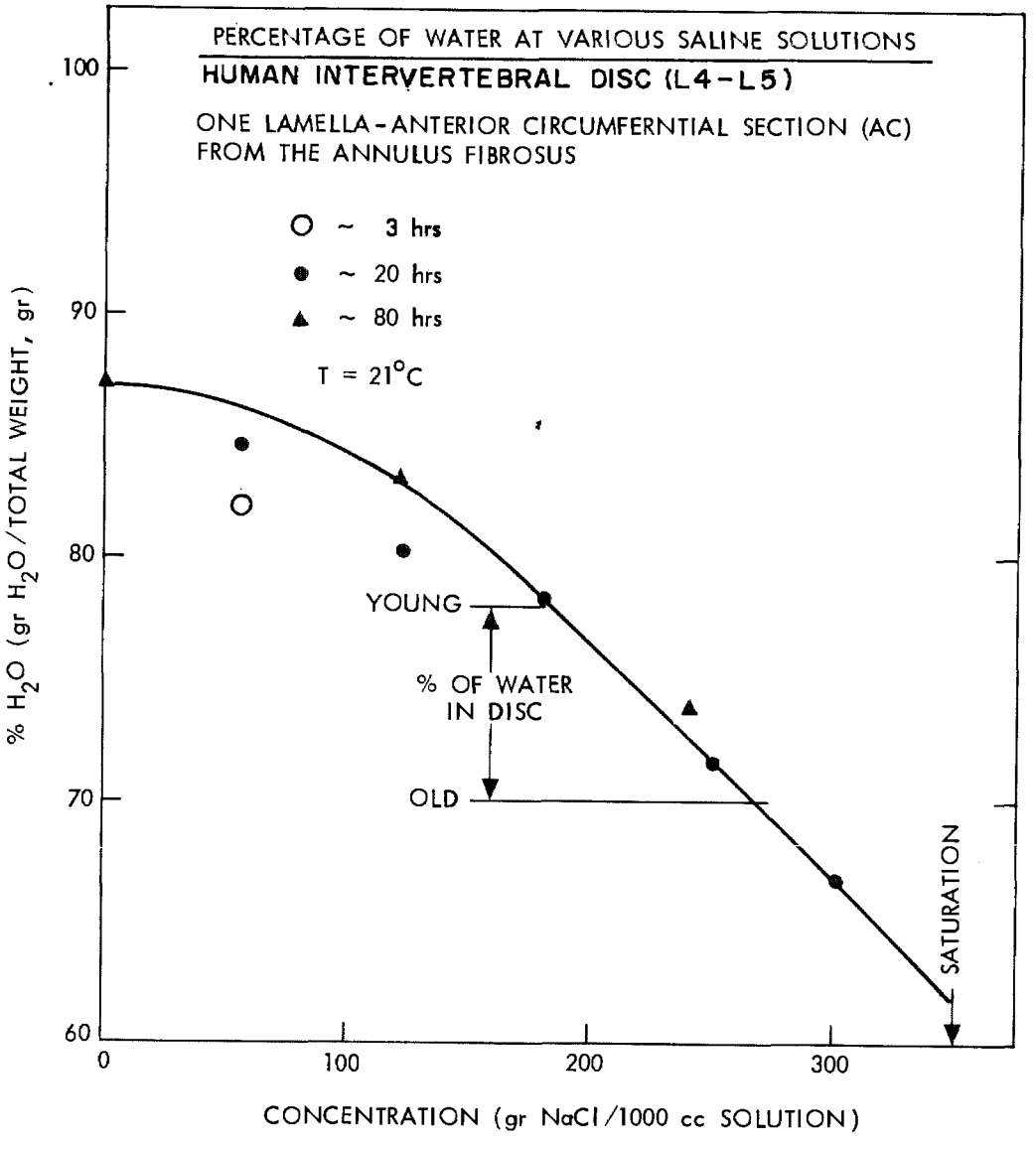

Figure 5.14. Percentage of Water for a One Lamella Specimen at Various NaCl Solutions

We observed that the dry specimens which have three lamellae or one lamella were always curved and twisted while the swollen specimens (at ~70% of water or more) were straight or only slightly curved). This natural twisting and curving was expected and is due to the anisotropic nature and anatomic character of the composite material of the annulus

fibrosus. The twisting and curving of the dried specimen introduces an error in the measurements of its dimensions. This error is rather large, especially in the cases of thickness and width measurements.

Furthermore, the density of the dried or swollen specimens was observed to be higher than any of the saline solutions used. That is, all the specimens drop to the bottom of the solutions after all the air bubbles in its surface were shaken off. The calculations of the density for dry specimens give 0.85 ± 0.2 gr/cm^3. However, it is known that the density of the saline solutions is slightly higher than unity so the upper limit of the calculated densities is more likely to be correct.

Galante observed appreciable swelling with respect to body water content when he placed specimens from the annulus fibrosus in solutions of 0.09% saline solution, blood plasma and dextran (10%) (Ref. 10). Our observations confirmed that swelling of the disc specimens occurred in almost all saline solutions. Especially when diluted ones were used, the water content was higher than body conditions (see Fig. 5.14). This fact may be surprising at first since the body fluids are reported to be approximately represented by dilute saline solutions and the disc is in indirect contact with such fluids through the ligaments and the vertebral bodies. However, we explain this observation by pointing out that in the body the disc is always under mechanical stress. According to Flory-Huggins theory (Ref.33) this mechanical stress shifts the equilibrium water content of the disc.

Saline solution at 38^{o}C offers the advantage of a better

environmental control for mechanical testing as compared to air at about the same temperature. That is, it does not have the problems present when moist air environment was used. However, only relatively high water content can be achieved by using this enrironment (i.e., 78%-83%). Therefore, if the saline solutions environment is used together with the previously discussed moist air one, the water content ranges covered for the triple lamella specimen are: 14%-46% for the moist air and 78%-83% for the saline solution at about 38°C temperature. Therefore, a third environment is needed to close the water content gap (i.e., 47% to 77% for a triple lamella specimen) and to assure the reproducibility of the data.

Liquid environments possess the disadvantage that any sol fraction in the material (such as newly formed collagen, low molecular weight polymers, ions, etc.) can be leached out. However, within the experimental errors involved in the measurement of dried specimens (such as balance weight errors $\pm$ 0.01 mg, unevenness in the conditions of the drier, i.e., wetness in the silica gel, etc.) we have noticed that the sol fraction extracted by immersion in water is less than a few percentages. This is shown by the two examples presented in Table 5.5. The low extractability from the disc specimens (which are in contact with body fluids) is in agreement with the biochemical fact that there are few cells in the old discs and that there is very little growth in them. Therefore, it is expected that the specimens contain only a small amount of new formed or extractable collagen.

Liquid environments containing salts also have the disadvantage

that the salts or its ions can penetrate the material. Nimni indicated that this problem may be significant only at rather high NaCl concentrations (Ref. 60). He also poined out that at low salt concentrations such interactions may not be problematic due to the fact that similar interactions are present in the human body.

Table 5.5. History of the Two Specimens

Specimen No.	Specimen Characterization	Specimen Weight [mgr]	Environment	Date	Comments
1	Triple-Lamella Circumferential	22.2	Air over silica gel	2/15	Dry
		--	Saline Solutions	2/15 - 3/14	--
		--	in H_2O	3/14 - 3/15	--
		19.9	Air over Silica gel	3/15 - 3/16	Average weight of two measurements taken on 3/16
		--	Low moist air of various temperatures from 38°C to 50°C	3/16 - 4/18	--
		20.6	Air over silica gel	4/18 - 4/21	Weight taken on 4/21
2	"	7.4	Air over silica gel	2/15	Dry
		8.8	Air over silica gel	2/15 - 3/14	Average weight of two measurements taken on 3/14
		--	In saline solution	3/14 - 4/15	--
		7.2	Air over silica gel	4/15 - 4/21	Average weight of two measurements taken on 4/21

(3) Other Environments. In order to achieve the desired intermediate water concentration (47% - 77%) the following media have been studied and discounted.

(a) Methanol-Water. Methanol swells the specimen appreciably. The exact equilibrium value is unknown, however, it is larger than 70%. It is unknown because the swelling was very slow and, therefore, very difficult to measure. The specimen was still

swelling after a week in this environment. Furthermore, methanol vaporized quickly at 38 C which makes it not practical for our research.

(b) $LiClO_4$ Solution. Since Li is one of the strongest cations, it seemed as a proper solute to drop the osmotic pressure of the water in the solution, therefore drying the specimen. The specimen was placed in a solution containing this salt at a near saturation level. However, the swollen specimen shows a strange appearance, like it has been cross-linked even further than its initial state (a tanning effect). This effect appeared irreversible. We demonstrated this by immersing the specimen in pure water for a week, and noticed that in this time interval no change was observed. The possible reasons for this "tanning" effect may be due to the ClO_4 anion since other perchlorates produce similar tanning effect, as Ninmi pointed out (Ref. 60).

(c) Chondroitin Sulfate Solution. This chemical is a polymer derivate of mucopolysaccharides. Our experiment with a 3 gr/10 cc solution showed that the specimen swells appreciably and absorbs more than 75% water. This solution is very viscous, and is difficult to use for mechanical testing. Therefore, we judged it not practical for our work.

(d) Others. In the near future we plan to study the following environments:

Glycerin and dimethyl sulfoxide which were suggested by Ninmi in a private communication (Ref. 60).

Silicone oil and water saturated silicone oil which was suggested by Silverberg based on work done by Witahelm (Ref. 61).

These silicone oil based environments will be used for mechanical testing under non-equilibrium conditions.

2) The Uncontrolled Environment Approach. In this case, initially the specimen is not in equilibrium with its environment. Therefore, its initial water concentration is not fixed (by the environment) and can be freely chosen provided that it is below the saturation level. In the time interval of interest (the term "time of interest" may include the time to place the specimen for testing, the testing time, the relaxation time between experiments, the repetition of the tests, etc.) a change in the water content of the specimen may be observed. If this change is such that no variation in the mechanical properties is detectable (i.e., due to drying of the specimen), we can consider the system to be approximately closed. The minimum time required to be able to detect such changes in the properties depends then on the interaction between the mechanical properties and the environment as well as the precision of the mechanical test and the speed of the diffusion process. However, the interactions between the mechanical properties and the environment are fixed for a given material. Therefore, we can extend the desired time interval as follows:

* By setting a lower accuracy for our mechanical data. We estimate that our error will be a few percent and we do not desire to increase it.

* By altering the diffusion process. That is, by changing the flow pattern of the moist air from the bulk of the environment to the surface of the specimen and vice versa

or by changing the medium in which the specimen is in (which then becomes a controlled environment experiment).

We discuss next two experiments performed under uncontrolled environmental conditions.

(1) The Reproducibility of Short Duration Experiments. Galante performed a short-duration loading-unloading experiment (less than one minute) on a specimen of 1 mm or 2 mm thickness immediately after the specimen was obtained from the disc (Ref. 10). Then he waited for some time (either 10 minutes or 30 minutes) for the water to diffuse out of the specimen and repeated the same loading-unloading experiments. He observed that the experiments performed within the time interval of 10 minutes were reproducible. On the other hand, experiments performed within the time interval of 30 minutes were not reproducible. From these experiments one can conclude that for specimens of such thickness the system can be considered as closed for the time interval $0 \text{ min} < t \leq 10 \text{ min}$.

(2) Detecting Abnormal Relaxation Behavior. We have used this method at room conditions for a multi-lamella specimen of irregular geometry obtained from the anterior circumferential section (AC) and found that closed system conditions were achievable for times up to two minutes (see Figure 5.15), therefore confirming Galante's observation (Ref. 10). This uncontrolled environment relaxation procedure enabled us to obtain the relaxation data shown in Figure 5.15 which covers a narrow experimental window approximately 10^{-2} min to 10 min). The lower limit is due to

INSTRON limitations. In order to extend this experimental time window to shorter times, another mechanical procedure (i.e., dynamic testing) is needed.

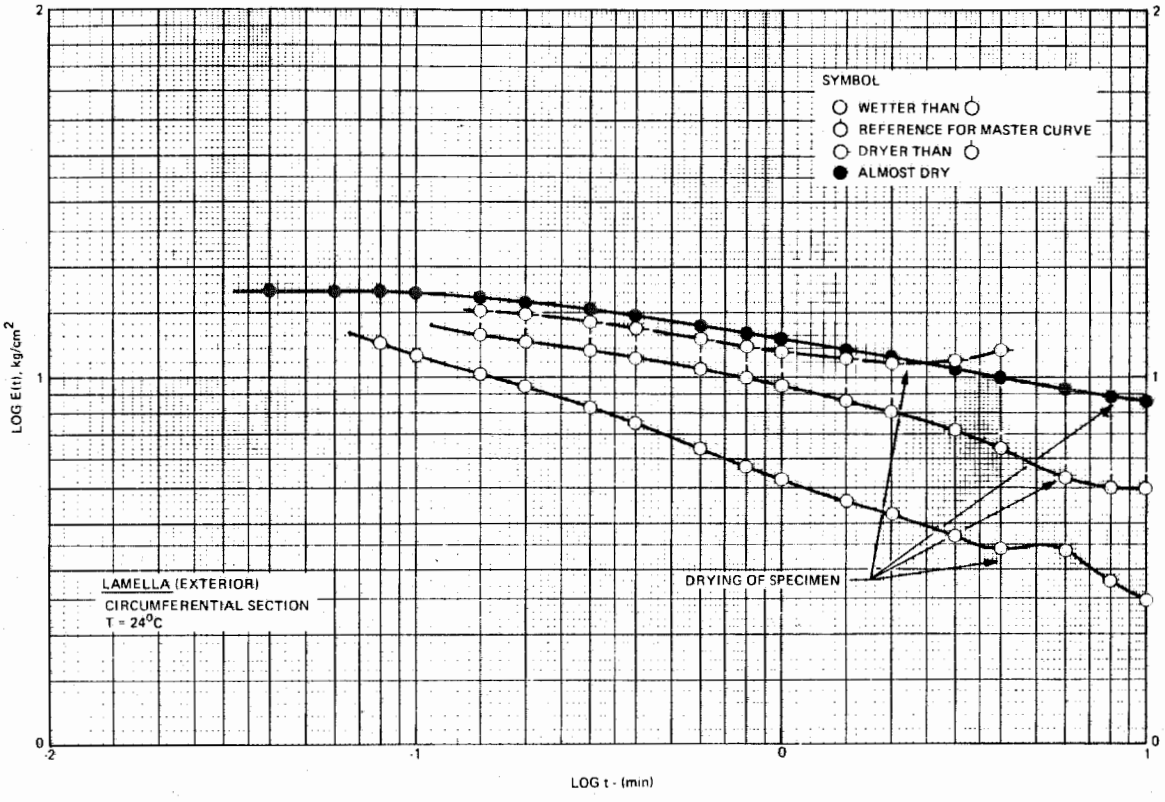

Figure 5.15. Relaxation Data for Exterior Lamella

4. Conclusions and Discussion on the Swelling of the Annulus Fibrosus

We now summarize our experimental findings described in previous paragraphs and speculate about their significance. These conclusions are no more than educated guesses since only limited data is available to date. Therefore, further work is needed for their verification.

(1) The Swelling of the Total Disc is Mainly in the Direction of the Spinal Axis. We observed that the specimen from the annulus fibrosus consisting of a triple lamella did not swell or swelled very little in the length direction compared to the swelling in the width and thickness directions (See Table 5.3). This corresponds to an almost zero growth in the disc circumference. The mechanism by which such swelling anisotropy is obtained is probably due to a particular balance between the swelling ability of the matrix and the fibers, as well as it may depend on the direction of the fibers in the lamellae. In order to understand this mechanism, further work is required (i.e., swelling experiments using the total disc and computer simulation based on the theory of swelling of angle-ply laminated composite materials).

We remark here that this inhomogeneous swelling of the annulus reduces the radial stresses at the contact points of the disc with the vertebral body (end effect). It also reduces any extra bulge of the disc due to swelling. Both effects would be present if the disc's material was isotropic. The reduction of these radial stresses and bulges may be one of the reasons that disc herniations do not occur easily during the normal operation of the disc.

This finding seems to be consistent with DePukey's observation that the average person is one percent shorter at the end of the day when compared to the body length in the morning on first rising (Ref. 27). This variation was attributed to changes in the disc's height which could be due either to a natural creep

and creep-recovery of its mechanical system, or to a water variation in the disc material, or, as it is more probable, a combination of both.

(2) The Fibers in the Annulus Swell Less Than the Matrix.

This result is expected from physical grounds if one considers that the molecules in the fibers are packed more closely than in the matrix. Also, phenomenologically the modulus along the fibers is higher than in the matrix. In addition, the matrix is more hydrophylic than the fibers therefore, the swelling along the fibers should be less than the average swelling of the material. This expectation was confirmed by our experiment as it is shown below.

From the swelling anisotropy, the swelling ratio along the direction of the fibers can be calculated as follows:
The angles and dimensions of this swollen specimen are given in Figure 5.16. From the experimental results presented in the previous section, the averaged swelling ratios of the specimen in saline solution environment were: $R_\ell \cong 1$, $R_W \cong 1.8$. Furthermore, it is known from the literature, or as confirmed from our microscope pictures, that $a/2 \cong 30$, therefore $\beta/2 \cong 60$.

The swelling ratio along the fibers (F_f = swollen length over dry length of the fiber) is given by:

$$F_f = \sqrt{\frac{\ell_o^2 + (R_W w_o)^2}{\ell_o^2 + w_o^2}} = \sqrt{\frac{1 + \tan^2 (a/2)}{1 + \frac{1}{R_W^2} \tan^2(a/2)}} \qquad (1)$$

Based on the given values for α and R_W one calculates $F_f \cong 1.16$, a value which is smaller than the averaged linear swelling in the surface of the specimen $\sqrt{R_\ell R_W}$ which is 1.34. This result implies that the fiber swells less than the matrix.

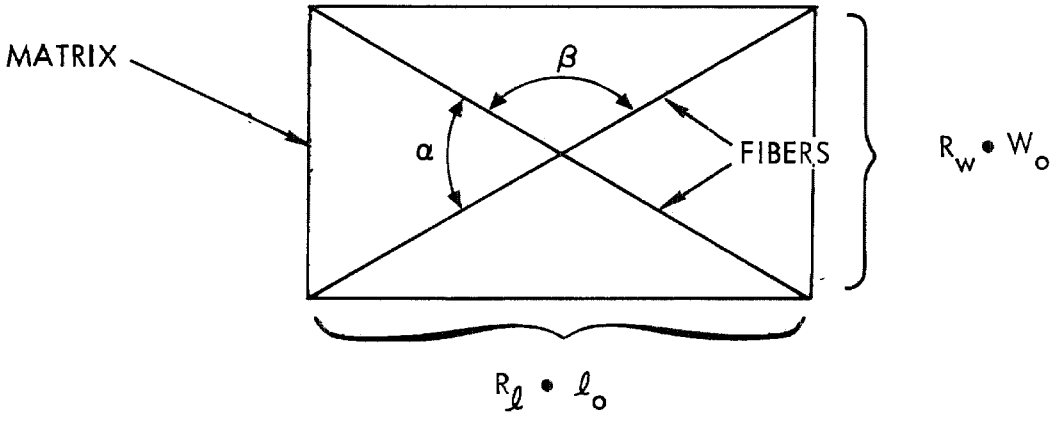

Figure 5.16. Direction of the Fibers in a Swollen Circumferential Specimen (AC-type) of two Lamellae (Where w_o is the Dry Width, ℓ_o is the Dry Length, R_ℓ, R_w are the Swelling Ratios of the Length and Width Respectively

(3) <u>There is Little or no Fiber Interweaving Between Lamallae in the Anterior Annulus Fibrosus for Nondegenerated Discs</u>. We noticed that this was true in the case of nondegenerated discs while appreciable interweaving was observed in two cases of degenerated discs. These facts were obvious during the micro-surgery performed for the specimen preparations. This probably explains some of the swelling characteristics of specimens taken from nondegenerated discs. That is, the swelling ratios in the thickness direction seem to be larger than the the one in the width direction.

(4) <u>The Water Diffusion Across the Annulus Fibrosus is Slow</u>. This finding follows from our experiments for triple-lamellae

specimens which reach equilibrium in about one hour. Therefore, for the annulus fibrosus which consists of 12 or more lamellae, the water diffusion process is expected to be rather slow. However, the exact proportion of diffusion along the spinal axis with respect to the diffusion in the radial direction in the disc is unknown. This expected anisotropy of diffusion is important for the understanding of the procedure by which water migrates in or out of the disc.

5. Discussion on the Experimental Procedures and the Errors Involved when Measuring the Disc's Mechanical Properties

A floor model INSTRON testing machine (Model TTB) was used in these experiments. The force measuring system uses load cells with an accuracy of $\pm$0.25 percent (in full scale), which could be reached if the internal voltage of the battery was held at 1 volt. This increases the stability of the recorded force. This step was necessary since it increases the stability of the recorded force and because some drift was noticed in the "balance" of the INSTRON.

Another source of error was due to the electronics of the INSTRON and could cause a drift in the "zero" of the recorded force. This error was eliminated by periodic zero adjustment and by calculating the correct zero position for each experiment. It was done by changing the scale of the force and then by matching the force values in both scales. In our experiments this error was found to be less than 2%. The speeds of the recorder chart were checked and found in good agreement with the specified ones. Similar checks were performed on the range of the force switch.

The crosshead provides a constant rate of specimen deformation independent of the load, with speeds varying from 0.02 in./min. to 20 in./min. However, the speed of the crosshead can't be achieved instantaneously, because of inertia, therefore there is always a lag of time in the response. This lag of time depends on the desired speed and makes the data for $t<0.01$ min. useless. Therefore, the INSTRON was restricted for 0.01 min.$<t<$1000 min. The upper limit is due to the drifts already discussed.

A problem that should be avoided is to achieve the maximum pen speed (full scale in 1.5 sec). This problem can be eliminated by a proper use of the force range switch.

The INSTRON tester used in our laboratory was equipped with a BEMCO environmental chamber. In this chamber the dry bulb temperature was measured using a copper-constantan thermocouple which was kept near the specimen for the case of moist-air environment and in a titanium well filled with silicone oil in the case of saline solution environment. The wet bulb temperature was obtained by wrapping the end of another copper-constantan thermocouple with a piece of wet cloth which was kept wet by immersing one end of the cloth in a container full of water. The dry and wet bulb temperatures of the environment were kept constant (dry bulb within $\pm.2^{\circ}$C and wet bulb within $\pm.5^{\circ}$C) over the duration of these experiments. This was done by circulating air of desired conditions generated and stored in the TENNEY environmental chamber. The large capacity of this environmental chamber allowed fast recovery in the changes of the conditions which occurred in the small BEMCO chamber when its door was opened. The transmission of the moist air from the TENNEY to

the BEMCO chamber and back to TENNEY was achieved by means of a PAR blower. The supply lines were plastic hoses properly insulated in order to minimize heat transfer problems.

The moist air current transmitted from the TENNEY to the BEMCO chamber hits the upper grip which holds the specimen and the wire that connects this grip with the load cell. It produced small oscillations in the force response. Although the effect of such oscillations was small, it was minimized by using appropriate buffers. These oscillations did not exist when saline solution environments were used.

From Figure 5.17 one can see that the dry and wet bulb temperature responses as well as the force response exhibit oscillatory behavior. Furthermore, one can see that the dry bulb oscillations had negligible effect in the force response to a step function of strain excitation. On the other hand, the wet bulb temperature oscillations affected the relaxation behavior rather significantly. The correspondence between the wet bulb temperature and the force response oscillations is clearly demonstrated in the same figure. We think that the force oscillations were due to the fact that the moisture variations produced dimensional changes, which for a specimen held at constant elongation resulted in stresses in it.

Since the amplitude of these oscillations was rather high, we attempted to reduce them by modifying the dry and wet bulb controllers of the TENNEY environmental chamber. However, this

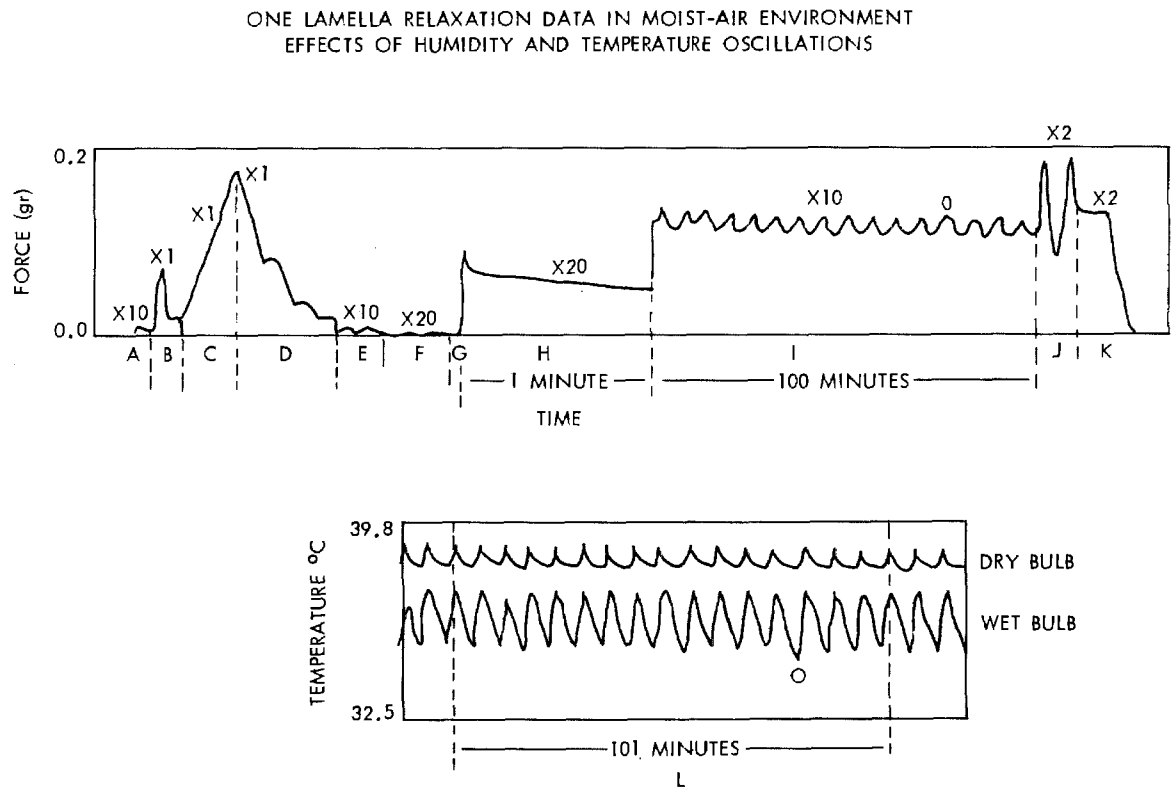

Figure 5.17. Raw Data* from the INSTRON Recorder and the Dry and Wet Bulb Measurements

modification did not reduce them significantly. Therefore since in our data these oscillations were always present, we had to uncouple them from the relaxation data. We achieved that by choosing as the starting point for all the experiments the lowest point of the oscillation since in the neighborhood of this point the force was approximately constant over the period of one to two minutes. The relaxation curve was thus constructed by connecting

---

*For more details regarding the meaning of A,B,C,...,K,L, See Appendix B

the lowest points of the oscillations, keeping in mind that the amplitude of the oscillations was always approximately constant.

The uncoupling of the oscillations is demonstrated in the Figure 5.18 where the uncoupled relaxation curve is shown by the dotted line.

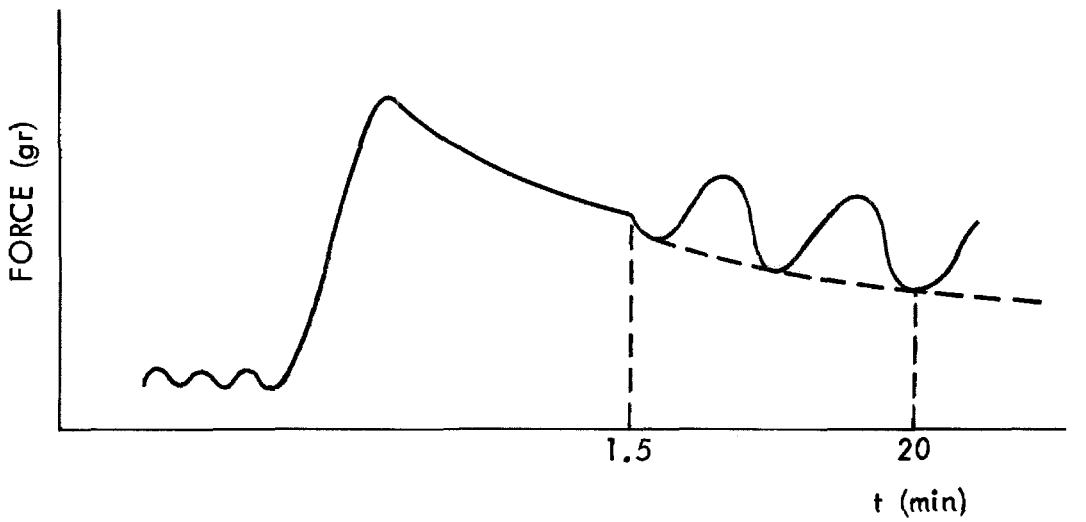

Figure 5.18. Uncoupling of the Relaxation Data

In the relaxation curve constructed in this way we think that the bump shown in Figure 5.19 was an experimental error (not a real data) and it was due to the existence of the oscillations. It occurred in the time inteval from 1.5 min to 20 minutes, its amplitude is probably due to the imperfection in the averaging procedure used and its position depends on the frequency of the oscillation.

We observed also that the volumetric changes due to swelling and deswelling caused by the changes of the environmental conditions produced a twisting in the specimen, thus

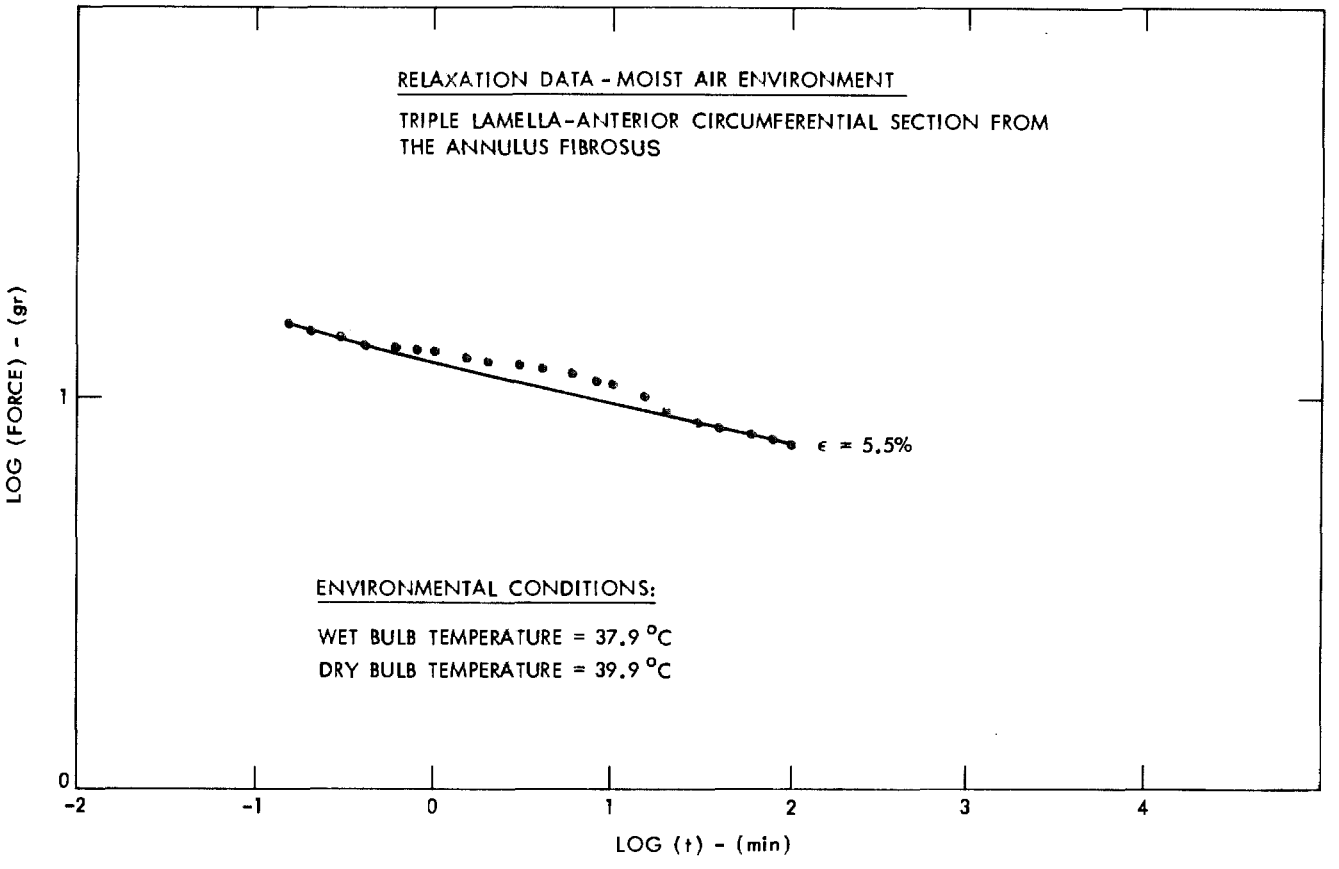

Figure 5.19. Relaxation Data with Bump

causing the upper grip to rotate with respect to the lower one. This rotation was possible because of the free rotating hinges which connected the upper grip with the load cell. We used the INSTRON crosshead displacement as a measure of the specimen's displacement. Since the specimen had a large length and a small cross sectional area, it could not withstand compressive forces without bending or buckling. This bending was detectable by a simple inspection and could be avoided by eliminating all compressive forces.

Furthermore, alignment problems occurred at the grips. We

minimized them by designing the grips appropriately. Part of the grip was made from plexiglass and in such a way so one can view the end of the specimen as it was gripped. Furthermore, at the center portion we had marks that enabled us to align the specimen during mounting. The surface of the grip in the area where the specimen was gripped had been serrated so that the specimen will not slip. However, this gripping procedure produced a squeezing of the specimen in the neighborhood of the gripping area accompanied by some twisting.

We minimize the end effects of the stress distribution in the specimen by making it narrow (1 or 2 mm. wide versus 10-20 mm. long) and by keeping the gripping area as small as possible.

An example of the differences possibly due to gripping effects is shown in Figure 5.27 and a brief review of the literature for the case of isotropic materials is given in References 62-64. These investigators considered the compression of a poker-chip (large diameter cylinder) and found by a detail stress-strain linear elastic analysis that:

(1) The end-effects introduced by the gripping depend on the aspect ratio (diameter/height for cylinders) and the higher the aspect ratio the higher the apparent modulus.

(2) This end-effect is a function of the Poisson ratio, and is more important for incompressible or near incompressible* (ν= 0.49 to 0.5) materials.

For the use of anisotropic composites of rectangular shape, work has been done by Pagano and Halpin (Ref. 65).

---

*The disc material is nearly incompressible, therefore, the end effect is important.

Since we had difficulties in producing specimens of absolutely uniform thickness, the cross-sectional area variations produced some inhomogenouity in the stress and strain fields. This error was unavoidable, and we had to use the average cross-section area. Furthermore, some significant errors in measuring the dimensions, or more specifically the thickness of the specimen, made the measurements of the cross section very difficult.

At this point we would like to discuss in some detail the measurement of the dimensions and the weight of the specimen.

The length and width were obtained by a ruler graduated in 0.01". The thickness was measured with a micrometer graduated in 0.0001". When measurements of dry specimens were performed, then due to the bending and twisting of the specimen, the dimensions could not be obtained accurately (estimated error: for length was $\pm$ 1%, for cross-sectional area was 40%, for width was $\pm$ 10%, and for thickness was $\pm$ 30 %). For a wet specimen the situation was better (estimated error: for length was $\pm$ 1%, for cross-sectional area was 30%, for width was $\pm$ 5%, and for thickness was $\pm$ 25%).

The weight was measured with a precision mechanical balance calibrated on 0.1 mgr. For the dry specimen the error was guessed to be $\pm$ 2%, for the wet specimen it was $\pm$ 4%, and was due to the existence of drops in the surface of the specimen and to diffusion effects.

Furthermore, we studied briefly the problems caused by the slipping of the specimen from the mechanical grips. When any of these problems occurred, it happened very fast. Therefore,

it was easy to detect from the force-time INSTRON recorder. In order to reduce the danger for the specimen to slip out of the grip, and at the same time minimize the chance to create an inhomogeneous stress-strain field in it, we had to use specimens with aspect ratios* of 1/5 to 1/10. However, we remark that for more accurate measurements this aspect ratio had to be reduced even further.

In a relaxation experiment, it is clear that the applied strain step function cannot be obtained experimentally. A reasonable approximation is a ramp function with an initially high rate of loading. The resulting response will, of course, deviate from that which would have been obtained if a true step function had been imposed (in the absence of material inertia). However, it can be shown that the two responses will differ by less than 1% for times $t \geq 10t'$, where t' is the time it took to achieve the constant strain. Thus, meaningful stress relaxation data can be taken after $10t'$.

We have noticed that when different specimens were used there was an appreciable scatter in the measured mechanical data. To reduce this scatter, we used the same specimen for a variety of tests.

Because of the viscoelastic nature of the material, the response obtained in a given experiment was affected by any previous deformation. In the absence of any permanent change

---

*Aspect ratio is defined to be the ratio between the area of the specimen fixed by the grip over the force area of the specimen.

in structure (i.e., due to oxidation), the longer the specimen was in the stress-free state between two experiments, the less was the effect caused by the previous experiment. Two ordering rules have been used:

1) tests requiring smaller deformations were made before those in which larger deformations were applied;

2) tests requiring longer times were made before those which extend to shorter times.

Furthermore, the time intervals, which were allowed between experiments, were never less than five times the duration of the previous experiment. Under these circumstances, the effect of the preceding experiment on the next one had been found, for some rubbery materials, to be within 1% (Ref. 34).

In addition to the previously discussed problems, damage (rupture) at the end of the specimen may occur. This is caused by the applied force due to gripping and it is important if repeated gripping is applied. We may also have ruptures due to excessive straining. We have reduced the possibility of this problem by performing experiments mostly at 5.5% strain and in few instances using higher strains.

We noticed that some rupture of the specimen occurred when it was left for a very long time (over a week) in deionized water. We observed that in this environment there were small strands of the specimen's material which had been separated from the specimen. We suspect that this was due to a rupture caused by excessive swelling of the material matrix. This rupture could be caused by

large internal stresses which developed during swelling. We minimized this problem by maintaining our specimens in saline solutions of relatively high concentration, thus reducing swelling.

Biochemical changes that led to an aging of the specimen during the experiments have been observed. These changes were probably caused by various types of chemical reactions; however, we think that oxidation (change in color) was the most probable source. We found that oxidation occurred only after prolonged exposure to high temperatures ($42\text{-}49^{\circ}$C) in moist air environment. No other changes were noticed either in moist air (below 42°C) or in saline solution (60-300 gr NaCl/1000 cc solution). It is possible that biochemical changes may occur in saline solutions (at high concentrations of NaCl) due to penetration of salt into the specimen but we have not observed such effects.

6. Results From the Relaxation Experiments and Discussion

We present here results obtained from the mechanical testing of specimens taken from the annulus fibrosus. The following types of specimens and environmental conditions have been used:

(a) Irregular specimen from the annulus fibrosus in air at room environmental conditions

(b) Single lamella specimen in moist air environment

(c) Triple lamella specimen in saline solution environment

(d) Triple lamella specimen in moist air environment

Furthermore, we report here some preliminary results obtained from an irregular specimen taken from the nucleus pulposus and tested in air at room environmental conditions.

a. Irregular Specimen in Air at Room Environmental Conditions

A number of short duration (~10 min.) relaxation experiments have been performed using a wet multi-lamella specimen of irregular geometry obtained from the anterior circumferential section. These experiments were performed under uncontrolled environmental conditions (i.e., the water content of the specimen was decreasing gradually) using the same specimen, the same gripping and the same step excitation of tensile strain (4%). Figure 5.15 shows the stress relaxation response to this excitation as a function of time for four such experiments. However, from this relaxation response only data obtained in the first two minutes were utilized for the construction of the master relaxation curve. This was due to the fact that the specimen started to dry at about two minutes (see the upswings in Figure 5.15) from the time of imposition of each step of strain.

It was observed that the changes which the water variations produced in the disc material were similar to the effect caused by solvents in synthetic polymers. In this case the solvent content effectively changes the glass transition temperature* of the material. As a result, the time dependence of the mechanical behavior was changed. This similarity was used to create the master relaxation curve shown in Figure 5.20.

---

*Temperature below which the thermal motions of the polymeric molecules essentially cease.

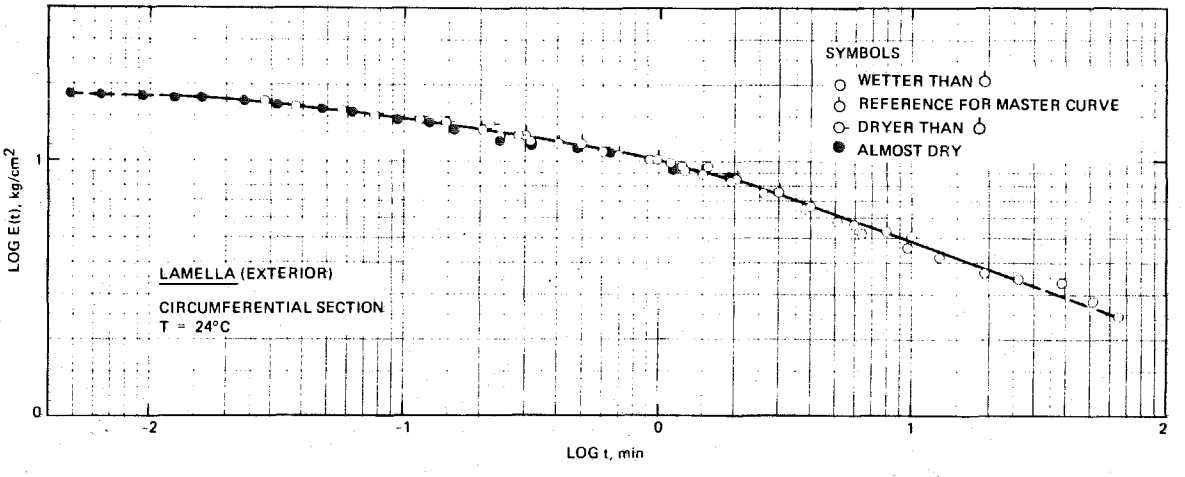

Figure 5.20. Relaxation Master Curve

From these data (Figure 5.15) we observed that the visco-elastic mechanical propeties of the specimen were sensitive to its water content. Furthermore, these data indicated that this uncontrolled environment approach can be used to obtain a master relaxation curve. Its advantage is that the water content can be freely chosen. However, if this approach is to be utilized in any future work, an accurate calibration of the specimen's water content as a function of time is necessary.

b. Single Lamella Specimen in Moist Air Environment

In these experiments a single lamella specimen of orthogonal parallelepiped shape obtained from the anterior circumferential section (AC) of the annulus fibrosus was used (Fig. 5.8). The specimen was first dried, weighed and subsequently placed inside the moist air controlled environment of the BEMCO environmental chamber until equilibrium was reached. Then the dimensions and the weight of the specimen were obtained.

Three sets of simple tension relaxation experiments were performed, at various strains and environmental conditions, by pulling the same specimen in the length (circumferential) direction. Each one of the first two sets (Figures 5.21 and 5.23(a) was obtained by using the same gripping (for each set) and the same environmental conditions, but varying the strains. The third set was performed by using the same grippings, but varying the environmental conditions and the strains too. However, since for each set we regripped the specimen, we introduced large errors in the absolute value of the relaxation data.

Figure 5.21 presents refined data (all the known errors have been appropriately incorporated) obtained from the first set of experiments.

We observed (Figure 5.21) that since these curves are parallel the time and strain effects can be separated.

$$\sigma(t) = f(t).g(\varepsilon) \qquad (2)$$

This implies that the time dependent behavior of the material f(t) is independent of the applied strain (Refs. 37 and 66). However, because of experimental errors (mainly gripping) and difficulties in the cross-sectional area measurements, only the shape of f(t) can be obtained accurately from the log (stress) versus log (time) plot and not its absolute value. Furthermore, again due to the gripping errors, the reference state ($\sigma = 0$, $\varepsilon = 0$) could not be determined accurately. Consequently, the determination of $g(\varepsilon)$ involves a large error.

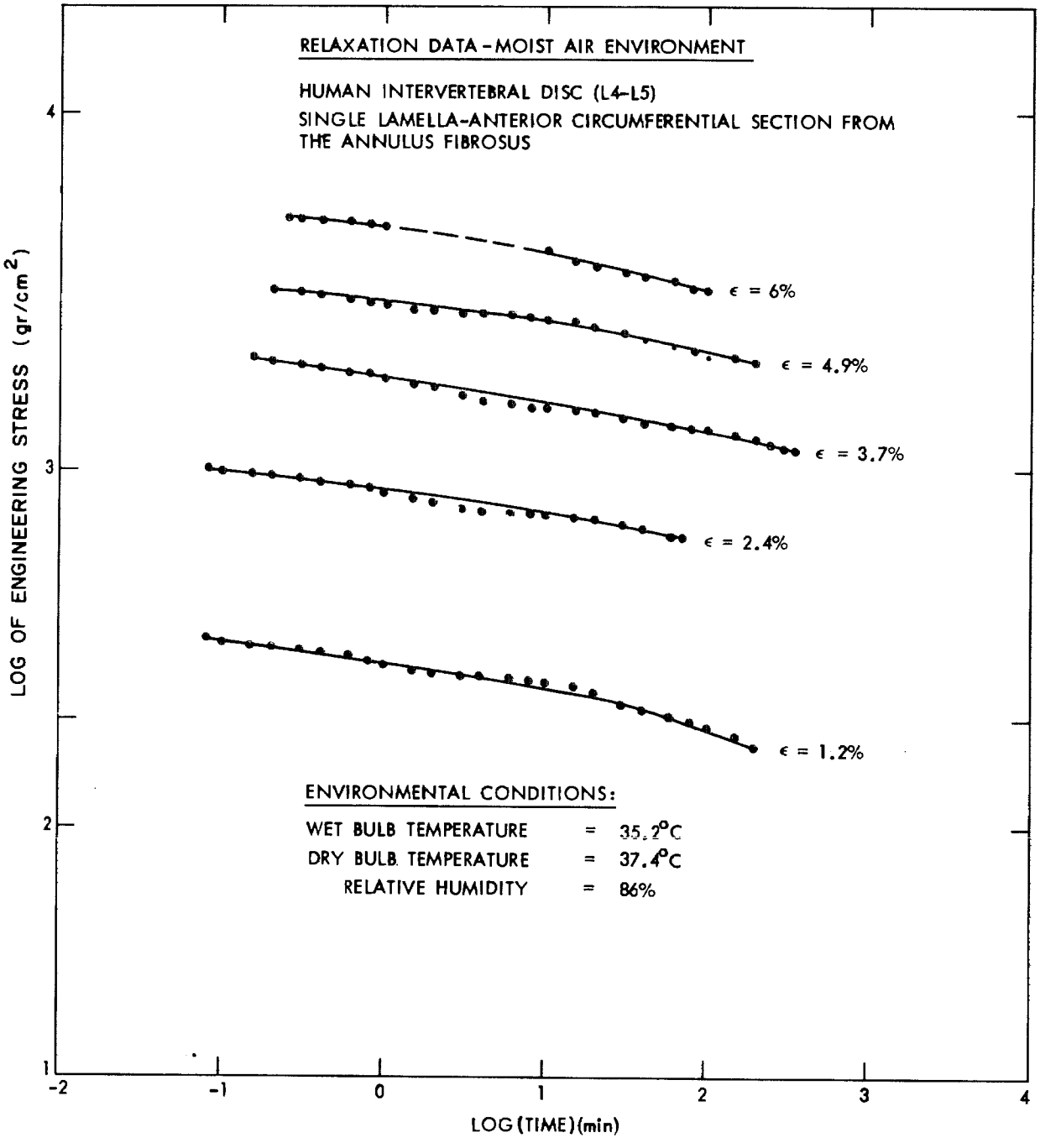

Figure 5.21. Single Lamella Relaxation Data

Based on the data presented in Figure 5.21, the isochronal stress-strain curve presented in Figure 5.22 was obtained.

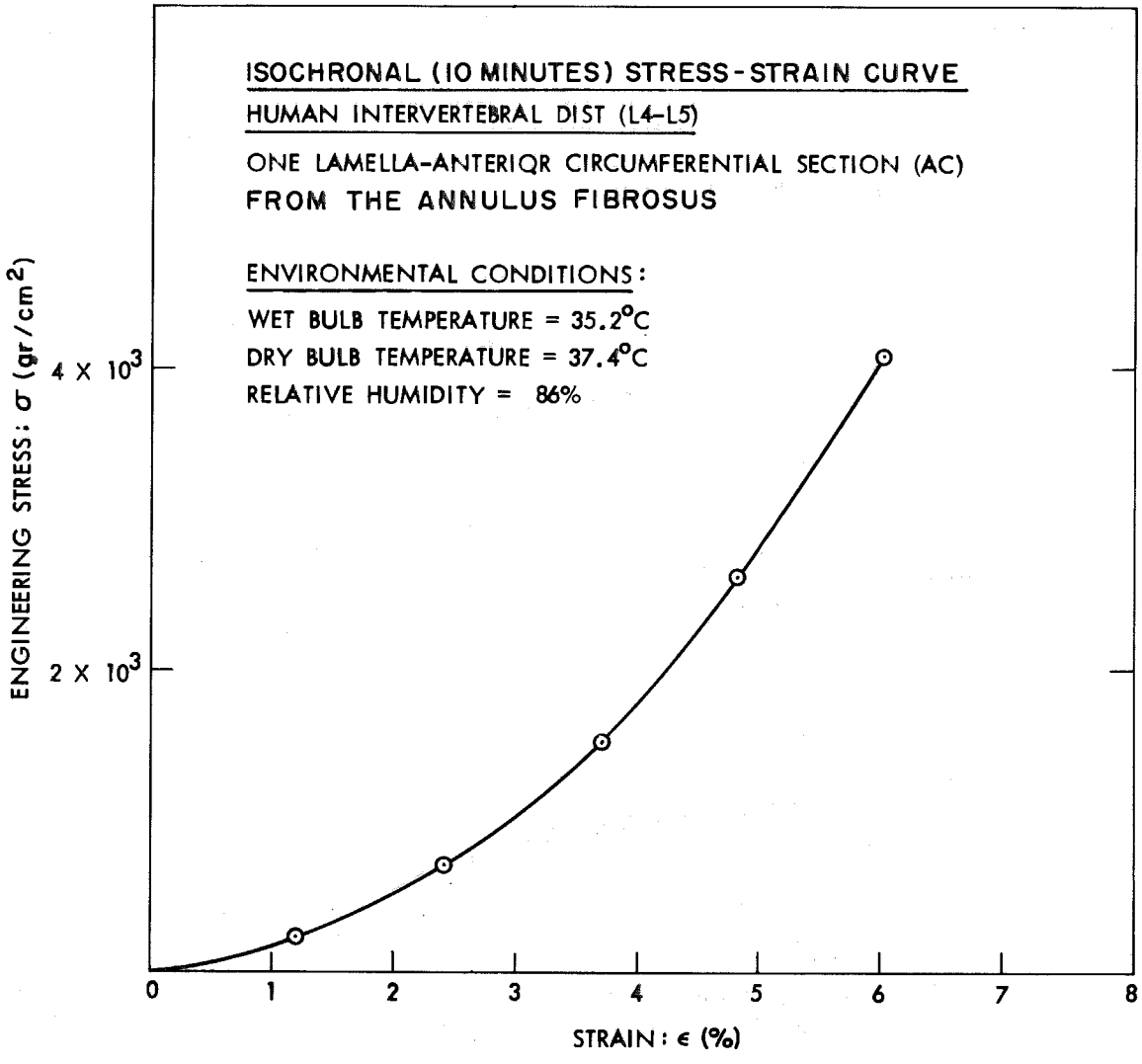

Figure 5.22. Isochronal Stress-Strain Curve

This curve shows that the stress-strain nonlinearities are significant.

At this point it is interesting to discuss the observation that the amplitude of the oscillations at the "reference or undeformed" state is smaller than the amplitude in the "deformed or stretched" state (Figure 5.17). The difference in amplitude can be explained by the nonlinear stress-strain law which holds for

this material. In other words, for changes in conditions near the reference state, we deal with an apparent modulus which is low compared to the apparent tangent modulus for the pre-stretched materials, which is high. We confirm this by imposing small ramps in both the reference (initial) state and in the stress (final) state (ε = 3.37%). We apply these ramps at the lowest point of the oscillations. From the original data presented in Figure 5.17 we can immediately observe that the modulus ratio of these ramps (4.38) is about the same as the amplitude ratio (4.37) of these oscillations. Furthermore, the same ratios were obtained from the stress-strain curve (Figure 5.22).

Furthermore, we remark that the relaxation data shown in Figure 5.21 cover only a narrow experimental time window of about three decades (0.1 min - 100 min). However, since we want to cover the useful time range in which the human body operates (i.e., milliseconds to a day or more, which is about eight decades), relaxation data are needed for a longer time window.

In order to cover these time requirements we combined similiar results obtained at various environmental conditions, using the fact that the water content in the specimen shifts the relaxation phenomena (Section III-5). This shift can be expressed by the following equation:

$$f(t;Co) = f\left(\frac{t}{a};\ C_1\right) \qquad (3)$$

which indicates a horizontal shifting of a curve in the log (a_c)

which indicates a horizontal shifting of a curve in the log (a_c) versus log (t) plot along the time axis. This leads to a superposition of the relaxation data obtained at different concentrations.

Based on these ideas and by making use of the data obtained from the other two sets of relaxation experiments (Figure 5.23), the relaxation curve (Fig. 5.24) was constructed. We observed that the master curve covers a section in the glassy region. The horizontal shift factor (a_c) versus the absolute humidity is given in Figure 5.25. Although the water content of the specimen was not measured for each environmental condition used, this curve still gives some representation of the water interaction with the internal relaxation phenomena and indicates the significant effect* of the water in the relaxation process.

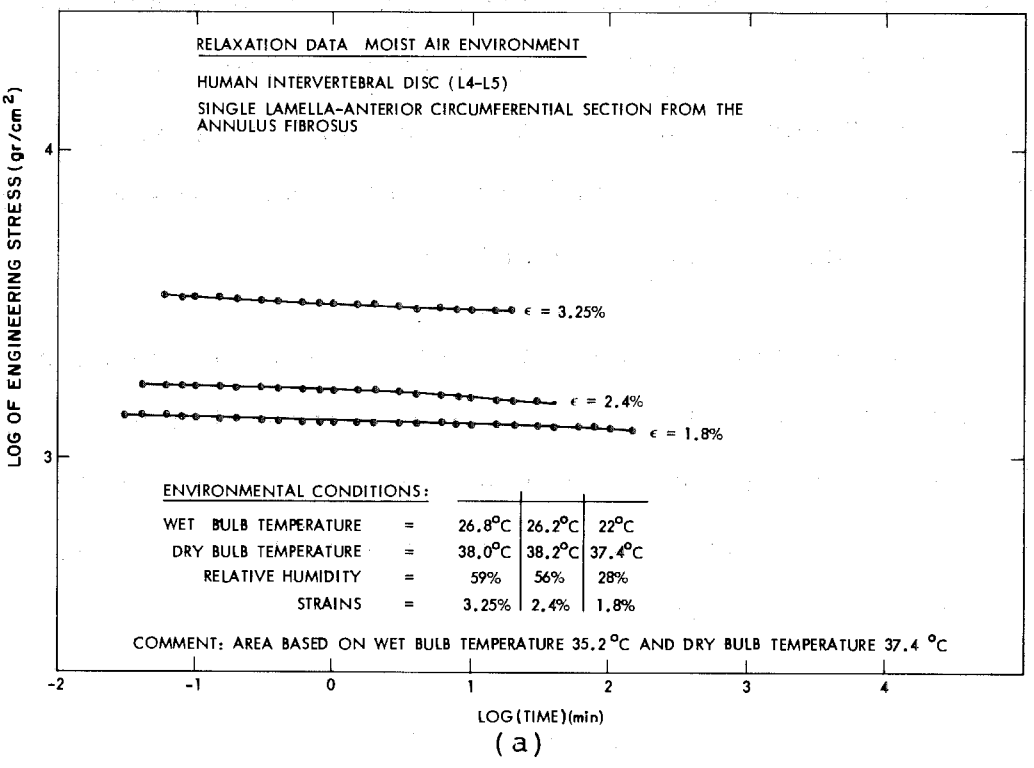

Figure 5.23. Relaxation Data at Various Environmental Conditions

*This effect is more clearly shown in the following relaxation experiments.

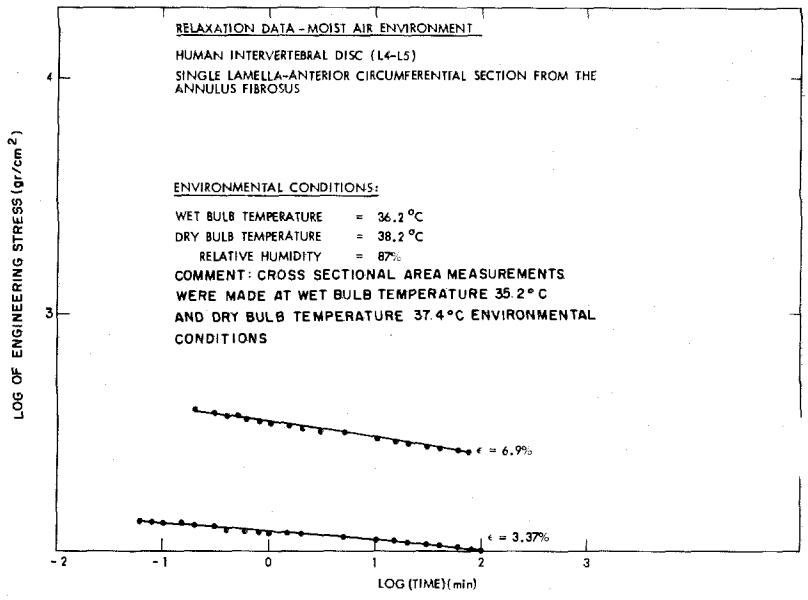

(b)

Figure 5.23. Relaxation Data at Various Environmental Conditions

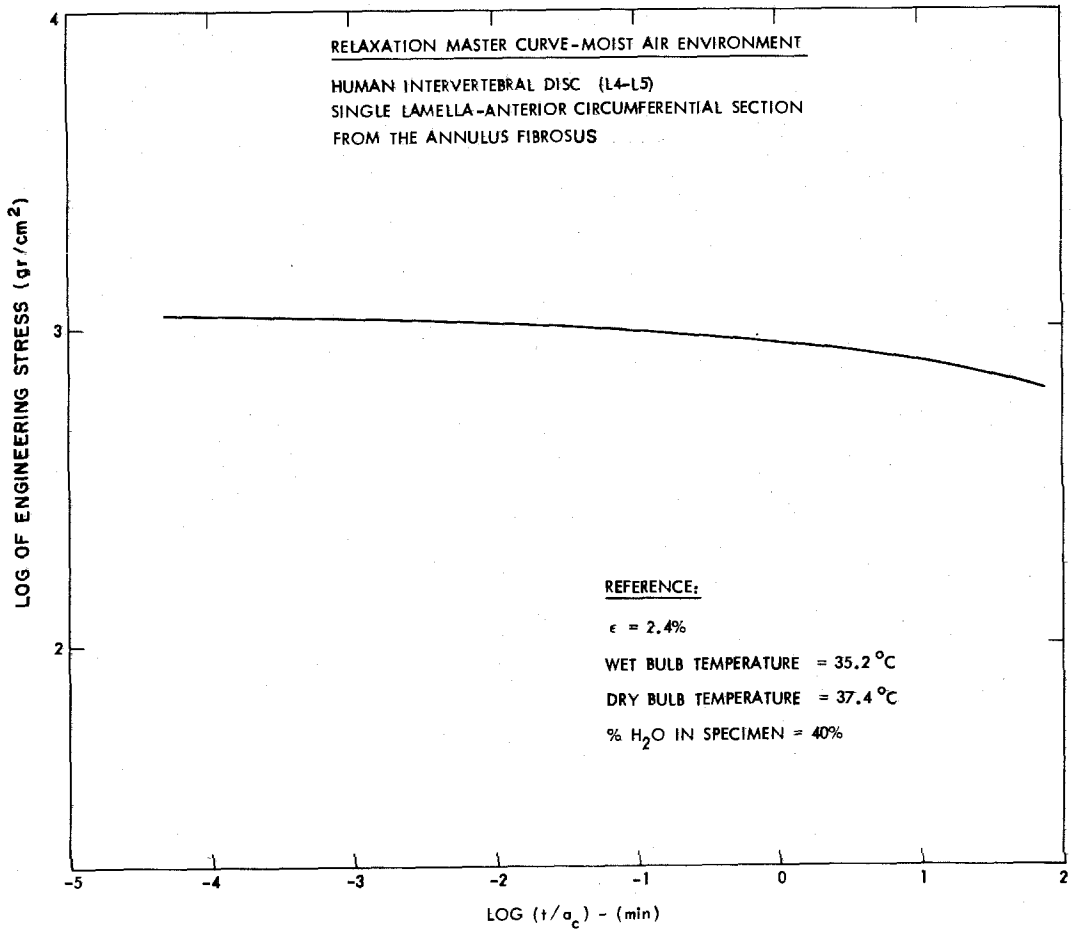

Figure 5.24. Master Relaxation Curve

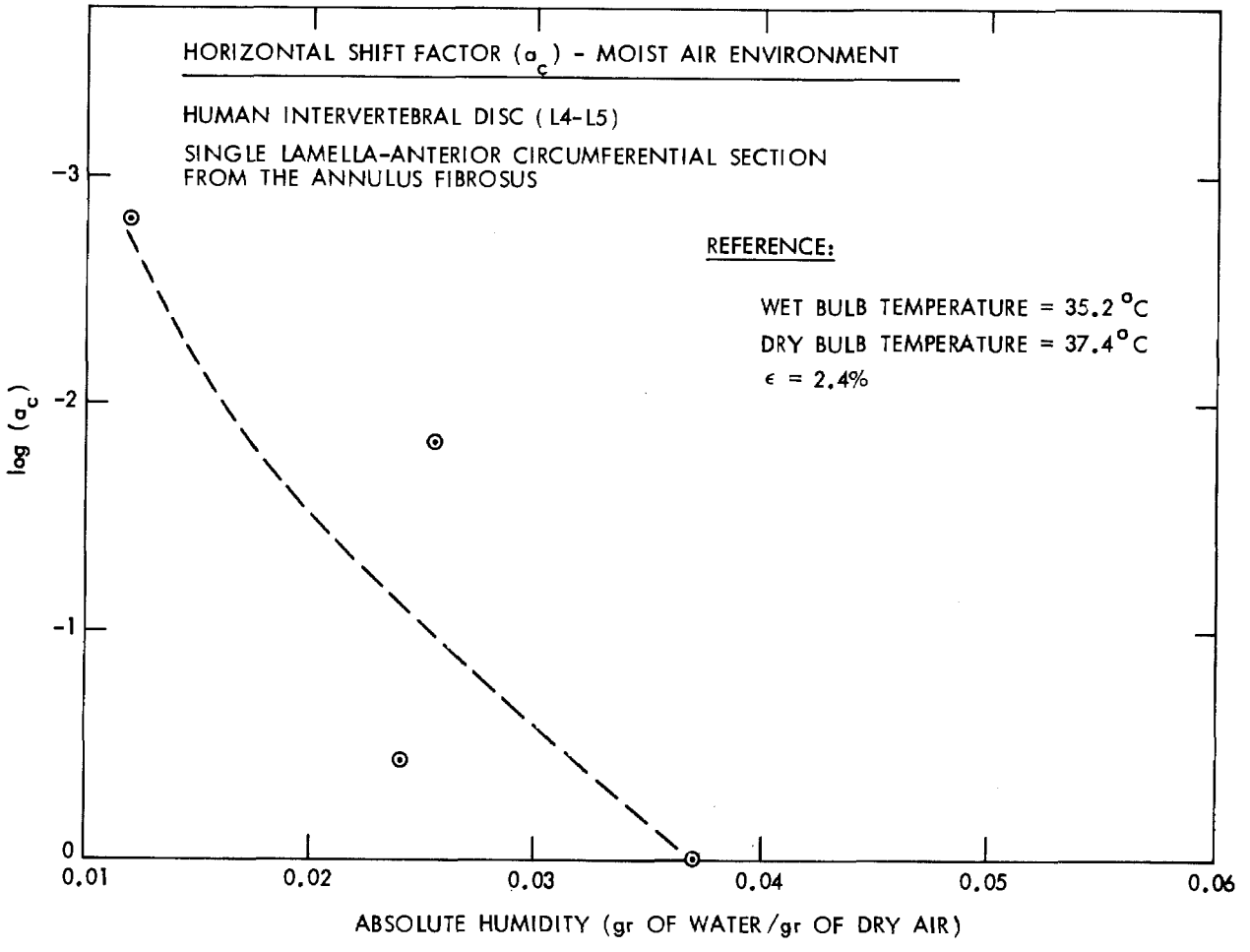

Figure 5.25. Horizontal Shift Factor

c. Triple Lamella Specimen in Saline Solution Environments

Four sets of simple tension relaxation experiments have been performed using a triple lamella specimen. The specimen was approximately of orthogonal parallelelepiped shape and was obtained from the anterior circumferential section (AC) of the annulus fibrosus (Figure 5.8).

These experiments have been performed in three saline solution environments (i.e., 60, 180 and 300 gr NaCl/1000 cc solution) around 38°C and with the specimen almost in equilibrium or in equilibrium with its environment. Furthermore, each of the

sets was carried out using the same gripping but varying the strains. The relaxation data and the corresponding environmental conditions for these experiments are presented in Figures 5.26(a), (b), (c) and (d).

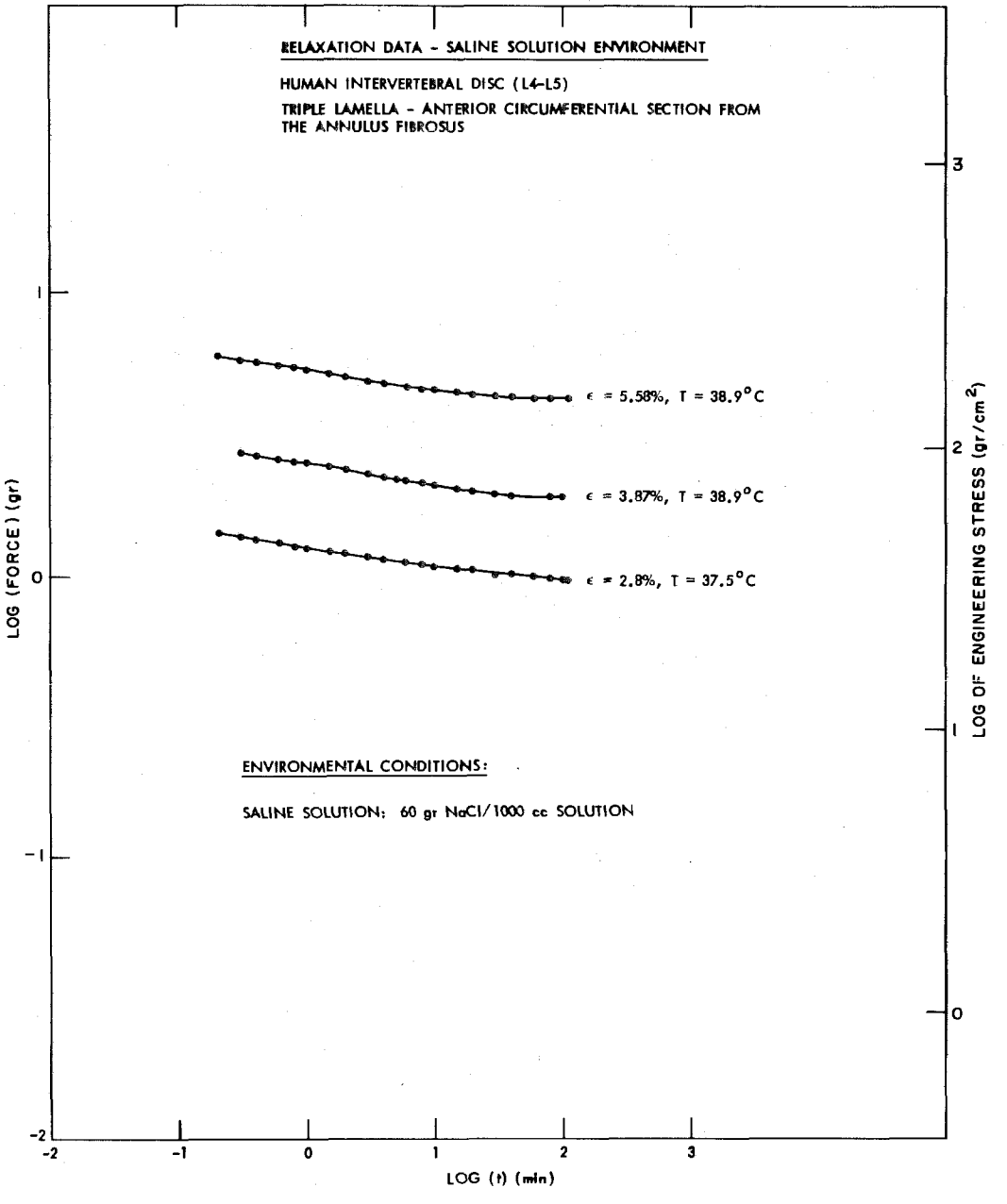

(a)

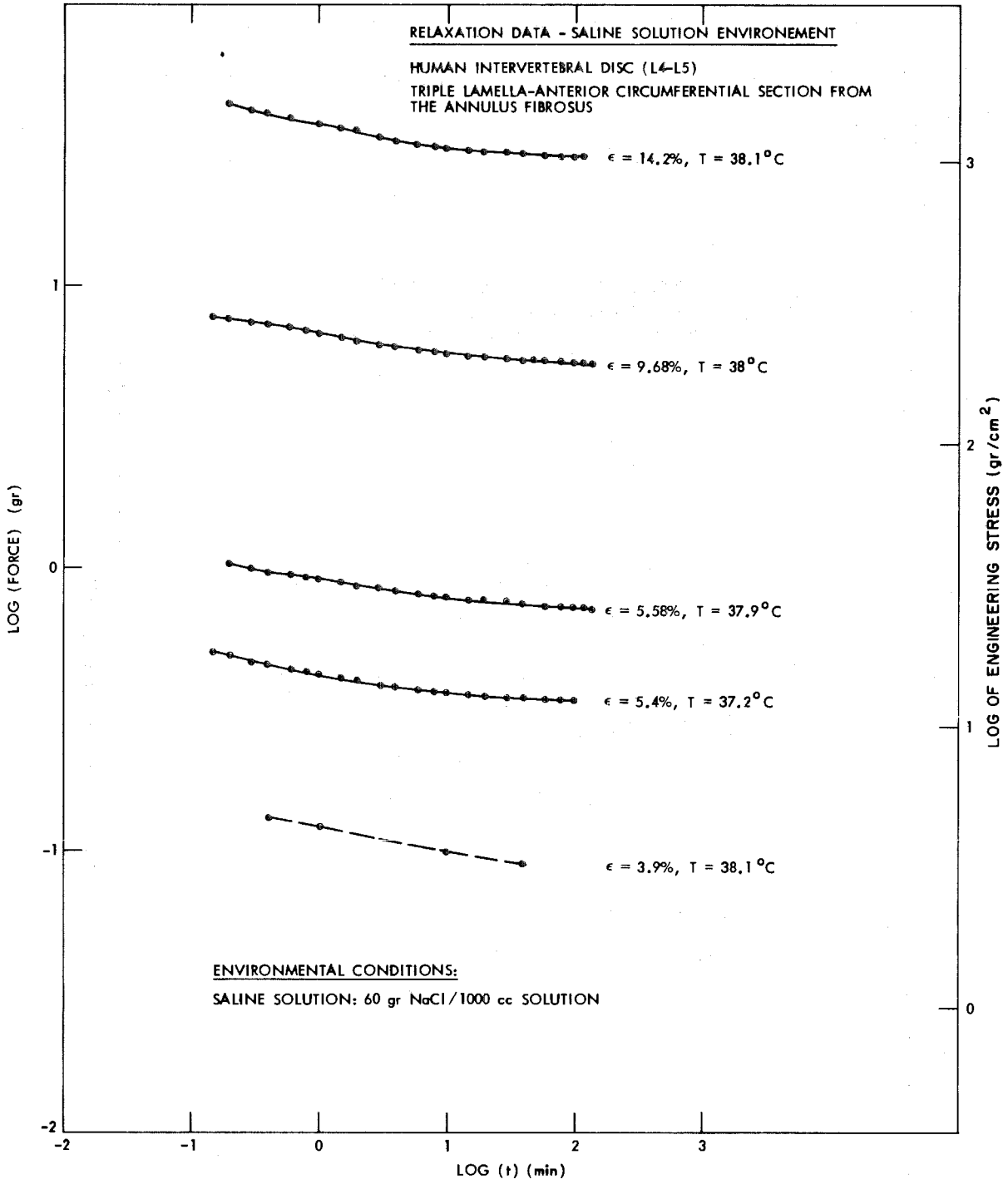
RELAXATION DATA - SALINE SOLUTION ENVIRONEMENT
HUMAN INTERVERTEBRAL DISC (L4-L5)
TRIPLE LAMELLA-ANTERIOR CIRCUMFERENTIAL SECTION FROM THE ANNULUS FIBROSUS
ε = 14.2%, T = 38.1°C
ε = 9.68%, T = 38°C
ε = 5.58%, T = 37.9°C
ε = 5.4%, T = 37.2°C
ε = 3.9%, T = 38.1°C
ENVIRONMENTAL CONDITIONS:
SALINE SOLUTION: 60 gr NaCl/1000 cc SOLUTION
LOG (FORCE) (gr)
LOG OF ENGINEERING STRESS (gr/cm²)
LOG (t) (min)
-2
-1
0
1
2
3

(b)

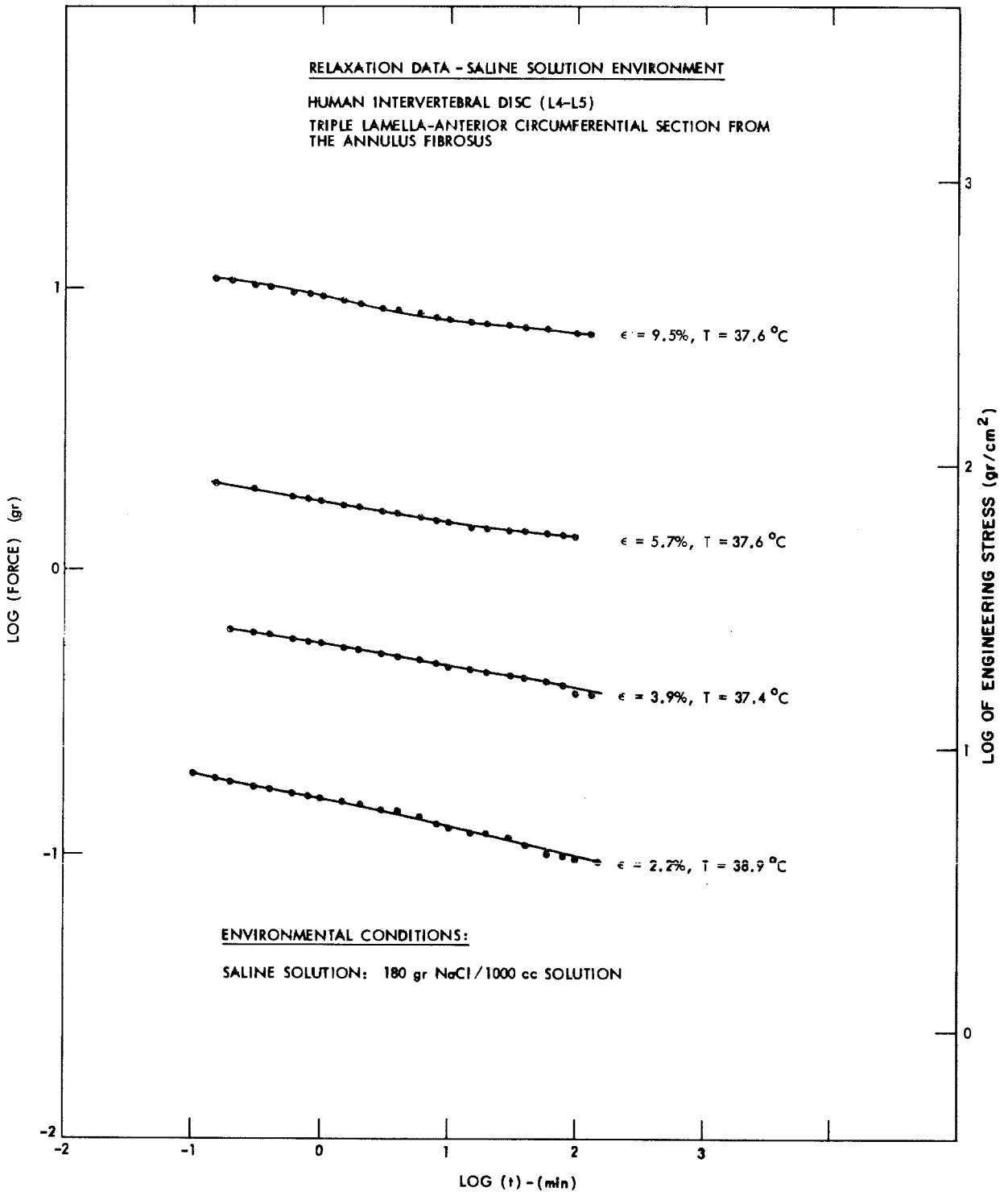
RELAXATION DATA - SALINE SOLUTION ENVIRONMENT
HUMAN INTERVERTEBRAL DISC (L4-L5)
TRIPLE LAMELLA-ANTERIOR CIRCUMFERENTIAL SECTION FROM THE ANNULUS FIBROSUS
ε = 9.5%, T = 37.6 °C
ε = 5.7%, T = 37.6 °C
ε = 3.9%, T = 37.4 °C
ε = 2.2%, T = 38.9 °C
ENVIRONMENTAL CONDITIONS:
SALINE SOLUTION: 180 gr NaCl / 1000 cc SOLUTION
LOG (FORCE) (gr)
LOG OF ENGINEERING STRESS (gr/cm²)
LOG (t) - (min)
-2
-1
0
1
2
3

(C)

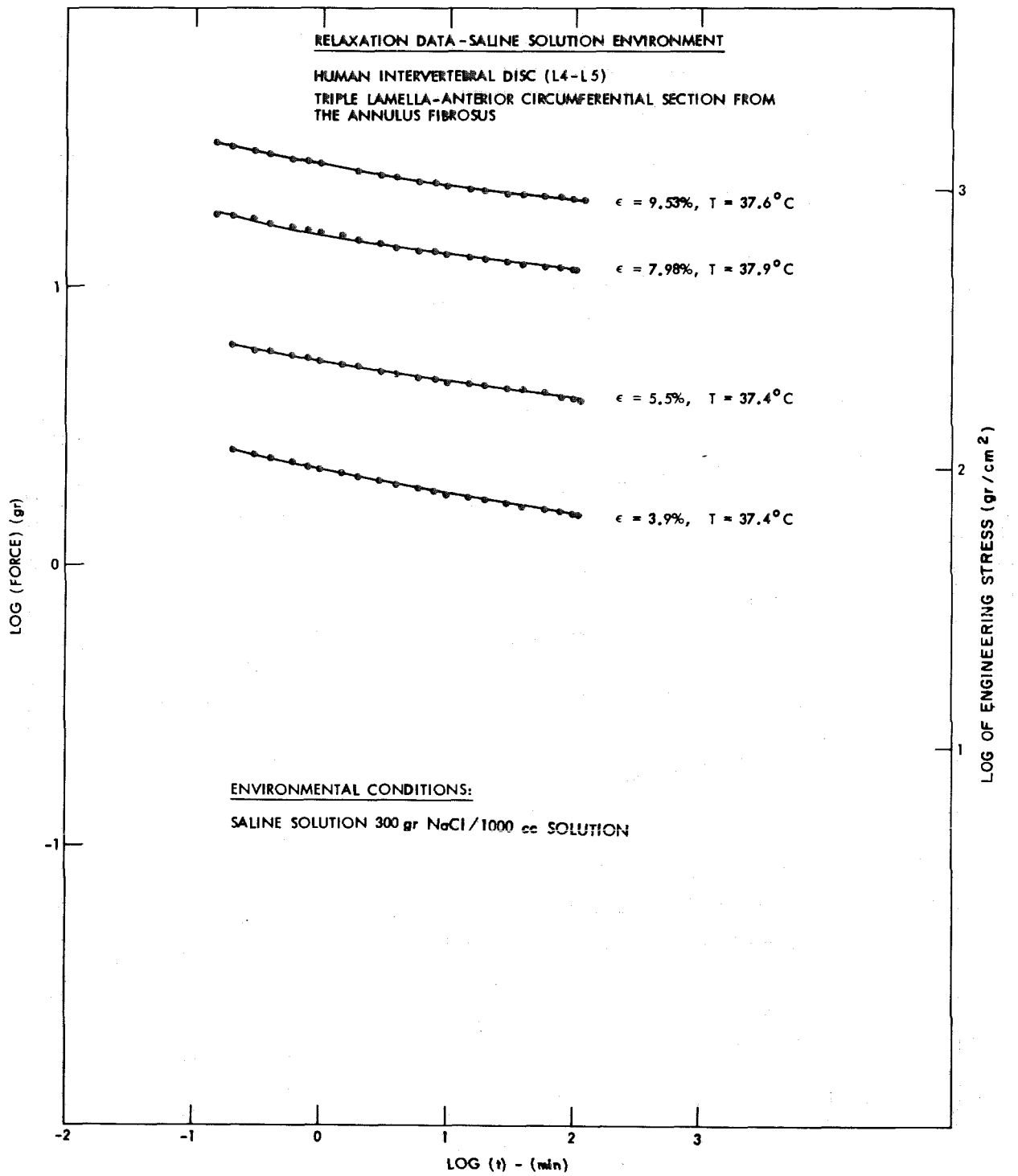

(d)

Figure 5.26. Relaxation Data for Various Saline Solution Environments

It is immediately apparent that time and strain effects can be separated. This is similar to what was observed for the single lamella case in the moist air environment. Based on these data, the following isochronal stress-strain curves were obtained (Figure 5.27).

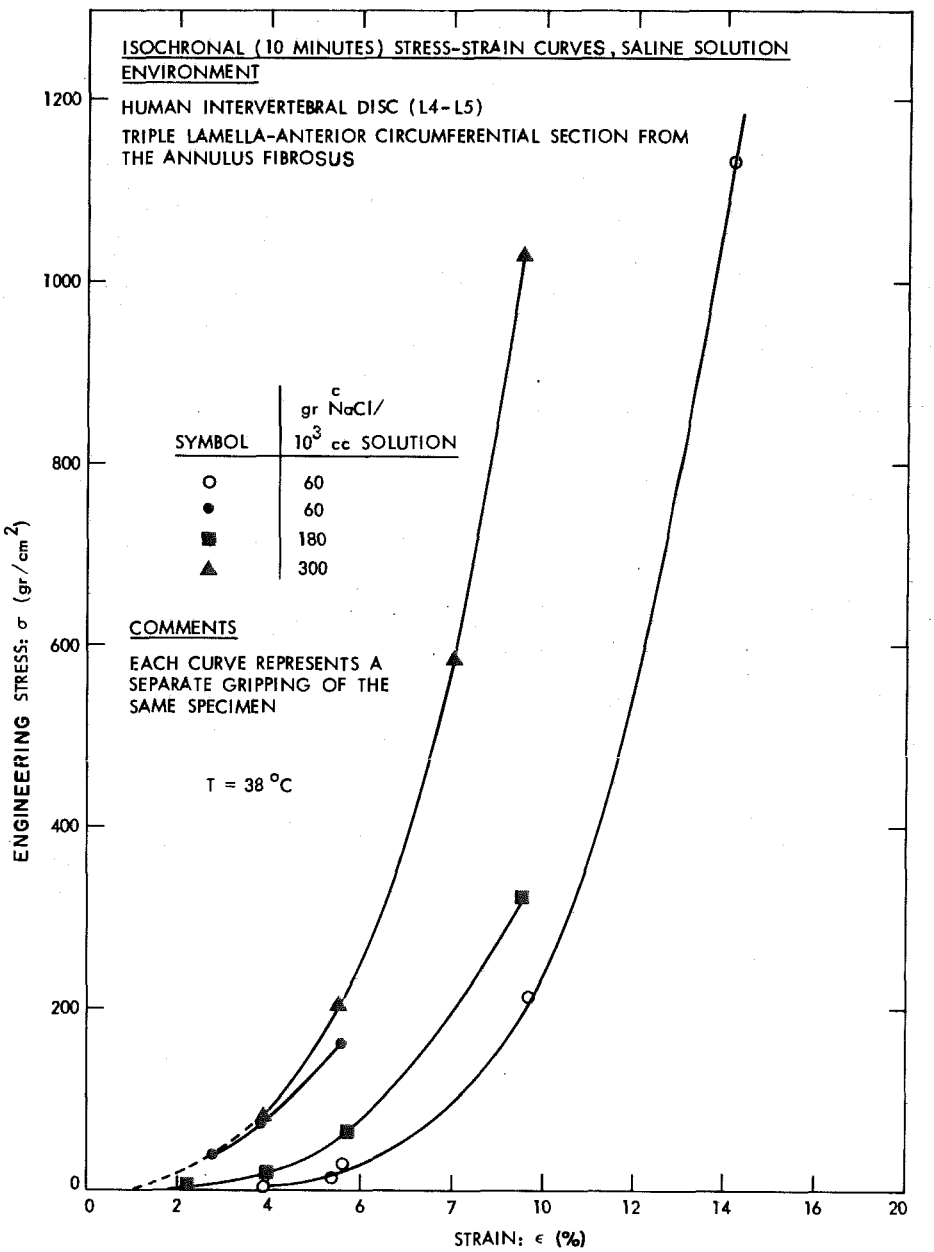

Figure 5.27. Isochronal Stress-Strain Curves

We observed that the stress-strain curves for the two experiments performed under the same environmental conditions (60 gr NaCl/1000 cc solution) were significantly different (in spite of the fact that they are supposed to be almost identical). The difference is due to the fact that for each experiment a different gripping was applied to the same specimen. However, the two curves could be superimposed if large horizontal and small vertical shifts were applied. This clearly demonstrates the importance of the gripping error; furthermore, it shows that this gripping error is mainly a shift in the reference state ($\sigma = 0, \varepsilon = 0$). In addition, the strong non-linear behavior of the material is shown in Figure 5.27. Based on these relaxation data, the relaxation master curve* shown in Figure 5.28 was constructed.

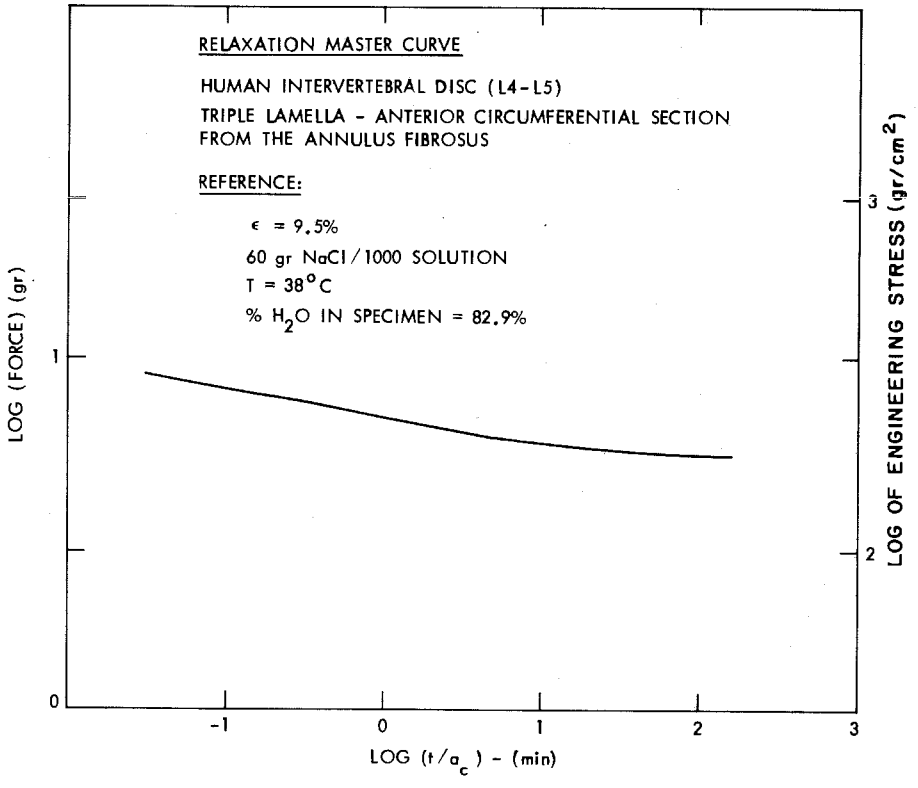

Figure 5.28. Relaxation Master Curve for Saline Solution Environments

*The shape and not the absolute value of the relaxation curve is obtained in this work.

We notice that the data presented by this relaxation curve are in the rubbery state. This was expected because of the large amount of water present in the specimen.

The horizontal shift factor (a_c) plotted versus the percentage of water in the specimen is presented in Figure 5.29.

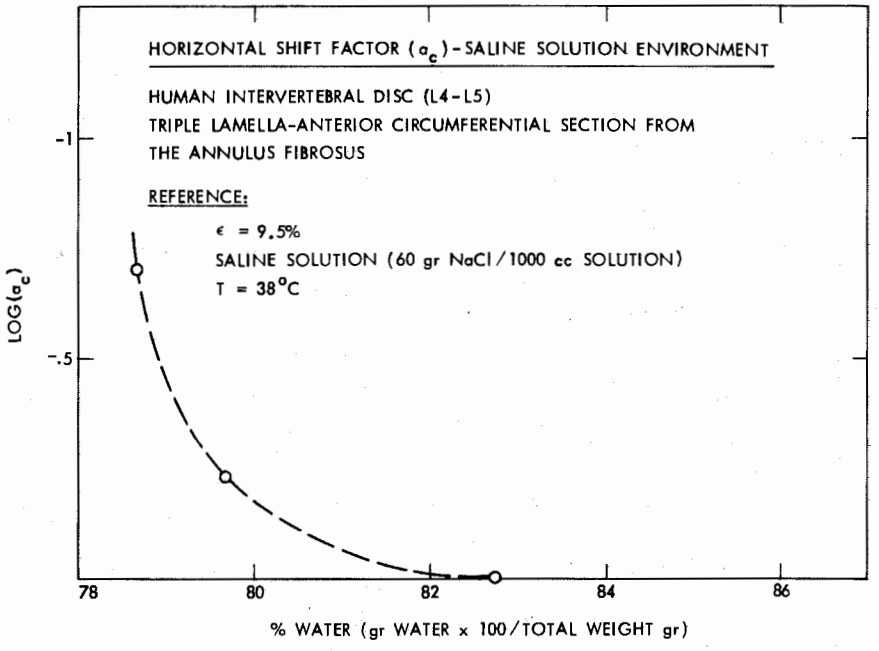

Figure 5.29. Horizontal Shift Factor for Saline Solution Environment

The reference state for both the master relaxation and the horizontal shift curves was above body conditions* (82.9% water content).

d. Triple Lamella Specimen in Moist Air Environment

A series of simple tension relaxation experiments were performed using the same triple lamella specimen as the one used in (c). These experiments were carried out using the same gripping, the same strain (ε= 5.5%) but varying the temperature and humidity environmental conditions (the range of absolute humidity covered

*Body condition corresponds to about 70% water content

was: 0.0275 - 0.076 gr of water/gr of dry air). In the course of these experiments measurements of the cross sectional area of the specimen as a function of the various environmental conditions have not been performed. This was done in order to minimize the large errors caused by the regripping of the specimen. The relaxation data obtained from these experiments are presented in Figures 5.30(a) and 5.30(b).

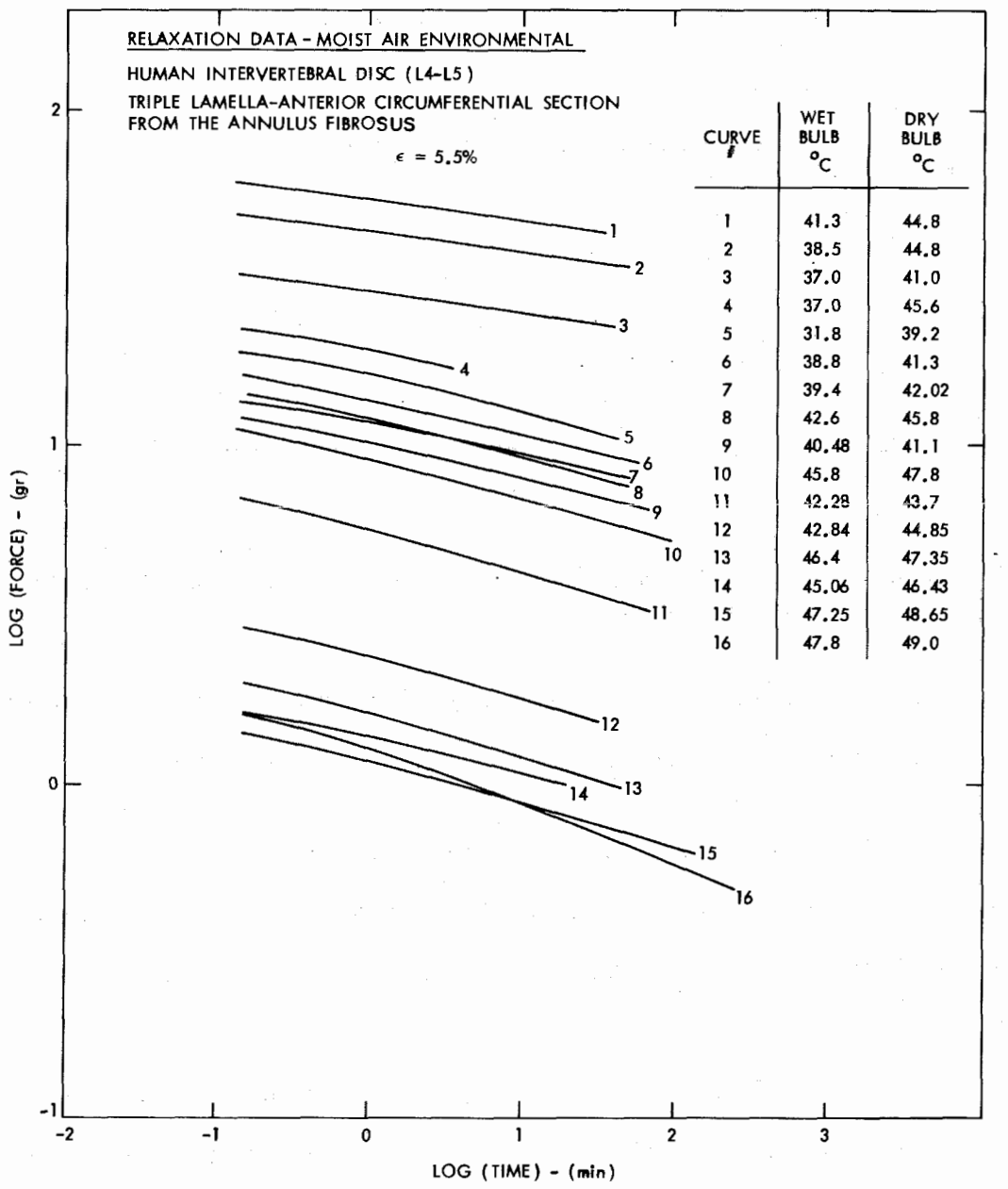

CURVE #	WET BULB °C	DRY BULB °C
1	41.3	44.8
2	38.5	44.8
3	37.0	41.0
4	37.0	45.6
5	31.8	39.2
6	38.8	41.3
7	39.4	42.02
8	42.6	45.8
9	40.48	41.1
10	45.8	47.8
11	42.28	43.7
12	42.84	44.85
13	46.4	47.35
14	45.06	46.43
15	47.25	48.65
16	47.8	49.0

(a)

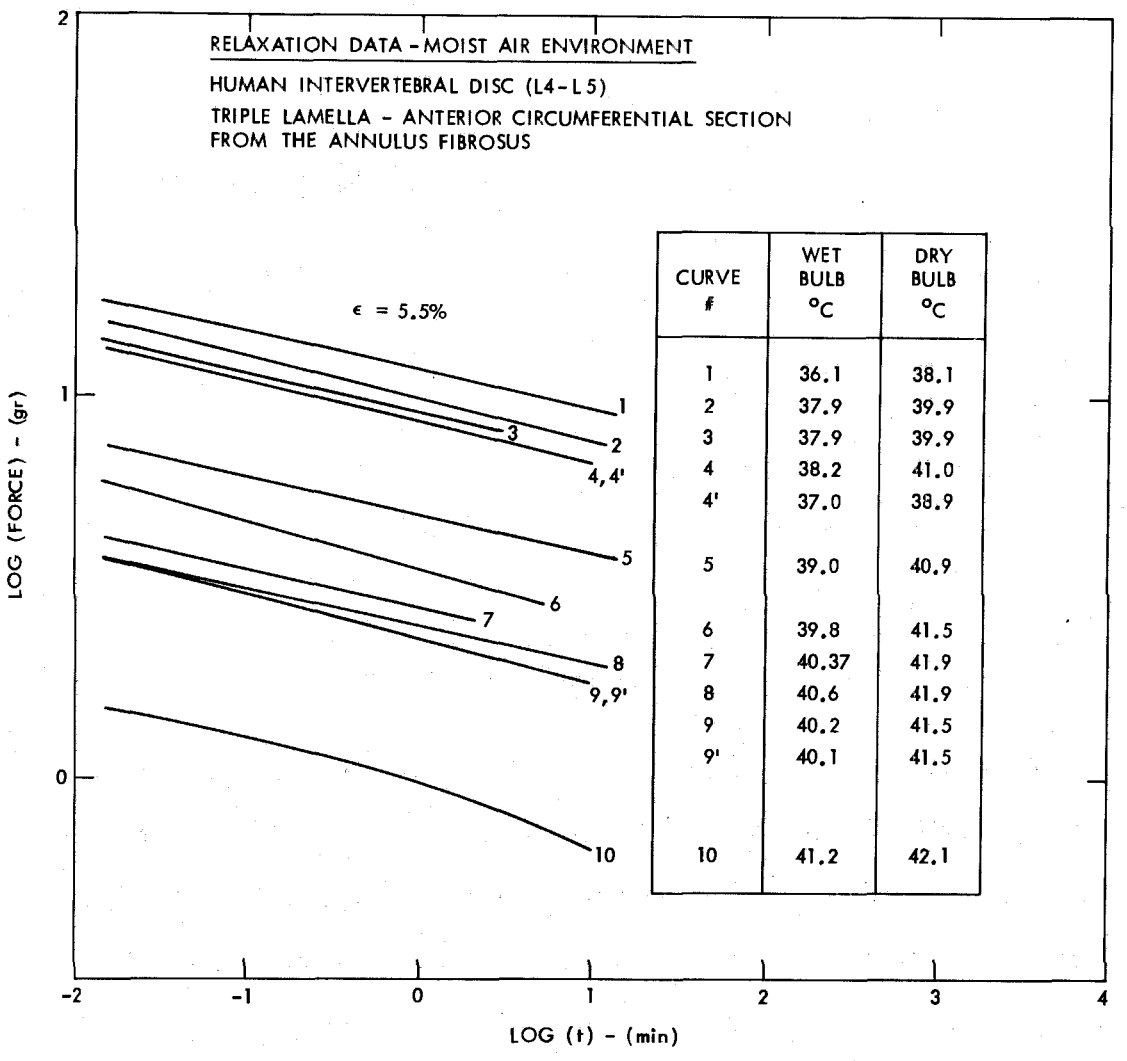

CURVE #	WET BULB °C	DRY BULB °C
1	36.1	38.1
2	37.9	39.9
3	37.9	39.9
4	38.2	41.0
4'	37.0	38.9
5	39.0	40.9
6	39.8	41.5
7	40.37	41.9
8	40.6	41.9
9	40.2	41.5
9'	40.1	41.5
10	41.2	42.1

(b)

Figure 5.30. Relaxation Data for α Triple Lamella Specimen in Moist Air Environment

Subsequently, we constructed the relaxation master curve* shown in Figure 5.31 by means of horizontal shifts of the relaxation data presented in Figures 5.30(a) and 5.30(b).

*The cross-sectional area on which the relaxation master curve was based was estimated on the basis of weight, length, and width measurements of the specimen at 46% water content and by assuming that its density is about 1.1 gr/cm3 since we know that the specimen is more dense than all the saline solutions used.

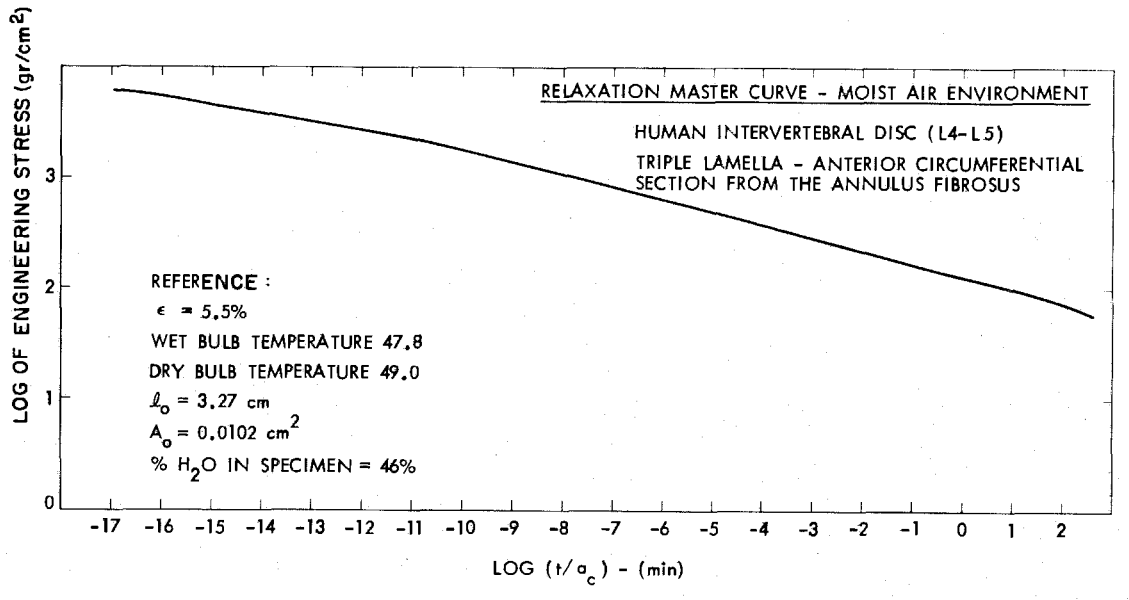

Figure 5.31. Relaxation Master Curve of Triple Lamella Specimen in Moist Air Environment

We observed that the data presented here belong to the transition region of the relaxation curve which seems to be rather broad for this material. The reference state of the relaxation master curve was based on the highest absolute humidity data available (wet bulb temperature = 47.8°C, dry bulb temperature = 49°C and 46% water) in the specimen which is still less than the 70% water content encountered in the human body's disc. Therefore, all the data in this region correspond to times shorter than the ones encountered in the normal operation of the human body (i.e., sitting, walking, jogging).

In the next figure (Figure 5.32) we present the horizontal shift factor (a_c) plotted versus the absolute humidity in the environment. We note that the scattering of the data is visualized in this figure and not in the relaxation master curve. This figure shows how the absolute humidity in the environment controls the relaxation process of this material.

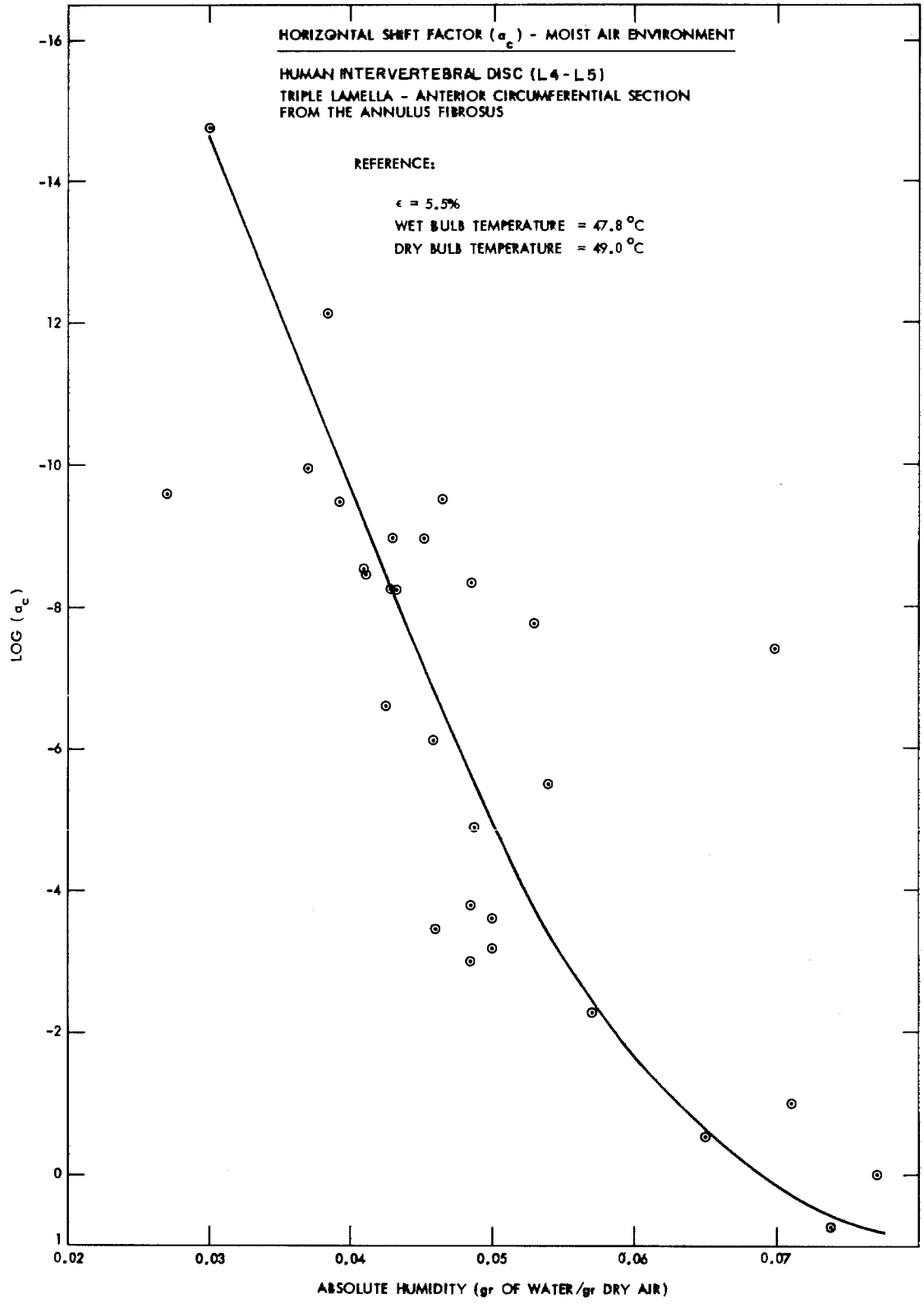

Figure 5.32. Horizontal Shift Factor for Triple Lamella Specimen in Moist Air Environment

At this point we examined the importance of temperature effects in the relaxation behavior as compared to similar effects caused by the concentrations. In order to do that the following two figures (Figures 5.33(a) and 5.33(b) are presented. We observed that in spite of the large scattering of the data, the effect of moisture (wet bulb temperature) is more significant than the one of temperature (dry bulb temperature). Furthermore, since the relaxation data (Figures 5.30(a) and 5.30(b) are parallel, the behavior of the material can be expressed by the following equation.

$$F(t,c) = f(t).G(c) \qquad (4)$$

where:

F(t,c) is the force

f(t) is a function of time, and

G(c) is a function of concentration

This empirical relation was based only on the fact of the parallelity in the relaxation data (Figures 5.30(a) and 5.30(b). We speculate that this parallelity may be due to the rather broad transition region of this material (Figure 31). The determination of the function G(c) could not be done from the isochronal plot presented in Figure 5.34 because of the large scattering of the data. If this were not the case, it could give a direct estimation of how the absolute humidity changes affected the properties of the material. Note that the same information could be obtained by analyzing the data in Figures 5.31 and 5.32.

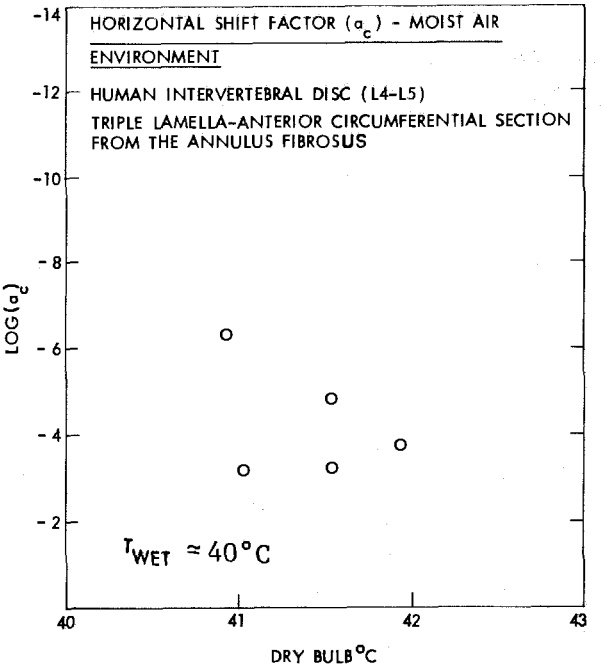

(a)

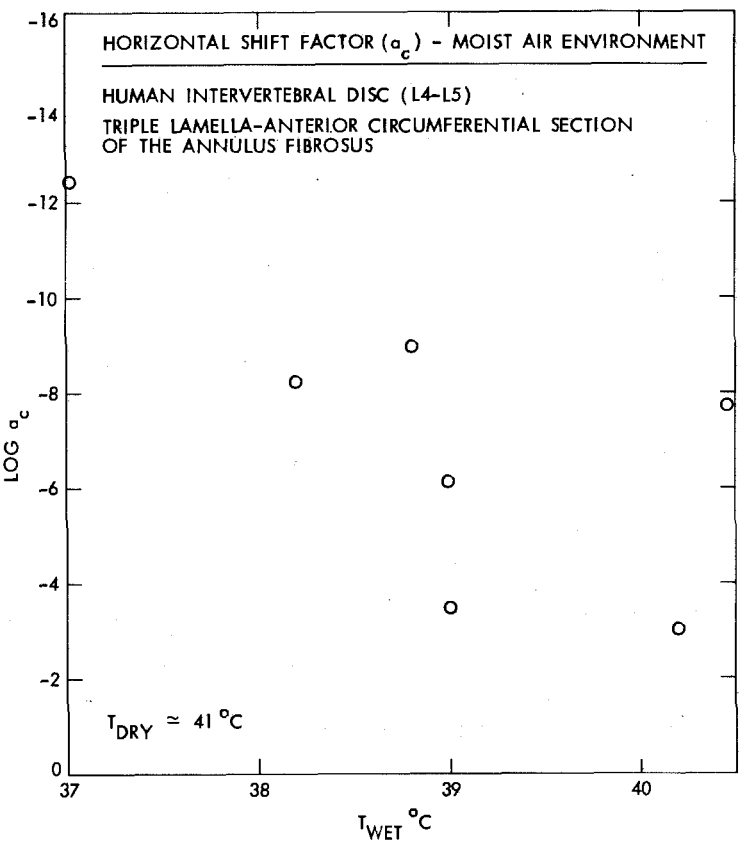

(b)

Figure 5.33. Horizontal Shift Factor (a_c)
(a) As Function of Dry Bulb Temperature for T_{wet} = constant
(b) As Function of Wet Bulb Temperature for T_{dry} = constant

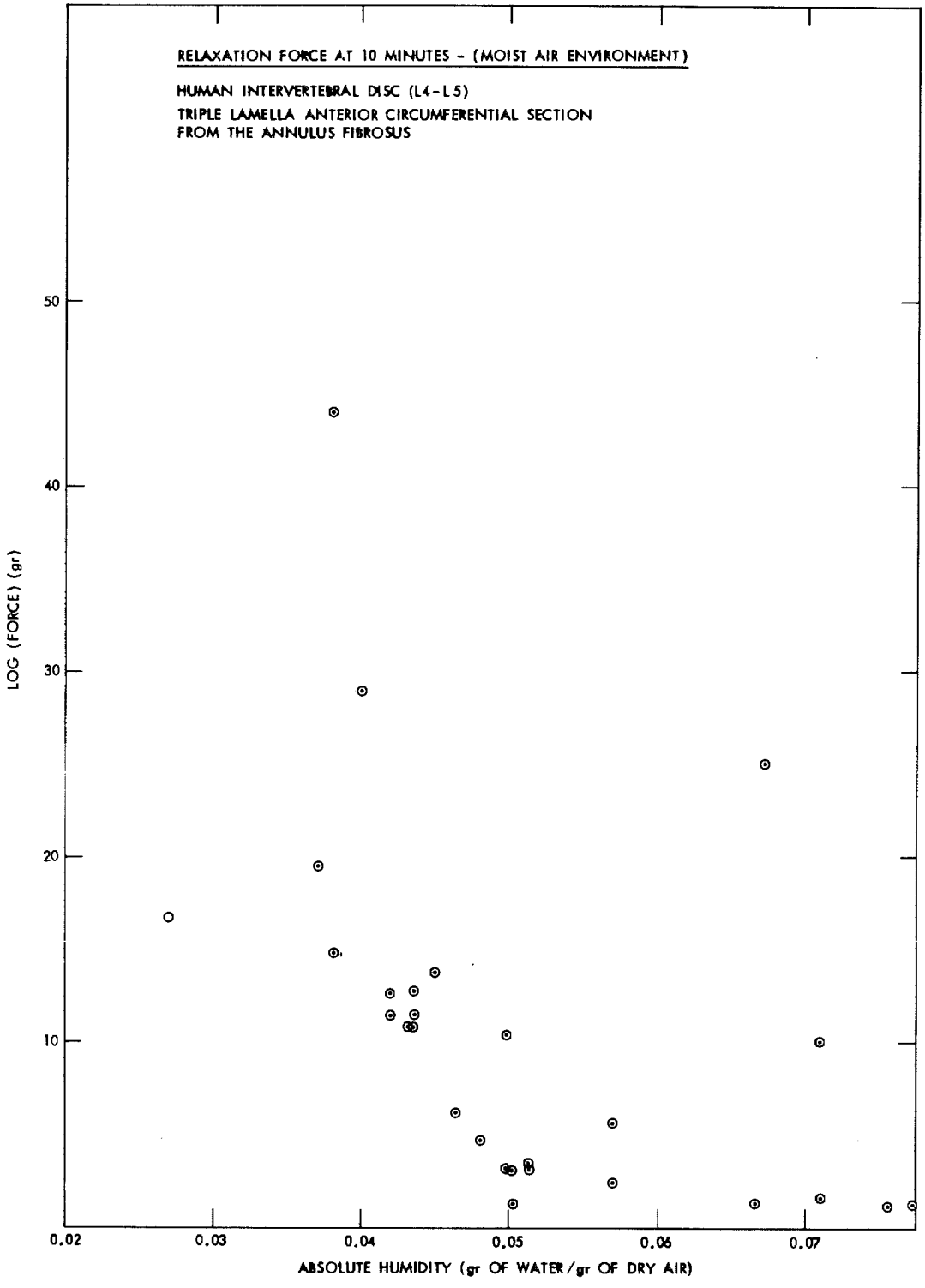

Figure 5.34. Effect of Absolute Humidity on the Relaxation

e. Irregular Specimen* from the Nucleus Pulposus in Air at 14°C

Figure 5.35 shows the relaxation data obtained from a specimen taken from the nucleus pulposus. The experiment was performed at about 14°C temperature and at room humidity conditions with the specimen not in equilibrium with its environment. It was observed that the material of the nucleus was not a fluid but a solid of low modulus (rubbery region).

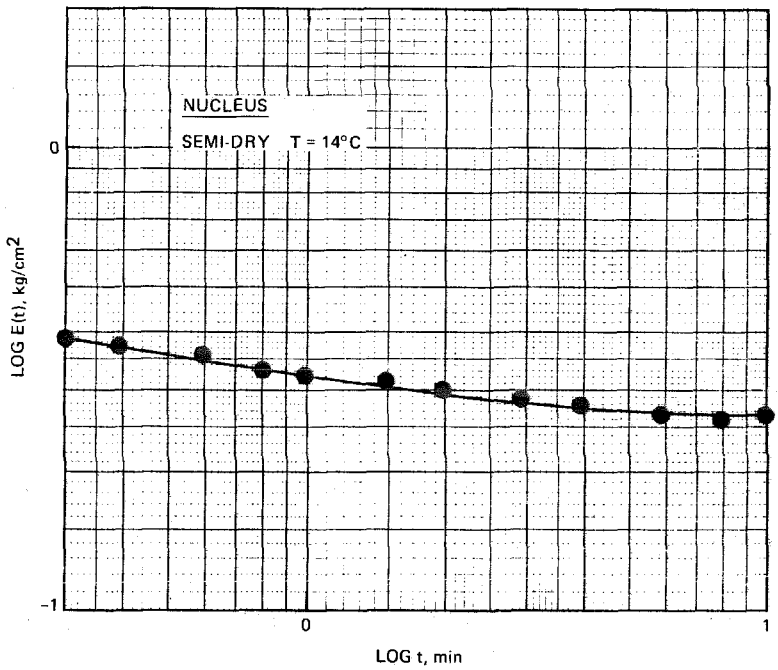

Figure 5.35. Relaxation Data from the Nucleus Pulposus

*Non-cylindrical type of specimens have been used due to gripping problems encountered otherwise.

7. Conclusions and Discussion On the Relaxation Experiments

We have considered the effect of water content of the human intervertebral disc material in connection to its viscoelastic behavior. We have shown that this effect is similar to that of temperature and that it is possible to obtain the disc's lamellae viscoelastic response for a wide time range based on relaxation data for a limited experimental time window.

To date, we have obtained sections of the master relaxation curves for:

(a) a non-uniform wet specimen from the annulus fibrosus referred to an unknown percent of water;

(b) a single lamella specimen referred to a dry state of about 40% water;

(c) a triple lamella specimen referred to a dry state of about 46% water;

(d) a triple lamella specimen referred to a wet state of about 82.9% water.

These master relaxation curves cover a wide time range (i.e., 4-19 decades) and are based on reference states that correspond to the highest absolute humidity data available which are less than the 70% water content encountered in the human disc.

From Figures 5.31 and 5.32 we can observe that the water indeed affects the relaxation spectrum. This is shown by the change in the horizontal shift factor (a_c) and by the corresponding change in the modulus.

A further evidence of the sensitivity of the relaxation data to water content was demonstrated in Figure 5.17. We can easily observe that the force response oscillations (raw relaxation data) are in phase with the wet bulb temperature oscillations. On the other hand, they are not in phase with the dry bulb temperature oscillations. The stronger dependence of the relaxation spectrum to humidity rather than to temperature is also shown in Figure 5.33.

Furthermore, from Figure 5.21 we can see that the relaxation spectrum does not depend on the magnitude of the applied strain. This means that the time and strain effects can be separated. The importance of this observation is in that a constitutive equation containing only a single integral may be more appropriate for the description of the viscoelastic properties over a strain range than the one containing multiple integrals. Similar behavior has been reported for the case of synthetic polymeric materials (Ref. 37). This behavior is a phenomenological description and no explanation in the molecular level is known to us today.

The effect of water content on the viscoelastic behavior of the disc's material is significant and useful because of its possible application to the study of the viscoelastic behavior of other biological materials. At present these effects are not completely understood, although their study should lead to a better understanding of the molecular processes involved in the time dependent mechanical behavior of biological materials.

Based on our experimental data and literature review

(Refs. 10 and 11), we conclude that:

The relaxation master curves for the lamellae and the nucleus are shifted relative to each other along the (log) time axis in accordance with their water content (Figure 6.3). This shift is similar to the one experienced by polymers in the presence of solvents.

We expect that the medical significance of this work will be in the fields of preventive and diagnostic medicine.

The fact of whether a disc is damaged is difficult at best and, at this time, involves invasive techniques which are not free of danger. Starting from our desire to develop a non-invasive diagnostic technique based on X-ray and computer aided image enhancement, we became interested in the structure and mechanical properties of the disc. In the near future we intend to gage X-ray detected information (water content, vertical and radial displacements) with the disc's water sensitive viscoelastic material properties. This seems to be possible since modern medical equipment such as EMI or body scanner can record quantitatively (via the absorption coefficient) water content of the internal body components. If this is true the diagnostic and preventive value of this technique will be invaluable since the mechanical performance of a disc will be estimated in-vivo.

The Figure 5.36 presents an example of how the EMI was able to visualize a section of the author's L4-L5 lumbar intervertebral.

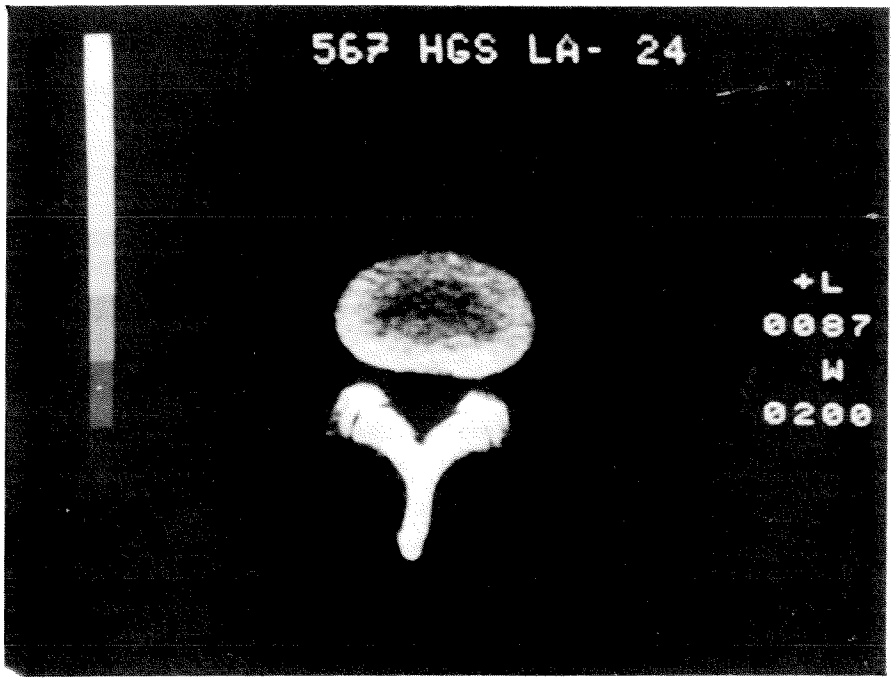

Figure 5.36. Example of a Section of an L4-L5 Disc Obtained via EMI (In-Vivo)

The importance of this and related future work will be in identifying which people would be more prone to develop disc problems. This is particularly important in screening people for special types of jobs (i.e., heavy labor, combat duty in the armed forces, etc.). This will be done by combining knowledge of the mechanical properties of the disc and its in-vivo water content measurements. Therefore, certain prophylactic restrictions may be established so the danger of further damage of a disc will be reduced. Needless to say, there is no technique available today which can provide this kind of information.

REFERENCES

1. Schultz, A. B., (1974), "Mechanics of the Human Spine." Applied Mechanics Reviews, ASME.

2. Schultz, A. B., and Belytschko, T. B., (19F4), Biomechanics Research and Education at UICE," American Society of Engineering Education, Annual Conference, Renselaer Polytechnique Institute, Troy, N. Y.

3. Finneson, B., (1973), "Low Back Pain," J. B. Lippincott Company, Philadelphia.

4. Cailliet, Rene, (1976), "Low Back Pain Syndrome," F. A. Davis Co., Philadelphia (Second Edition).

5. Castleman, K. R., (1974), "Digital Image Processing," Caltech Course Notes.

6. Selzer, R. H., (1968), "Improving Biomedical Image Quality with Computer," JPL Technical Report 32, 1336.

7. Kruger, R., Dwyer, S., Lodwick, (1970), "Digital Techniques for Image Analysis of Radiography," Eighth Annual Symposium on Biomathematics and Computer Science in Life Sciences, Proceedings, Houston, March 23-24.

8. Ziskan, M., Shea, F., (1972) "Linear Spatial Filtering for Enhancement of Radiographic Images," Radiology 103, 101.

9. Hall, E., Kruger, R., Turner, A., (1975), "An Optical Digital System for Automatic Processing of Chest X-Rays," Optical Engineering.

10. Galante, J. O., (1967), "Tensile Properties of the Human Lumbar Annulus Fibrosus." Acta Orthop. Scand. Suppl. 100.

11. Virgin, W. J., (1951), "Experimental Investigations into the Physical Properties of the Intervertebral Disc," J. Bone Jt. Surg., Vol. 33B, No. 4, 607-611.

12. Kazarian, L., (1975), "Creep Characteristics of the Human Spinal Column." The Orthopedic Clinics of North America, Vol. 6, No. 1.

13. Pope, M. H., et al., (1977), "Measurements of Intervertebral Disc Space Height," (To appear in SPINE).

14. Rouviere, H., (1921), "Sur la texture des disques intervertebraux," C. R. Societe de Biologie, 85, 156-157.

15. Horton, W. G. (1958), "Further Observations in the Elastic Mechanism of the Intervertebral Disc," The Journal of Bone and Joint Surgery, 40-B, 552-557.

16. Kazarian, L., (1975), Private communication.

17. Farfan, H. F., (1973), "Mechanical disorders of the low back," published by Lea and Febiger, Philadelphia.

18. Crough, J. E., McClintic, J. R., (1971), "Human Anatomy and Physiology," Wiley.

19. Gross, J., (1961), "Collagen," Scientific American 204:121

20. Jackson, D.S., (1964), "Aging: Temporal changes in Collagen-Aging or Essential Maturation," Advances in Biology of Skin, Vol. 6, Edited by W. Montagna, Chapter XIV, pp 219-238.

21. Smith, J. G., et al., (1964), "Aging: Human Cutaneous Acid Mucopolysaccharides: The effects of age and chronic sun damage,: Advances in Biology of Skin, Vol. 6, Edited by W. Motagna, Chapter XIII, pp. 211-218.

22. Bentley, J. P., (1968), "The Dermis: The biological Role of the Ground Substance Mucopolysaccharides," Advances in Biology of Skin, Vol. 10, Edited by W. Montagna, Cahpter VII, pp. 103-121.

23. Dickson, I. R., Naylor, A., et al. (1967), "Variations in Protein Components of Human Intervertebral Disc with Age," Nature, Vol. 215.

24. Naylor, A., (1976), "Intervertebral Disc Prolapse and Degeneration: The Biochemical and Biophysical Approach," Spine, Vol. 1, No. 2, pp. 108-114.

25. Lyons, H., Jones, E., Quinn, F. K., and Sprunt, D. H., (1966), "Changes in the protein-polysaccharide fractions of nucleus pulposus from human intervertebral disc with age and disc herniation," J. Lab. Clin. Med., 68:930.

26. Püschel, J., (1930), Der Wassergehalt Normaler und degenerieter Zwischenwirtelscheiben," Beitr. path. Anat. 84, 123.

27. De Pukey, P., (1935), "The physiological Oscillation of the length of the Body," Acta Orthop. Scand. 6:338.

28. Tschoegl, N. W., (1976) "Introduction to the Mathematical Theory of Viscoelastic Behavior," CIT, Class Notes
Tschoegl, N. W., (1974), "The Encylcopedia of Physics," edited by Besancon, R., Rheinhold Publishing Corporation.

29. Lekhnitskii, S. G., (1963), "Theory of Elasticity of an Anistropic Elastic Body," Hollen-Day Inc.

30. Jayne, B. A., and Suddarth, S. K., (1966), "Matrix-Tensor Mathematics in Orthotropic Elasticity," From Orientation Effects in the Mechanical Behavior of Anisotropic Structural Materials," An ASTM (stp 405) Publication.

31. Knauss, W. G., (1965-66), Lecture notes "Theory of Viscoelasticity," California Institute of Technology.

32. Ferry, J. D., (1961), "Viscoelastic Properties of Polymers," published by J. Wiley and Sons.

33. Treloar, L. R. G., (1958), "The Physics of Rubber Elasticity," Oxford University Press, London.

34. Bloch, R., (1976), "Viscoelastic Behavior of Polymers under Large Deformation," Ph.D. Thesis, California Institute of Technology, Pasadena, California.

35. Blatz, P. J., Shards, S. C., and Tschoegl, N. W., (1974), "Strain Energy Function of Rubberlike Materials Based on Generalized Measure of Strain," Transactions of the Society of Rheology 18:1, 145-161.

36. Ogden, R. W., (1973), Rubber Chem. Tech. 46, 398-416.

37. Chang Wenji Victor, (1976), "Theoretical and Experimental Studies of the Viscoelastic Behavior of Soft Polymers," Ph.D. Thesis, California Institute of Technology.

38. Green, A. E., and Adkins, J. E., (1970), "Large Elastic Deformations," Clarendon Press, Oxford.

39. Greene, A., Smith, K. J., and Cifem, A., (1967), "Elastic Properties of Networks Formed from Oriented Chain Molecules. II. Composite Network," Rubber Chemistry and Technology.

40. Cheung, J. G., and Hsiao, C-C., (1972), "Nonlinear Anisotropic Viscoelastic Stress in Blood Vessels," J. of Biomechanics, Vol. 5.

41. Knauss, W. G., (1967), "An Upper Bound of Failure in Viscoelastic Materials Subjected to Multiaxial Stress States," International Journal of Fracture Mechanics, Vol. 3, No. 4, 267-277.

42. Knauss, W. G., (1969), "Stable and Unstable Crack Growth in Viscoelastic Media," Transactions of the Society of Rheology, 13:3, 291-313.

43. Knauss, W. G., (1970), "Delayed Failure - The Griffith Problem for Linearly Viscoelastic Materials," International Journal of Fracture Mechanics, Vol. 6, No. 1.

44. Wnuk, Milosz P., Knauss, W. G., (1970), "Delayed Fracture in Viscoelastic-Plastic Solids," Int. J. Solids Structures, Vol 6, 995-1009.

45. Knauss, W. G., (1974), "The Mechanics of Polymer Fracture," Applied Mechanics Reviews.

46. Brown, T., Hansen, R. J., and Yorra, A. J., (1957), "Some Mechanical Tests on the Lumbosacral Spine with Particular Reference to the Intervertebral Dis." J. Bone Jt. Surg., 39A, 1135-1164.

47. Yamada, H., (1970), "Strength of Biological Materials." Williams and Wilkins, Baltimore. (work done by T. Sonada (1962) and edited by H. Yamada.)

48. Wu, Han-Chiu; Yao, Ren-Feng, (1976), "Mechanical Behavior of the Human Annulus Fibrosus," J. Biomechanics Vol. 9, pp. 1-7.

49. Spencer, A.J.M., (1972), "Deformations of Fibre-Reinforced Materials," Oxford Science Research Papers.

50. Fung, Y.C.B., (1967), Elasticity of Soft Tissues in Simple Elongation," Am. J. Physical 213, 1332-1544.

51. Kulak, R. F., Belytschko, T. B., Schultz, A. B., and Galante, J. O., (1975), "Non-Linear Behavior of the Human Intervertebral Disc under Axial Load," (ASME publication).

52. Nachemson, A., (1960), "Lumbar Intradiscal Pressure." Acta Orthopedic Scand. Suppl. 43.

53. Krauss, H., (1973), "Mechanical Disorders of the Low Back," Chapter 6, "Stress Analysis," edited by H. F. Farfan, published by Lea & Febiger, Philadelphia.

54. Sonnerup, Lars, (1972), "A Semi-Experimental Stress Analysis of the Human Intervertebral Disc in Compression." Experimental Mechanics, 142-147.

55. Belytschko, T., Julak, R. F., Schultz, A. B., and Galante, J. O., (1974), "Finite Element Stress Analysis of an Intervertebral Disc." J. Biomechanics, Vol. 7, 227-285.

56. Kulak, R. F., Belytschko, T. B., Schultz, A. B., and Galante, J. O., (1975), "Non-linear Behavior of the Human Intervertebral Disc. Under Axial Load," (ASME publication).

57. Nathan, R., (1966), "Digital Video-Data Handling," JPL Technical Report 32-877.

58. Beckenbach, E. S., Selzer, R. H., Crawford, D. W., Brooks, S. H., Blankenhorn, D. H., (1974), "Computer Tracking and Measurement of Blood Vessel Shadows from Arteriograms," Medical Instrumentation, Vol. 8, No. 5.

59. Vrentas, J. C. , and Duda, J. L., (1976), "Diffusion of Small Molecules in Amorphous Polymers," Macromolecules, Vol. 9, No. 5, pp. 785-790.

60. Nimni, M. E., (1977), Private Communication.

61. Silverberg, (1977), Private Communication.

62. G. H. Lindsey, R. A. Shapery, M. L. Williams and A. R. Zak. The Triaxial Tension Failure of Viscoelastic Materials ARL 63-152, September 1963.

63. A. N. Gent, and P. B. Lindley, Proc. Inst. Mech. Eng. 173, 111 (1959).

64. S. R. Moghe, H. F. Neff, J. Appl. Mech. 38, 393 (1973).

65. Pagano, N. J., and Halpin, J. C. , (1968), "Influence of End Constraints in the Testing of Anisotropic Bodies," Journal of Composite Materials 2, 18.

66. Guth, E., et al., (1946), J. Appl. Phys. 17, 347.

APPENDIX A

EXPERIMENTAL DETERMINATION OF MODULI

A. Creep Experiments

$$\{\varepsilon\} = \{K\}\{\sigma\} \tag{A-1}$$

where the compliance matrix $\{K\}$ for the case of transversely isotropic materials is given by:

$$\{K\} = \begin{bmatrix} K_{11} & K_{12} & K_{13} & 0 & 0 & 0 \\ K_{12} & K_{11} & K_{13} & 0 & 0 & 0 \\ K_{13} & K_{13} & K_{33} & 0 & 0 & 0 \\ 0 & 0 & 0 & K_{44} & 0 & 0 \\ 0 & 0 & 0 & 0 & K_{44} & 0 \\ 0 & 0 & 0 & 0 & 0 & \frac{K_{11}-K_{22}}{2} \end{bmatrix} \tag{A-2}$$

Experiment 1: Specimen pulled along the direction of the fibers.

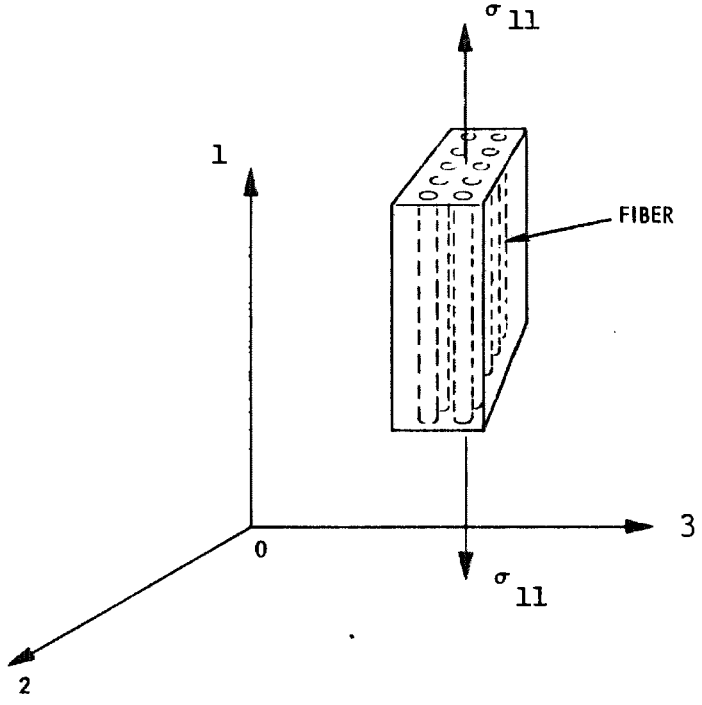

In this case

$$\left.\begin{array}{l} \sigma_{11} \neq 0,\ \sigma_{22} = \sigma_{33} = 0 \text{ and } \sigma_{ij} = 0 \text{ for } i \neq j \\ \text{and} \\ \varepsilon_{11} \neq 0,\ \varepsilon_{22} \neq 0,\ \varepsilon_{33} \neq 0 \end{array}\right\} \quad \text{(A-3)}$$

using these relations, equation (A-1) reduces to

$$\left.\begin{array}{l} \varepsilon_{11} = K_{11}\sigma_{11} \\ \varepsilon_{22} = K_{12}\sigma_{11} \\ \varepsilon_{33} = K_{13}\sigma_{11} \end{array}\right\} \quad \text{(A-4)}$$

from which K_{11}, K_{12} and K_{13} can be determined.

Experiment 2: Specimen pulled in a direction perpendicular to the fiber.

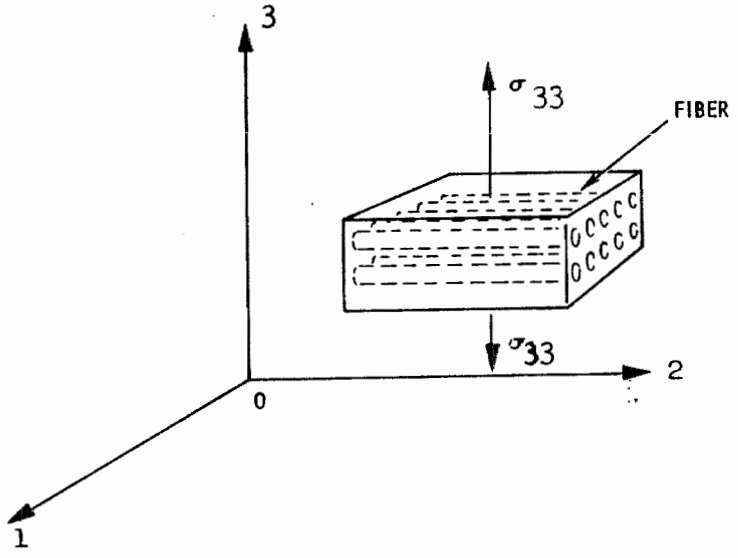

In this case

$$\left.\begin{array}{l} \sigma_{33} \neq 0,\ \sigma_{11} = \sigma_{22} = 0 \text{ and } \sigma_{ij} = 0 \text{ for } i \neq j \\ \text{and} \\ \varepsilon_{11} \neq 0,\ \varepsilon_{22} \neq 0,\ \varepsilon_{33} \neq 0 \end{array}\right\} \quad \text{(A-5)}$$

Again using the relations (A-5), equation (A-1) reduces to:

$$\left.\begin{aligned} \varepsilon_{11} &= K_{13}\,\sigma_{33} \\ \varepsilon_{22} &= K_{13}\,\sigma_{33} \\ \varepsilon_{33} &= K_{33}\,\sigma_{33} \end{aligned}\right\} \qquad \text{(A-6)}$$

from which K_{13} and K_{33} can be determined. Obviously the values for K_{13} obtained by the two experiments should agree.

Therefore, K_{11}, K_{12}, K_{13} and K_{33} can be determined in terms of the known stresses σ_{11} and σ_{33} and the strains ε_{11}, ε_{22}, ε_{33}. We hope to be able to determine these strains by means of an optical obscurator shown in the figure below.

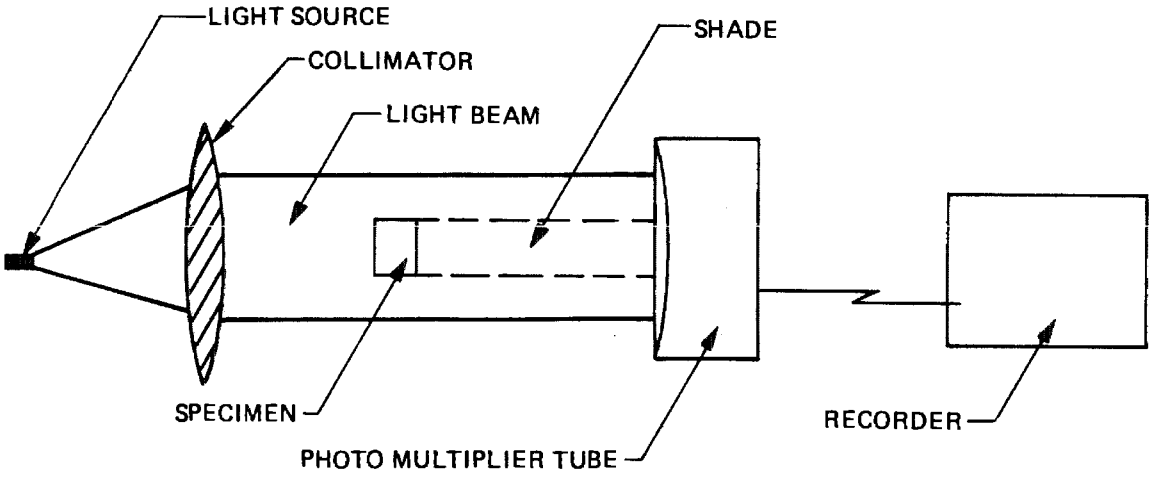

B. Relaxation Shear Experiment

Consider the disc specimen in figure below

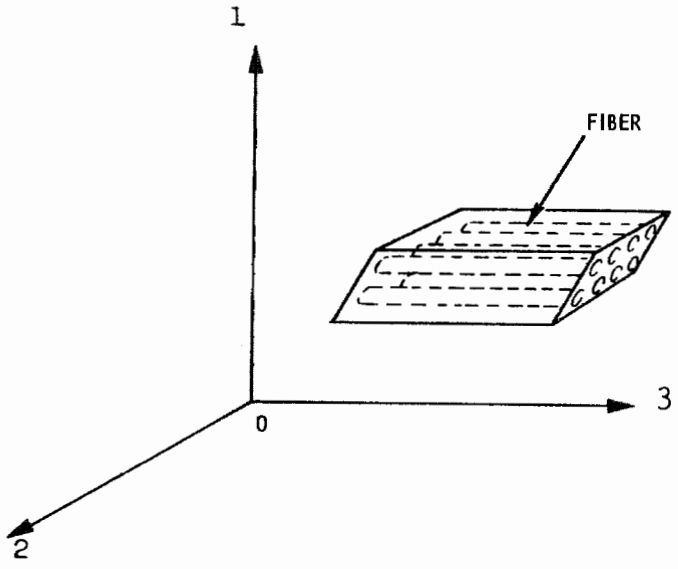

subjected to the excitation:

$$\left.\begin{aligned} \varepsilon_{23}(t) &= \varepsilon_{32}(t) = \varepsilon^{\circ}_{32} h(t) \\ \varepsilon_{ij}(t) &= 0 \text{ for } i \neq j \\ \varepsilon_{12}(t) &= \varepsilon_{13}(t) = 0 \end{aligned}\right\} \qquad \text{(B-1)}$$

where $h(t)$ = heavy side unit step function, $\varepsilon^{\circ}_{32}(t)$ = strain amplitude applied at time $t = 0$. Then, using relations (B-1) equations (2) and (6) of Section III-5, reduce to:

$$C_{44}(s)\varepsilon^{\circ}_{32} = \sigma_{32}(s) \qquad \text{(B-2)}$$

In this equation ε_{32} is given and $\sigma_{32}(t)$ is the response that must be measured.

APPENDIX B

MEANING OF THE VARIOUS REGIONS IN FIGURE 5.17

REGION IDENTIFIER	DESCRIPTION
A	Force cycling due to temperature variations (Force Scale 10) (Time Scale 7.5 cm = 100 min)
B	Same as A (Force Scale 1)
C	Pull ramp at 0.02"/min (Force Scale 1) (Time Scale: 3.75 cm = 1 min)
D	Here by steps we returned the cross head to the same reference state as A. Return ramps 0.02"/min (i.e. strain rate = 0.024"/min) Force and Time Scale the same as C.
E	Force cycling due to temperature variations (Force Scale 10) Time Scale the same as A.
F	After 1 hour of relaxation, cycling as in E with Force Scale 20.
G	Pull ramp at 5"/min (i.e., strain rate 6.02"/min). Force Scale 20. Time Scale the same as C.
H	Relaxation (Force and Time Scale the same as G) $\Delta\ell$ = 0.028", ε = 3.3 %
I	Relaxation (Force Scale 10, Time Scale the same as A)
J	Relaxation from which a force was substructed to increase sensitivity of cycles. (Force Scale 2, Time Scale the same as I.)

REGION IDENTIFIER	DESCRIPTION
K	Return pull at 0.02"/min (i.e., strain rate = 0.024"/min). Force Scale 2. Time Scale the same as C.
L	Temperatures for wet and dry bulbs recorded during the time intervals H and I.

Note the correspondence between the point "O" in both figures (the oscillations in both, relaxation and humidity curves are in phase).